February 1996 • NREL/TP-411-20588

Continuous Roll-to-Roll a-Si Photovoltaic Manufacturing Technology

Final Subcontract Report
1 April 1992 – 30 September 1995

M. Izu
Energy Conversion Devices, Inc.
Troy, Michigan

National Renewable Energy Laboratory
1617 Cole Boulevard
Golden, Colorado 80401-3393
A national laboratory of the U.S. Department of Energy
Managed by Midwest Research Institute
for the U.S. Department of Energy
under Contract No. DE-AC36-83CH10093

NREL/TP-411-20588 ● UC Category: 1280 ● DE9696000531

Continuous Roll-to-Roll a-Si Photovoltaic Manufacturing Technology

Final Subcontract Report
1 April 1992 – 30 September 1995

M. Izu
Energy Conversion Devices, Inc.
Troy, Michigan

NREL technical monitor: R. Mitchell

National Renewable Energy Laboratory
1617 Cole Boulevard
Golden, Colorado 80401-3393
A national laboratory of
the U.S. Department of Energy
Managed by Midwest Research Institute
for the U.S. Department of Energy
under contract No. DE-AC36-83CH10093

Prepared under Subcontract No. ZM-2-11040-7

February 1996

Available to DOE and DOE contractors from:
Office of Scientific and Technical Information (OSTI)
P.O. Box 62
Oak Ridge, TN 37831
Prices available by calling (615) 576-8401

Available to the public from:
National Technical Information Service (NTIS)
U.S. Department of Commerce
5285 Port Royal Road
Springfield, VA 22161
(703) 487-4650

Printed on paper containing at least 50% wastepaper, including 10% postconsumer waste

Preface

This Final Subcontract Report covers the work performed by Energy Conversion Devices, Inc. (ECD), under DOE/NREL Subcontract number ZM-2-11040-7 entitled "Continuous Roll-to-Roll a-Si Photovoltaic Manufacturing Technology." The total period covered under this subcontract is April 8, 1992 to September 7, 1995. The following personnel participated in the research program:

T. Barnard
H. Bianchi
R. Ceragioli
J. Chema
B. Clark
R. Crucet
X. Deng
J. Doehler
T. Ellison
J. Evans
C. Harrison
M. Izu, Principal Investigator
S. Jones
R. Kopf
A. Krisko
A. Kumar
T. Laarman
A. Myatt
K.L. Narasimhan
H. Ovshinsky
S.R. Ovshinsky
G. Pietka
R. Souleyrette
S. Sullivan
B. Viers
K. Whelan

We would like to thank Drs. H. Fritzsche, S. Guha, and J. Yang for helpful discussions.

Executive Technical Progress Summary

Objectives and Goals

The overall objective of this three-year program is to advance roll-to-roll, triple-junction photovoltaic (PV) manufacturing technologies, to reduce the module production costs, to increase the stabilized module performance, and to expand commercial production capacity utilizing such roll-to-roll technology.

The specific three-year goal is to develop advanced large-scale manufacturing technology incorporating ECD's earlier research advances with the capability of producing modules with stable 10.2% efficiency at a cost of approximately $1.00 per peak watt.

Major efforts during this subcontract include: Task I: Optimization of the high performance back-reflector system; Task II: Optimization of the Si-Ge Narrow Bandgap Solar Cell; Task III: Optimization of the Stable Efficiency of Photovoltaic Modules; Task IV: Demonstration of Serpentine Web Continuous Roll-to-Roll Deposition Technology; Task V: Material Cost Reductions; and Task VI: Improving the Module Assembly Process.

Approaches

We have performed manufacturing technology development work utilizing two advanced continuous roll-to-roll amorphous silicon (a-Si) alloy solar cell manufacturing machines, both were engineered and manufactured by ECD at ECD's expense.

1. A 2 MW Production Line

   This 2 MW production plant consists of a continuous roll-to-roll substrate washing machine, a continuous roll-to-roll back-reflector deposition machine, a continuous roll-to-roll amorphous silicon alloy deposition machine and a continuous roll-to-roll transparent conductor deposition machine.

   The production line produces triple-junction two bandgap a-Si alloy solar cells consisting of an a-Si/a-Si/a-SiGe structure on a 5 mil. thick, 14 in. wide, 2500 ft. long stainless steel roll at a speed of 1 ft./min. This production line represents the world's first commercial production line of high efficiency a-Si alloy solar cells utilizing a multi-junction spectrum-splitting cell design and high performance back-reflector.

2. A 200 kW Pilot Line

   This multipurpose continuous roll-to-roll a-Si alloy solar cell deposition machine consists of n-i-p chambers to deposit a-Si n-i-p solar cells, a sputtering chamber to deposit textured Ag/ZnO back-reflector and TCO top conductor, and a serpentine deposition chamber to develop new high throughput serpentine deposition processes.

Major Accomplishments

- Successful incorporation of a high-performance Ag/ZnO back-reflector system into our continuous roll-to-roll commercial production operation.

- Incorporation of high quality a-SiGe narrow bandgap solar cells into a commercial continuous roll-to-roll manufacturing process.

- Demonstration that the continuous roll-to-roll production of high efficiency triple-junction two bandgap solar cells is consistent and uniform throughout a 2500 ft. run with high yield. The average initial subcell efficiency and yield were 10.21% and 99.7%, respectively. (7.35 cm^2, 2/93)

- Achievement of 11. 1 % initial subcell efficiency of triple-junction two bandgap a-Si alloy solar cells manufactured in continuous roll-to-roll production. (test cell 0.25 cm^2, 2/93)

- Production of the world's first 4 $ft.^2$ PV modules utilizing triple-junction two bandgap solar cells manufactured in a commercial, continuous roll-to-roll production line. These 4 $ft.^2$ modules had 9.5% initial efficiencies and 8% stable aperture-area module efficiencies. (4/93)

- Demonstration of the long-term stability of ECD's 4 $ft.^2$ production module. The stable module efficiency after 2,380 hours of sunlight soaking at 50°C is 7.9%. Light soak testing of ECD modules performed at NREL under one sun at 50°C showed 15% degradation after 600 hours. ECD modules have passed heat and humidity/freeze cycles of NREL recommended module reliability testing procedure.

- Process optimization to reduce the layer thickness and to improve gas utilization resulted in a 77% material cost reduction for germane and a 58% reduction for disilane have been achieved.

- Design, construction (at ECD's expense) and completion of initial optimization of a 200 kW multi-purpose continuous roll-to-roll a-Si alloy solar cell deposition machine having upgraded machine and construction specifications;

- Design and construction, at ECD's expense, of a serpentine deposition chamber which has demonstrated a compact, low-cost deposition machine design with improved throughput and gas utilization factor.

- Demonstration of triple-junction solar cells with 9.5% initial efficiency with top a-Si cells deposited in the serpentine deposition chamber. (10/94)

- Development of a new back-reflector evaluation technique using PDS to effectively analyze the optical losses of textured back-reflector and develop an improved textured Ag/ZnO back-reflector system demonstrating 26% gain in J_{sc} over previous textured Al back-reflector systems.

- Development of a new grid/busbar design utilizing thin wire grids which improved the efficiency by approximately 3 - 4% and reduced the grid/busbar cost by approximately 50%.

- Development of a concept design for an automated high volume (100 MW/yr) PV manufacturing plant for producing a low-cost large-area PV module with an expected material cost reduction of 71%. The module manufacturing cost is estimated to be $1.00 per peak watt.

Table of Contents

List Of Figures

Figure Number

List Of Figures
(Cont'd)

Figure Number

List Of Figures
(Cont'd)

Figure Number

List Of Tables

Table Number

Introduction

During the past fifteen years, ECD has made important progress in the development of materials, device designs, and manufacturing processes required for the continued advancement of practical photovoltaic technology[1-23]. Among these accomplishments, ECD has pioneered and continues further development of two key proprietary technologies, with significant potential for achieving the cost goals necessary for widespread growth of the photovoltaic market: (1) a low cost, roll-to-roll continuous substrate thin-film solar cell manufacturing process; (2) a high efficiency, monolithic, multiple-junction, spectrum-splitting thin-film amorphous silicon alloy device structure.

Commercial production of multiple-junction a-Si alloy modules has been underway at ECD and its joint venture company for a number of years using ECD's proprietary roll-to-roll process and numerous advantages of this technology have been demonstrated. These include relatively low semiconductor material cost, relatively low process cost, a lightweight, rugged and flexible substrate that results in lowered installed costs of PV systems, and environmentally safe materials. Nevertheless, the manufacturing cost per watt of PV modules from our current plant remains high.

In order to achieve high stable efficiency and low manufacturing cost, ECD has, at ECD's expense, engineered and constructed a 2 MW production line and a 200 kW pilot line, incorporating earlier ECD research advances in device efficiency through the use of multi-junction spectrum-splitting and high performance back-reflector cell design. Under this subcontract six tasks were directed towards achieving this goal. They are: **Task I:** Optimization of back-reflector system; **Task II:** Optimization of the Si-Ge narrow bandgap solar cells; **Task III:** Optimization of the stable efficiency of photovoltaic modules; **Task IV:** Demonstration of serpentine web continuous roll-to-roll deposition technology; **Task V:** Material cost reductions; and **Task VI:** Improving the module assembly process.

ECD's Continuous Roll-to-Roll Amorphous Silicon Photovoltaic Manufacturing Technology

Features and Advantages of ECD's PV Manufacturing

Spectrum Splitting, Triple-Junction Cell Design

The key feature of our continuous roll-to-roll production is the use of triple-junction multiple bandgap solar cells with high quality, bandgap profiled a-Si alloy as the bottom intrinsic layer. The cell structure is shown in Figure 1.

ECD has demonstrated 13.7% initial active-area conversion efficiency in small a-Si alloy solar cell devices with a-Si/a-Si/a-SiGe triple-junction design. The manufacturing line has been designed and engineered to produce solar cells incorporating this advanced cell design for obtaining high stable efficiency modules. ECD has demonstrated the production of triple-junction 4 $ft.^2$ modules with stable 8% efficiency under this PVMaT Program, as is shown in Figure 2.

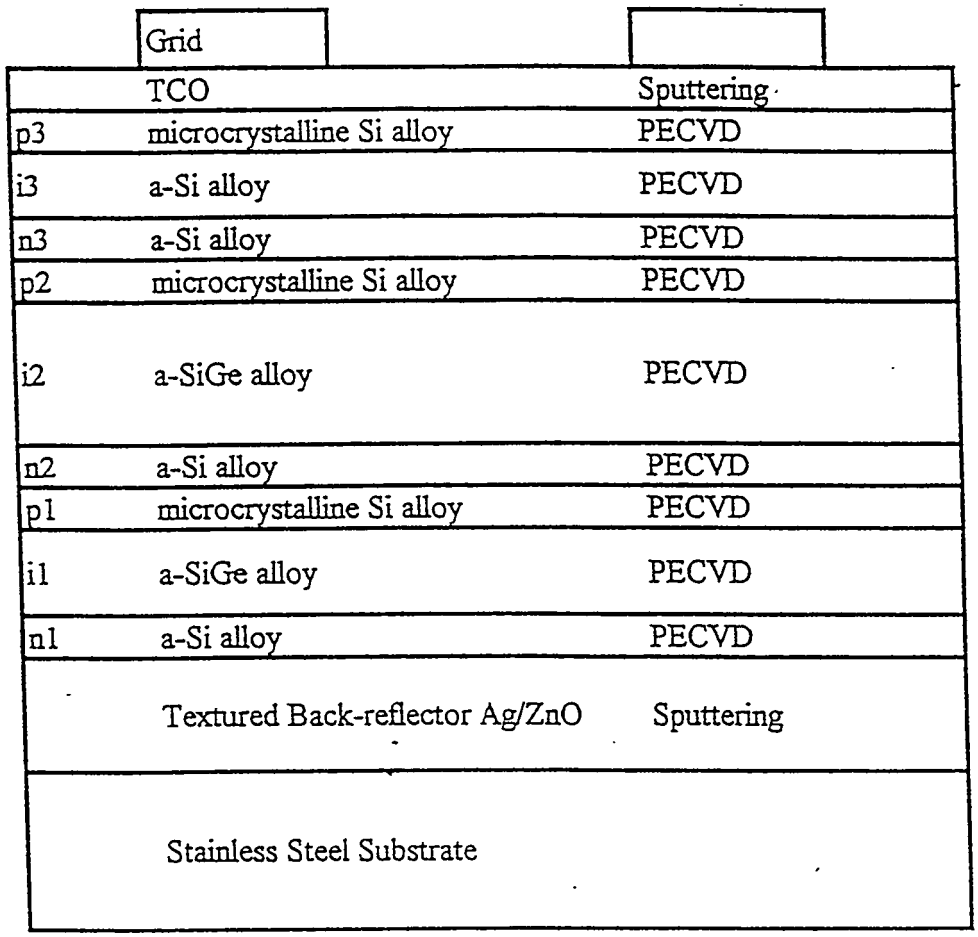

Figure 1. Structure of a triple-junction spectrum-splitting solar cell produced in ECD's continuous roll-to-roll manufacturing process.

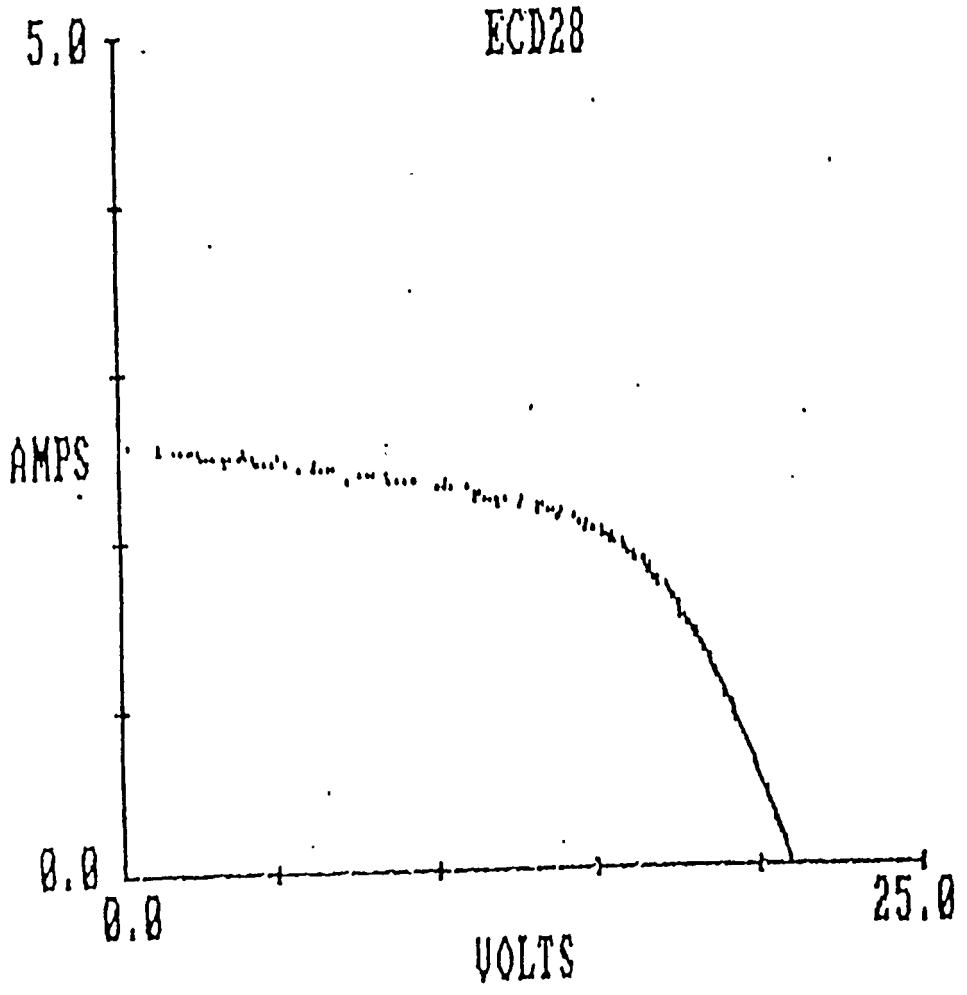

(no filename)
ID. No. M28-625H
19-04-1993, 08:33:46
Sun = 100 mW/cm2
Temp = 22 degC, 22
Voc = 20.99 V
Isc = 2.62 A
Pmax = 31.38 W
Vmp = 15.32 V
Imp = 2.05 A
FF = .57
Rs = 1.82 Ohms
Ef,c = 8 %

No. of flashes = 286

Figure 2. I-V curve of a 4 ft2 a-Si alloy PV module showing 8% stable module efficiency.

Low Cost, Large Scale Continuous Roll-To-Roll Operation

In the roll-to-roll deposition of a-Si alloy solar cells, nine layers of a-Si alloys are deposited onto a 2500 ft. substrate in a single pass. This stable steady-state process has proven reliable, and provides uniform cells. The operating cost, which includes maintenance and labor, is low. Figure 3 shows the excellent uniformity of solar cell efficiency, both along the web and across the web, of a production run.

Flexible Thin Stainless Steel Substrate

The substrate is a 5 mil. thick, 14 in. wide, 2500 ft. long stainless steel roll. It offers many advantages compared to glass substrates. Stainless steel does not shatter during operation and handling. This thin stainless steel substrate can be heated and cooled quickly during deposition, i.e., no waiting time is needed for temperature stabilization. During deposition, the substrate transport mechanism is simple and reliable, and component wear is low. This keeps maintenance costs low. Also, the substrate is lightweight and flexible.

Lightweight Polymer Encapsulated PV Module

EVA/Tefzel is used for module encapsulation. Modules are lightweight and shatter-proof.

ECD's Continuous Roll-to-Roll Manufacturing Line

In the 2 MW PV manufacturing line, we deposit triple-junction, two bandgap a-Si alloy solar cells in a continuous roll-to-roll process on a 5 mil. thick, 14 in. wide and 2500 ft. long web of stainless steel at a speed of 1 ft./min. Figure 4 is a picture of ECD's 2 MW PV manufacturing line.

The front end of the manufacturing line consists of four continuous roll-to-roll machines:

Substrate Washing Machine

Prior to the film deposition, the stainless steel is loaded into a roll-to-roll substrate washing machine that transports the stainless steel web through a detergent cleaning station, multiple deionized water rinsing baths, and an infrared oven drying stage, to produce a clean, dry, particle-free substrate suitable for amorphous silicon deposition.

Back-Reflector Machine

After washing and drying, the roll is loaded into a roll-to-roll back-reflector machine that deposits a reflective metal layer and a metal oxide layer on the cleaned, stainless steel web. Both the metal and the metal oxide layer are vacuum deposited by DC magnetron sputtering onto the heated substrate.

The metal adheres to the stainless steel and textures the surface to provide a diffuse, highly reflective layer. This enhances absorption of the infrared portion of the solar spectrum by providing an increased optical path length for reflected light in the thin film solar cell structure and by increasing reflectivity over that of the stainless steel. The metal and oxide layers provide ohmic contact to the solar cell as well as improved infrared response.

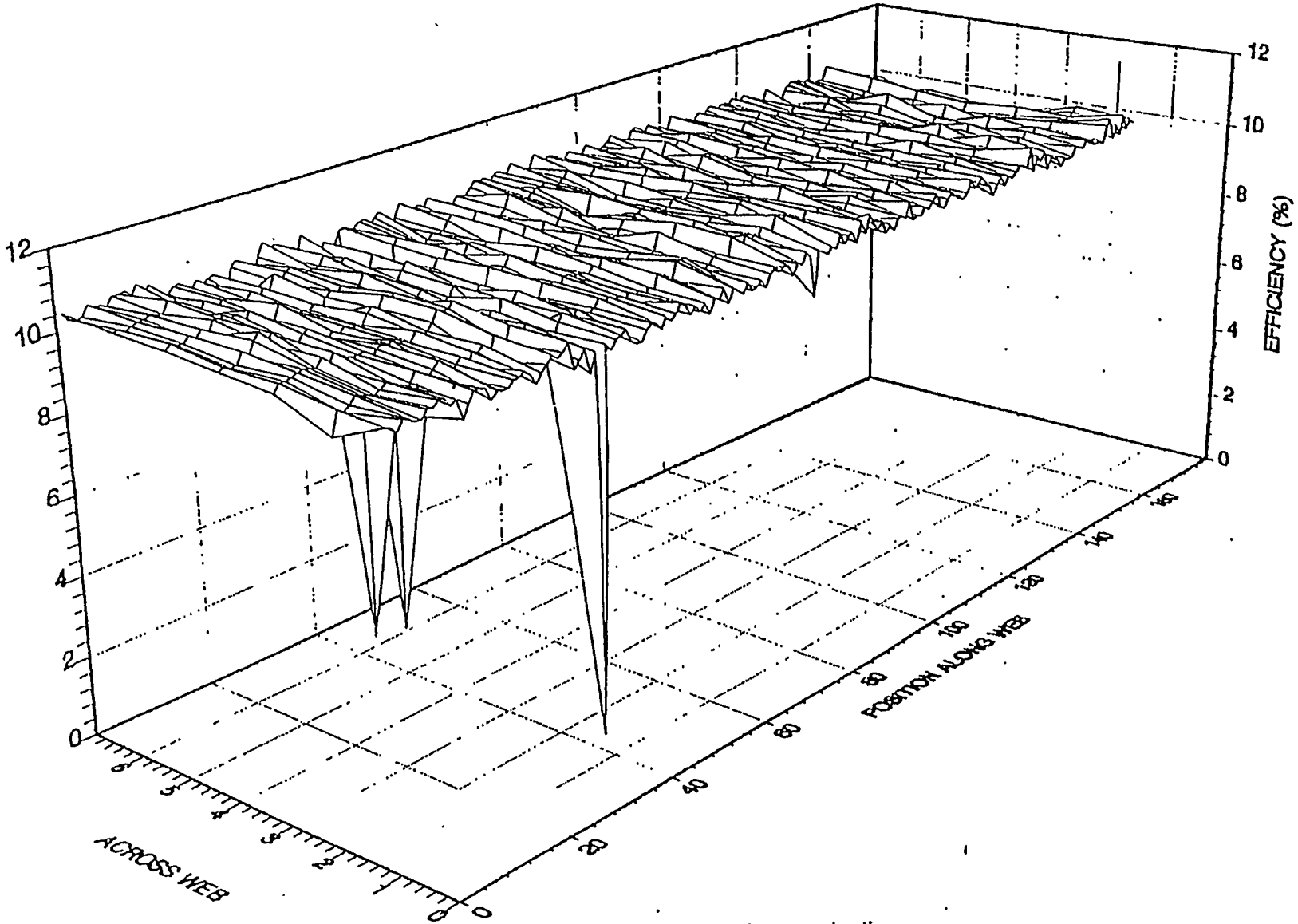

Figure 3. Cell efficiency of a 600 m production run.

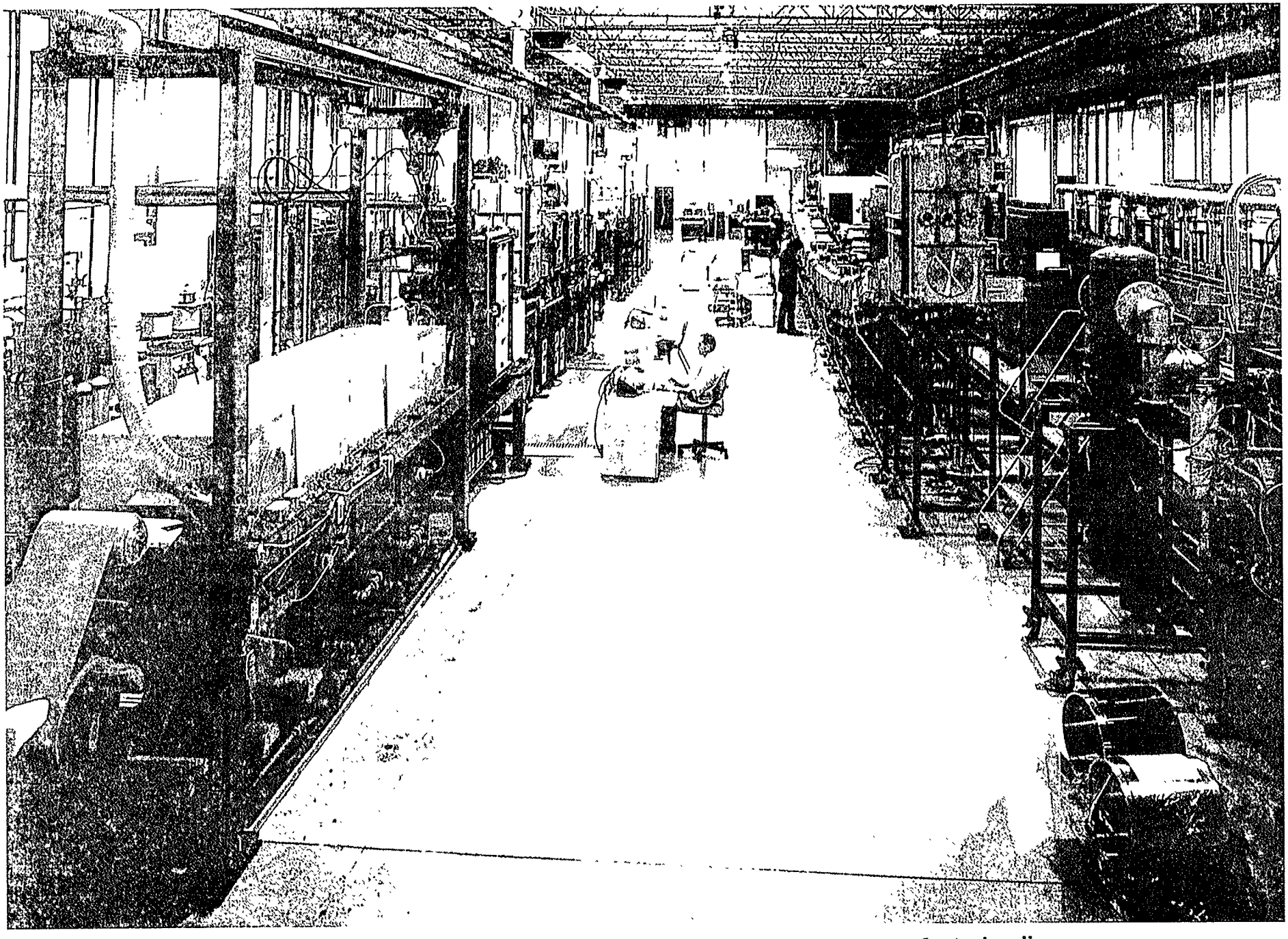

Figure 4 **ECD's continuous roll-to-roll a-Si alloy solar cell manufacturing line.**

Amorphous Silicon Alloy Deposition Machine

After the back-reflector deposition, the roll is loaded into the amorphous silicon alloy roll-to-roll deposition machine that produces, in a single pass, sequentially deposited thin films of doped and undoped amorphous silicon alloy material. Mixtures of feedstock gases are decomposed at a pressure of approximately 1 Torr in a series of RF CVD plasma chambers to continuously deposit layers of amorphous silicon alloy material onto the coated stainless steel substrate heated to approximately 250°C to 300°C. The multi-section amorphous silicon alloy deposition machine consists of a pay-off chamber section, nine process chamber sections for the triple device structure and a take-up section. The process gas mixtures in each section are dynamically isolated from adjacent sections by proprietary "gas gates." The "gas gates" utilize laminar gas flow through constant geometrical cross section conduits in a direction opposite to the diffusion gradient of the dopant gas concentrations. In this way, migration of dopants between chambers is essentially eliminated and gas mixtures in adjacent chambers are effectively isolated even though no actual physical impediment is present. Substrate transport is accomplished with controlled tension and magnetic rollers for accurate positioning of the substrate in the various process chambers. The web is steered in the take-up chamber to insure that the substrate is properly wound. Substrate passage through the process chambers is such that deposition takes place on the underside, which minimizes film defects due to particulate accumulation. The production equipment has nine RF-plasma deposition chambers to produce a-Si/a-Si/a-SiGe triple-junction two bandgap solar cells. Figure 5 is a picture of ECD's continuous roll-to-roll a-Si alloy deposition machine.

Transparent Conductor Deposition Machine

The solar cell roll is then transferred to the transparent conducting oxide (TCO) roll-to-roll deposition machine, which vacuum-deposits a transparent, electrically conductive layer on top of the solar cell structure. Metal is reactively evaporated in an oxygen atmosphere. The substrate is heated to approximately 200°C during this deposition process. The TCO layer has two functions. First, it provides an electrical top contact between the current generating photovoltaic layers and the current collection grid. Second, its thickness is selected so that it acts as an anti-reflective coating to pass more incident light.
These four continuous roll-to-roll machines are highly automated. We are able to reference the actual deposition conditions of each process for every module we build. Complete records for the deposition conditions are stored in the computer.

The PV module assembly process consists of the following procedures:

1. Slabbing

   A finished roll of TCO coated a-Si solar cell material is cut by a slab cutter into 16" long, 14" wide "slabs".

2. QA/QC

   Forty to one hundred samples (4" x 14") are sheared and processed into test solar cells for QC qualification of each 2,500 foot roll.

3. Scribing

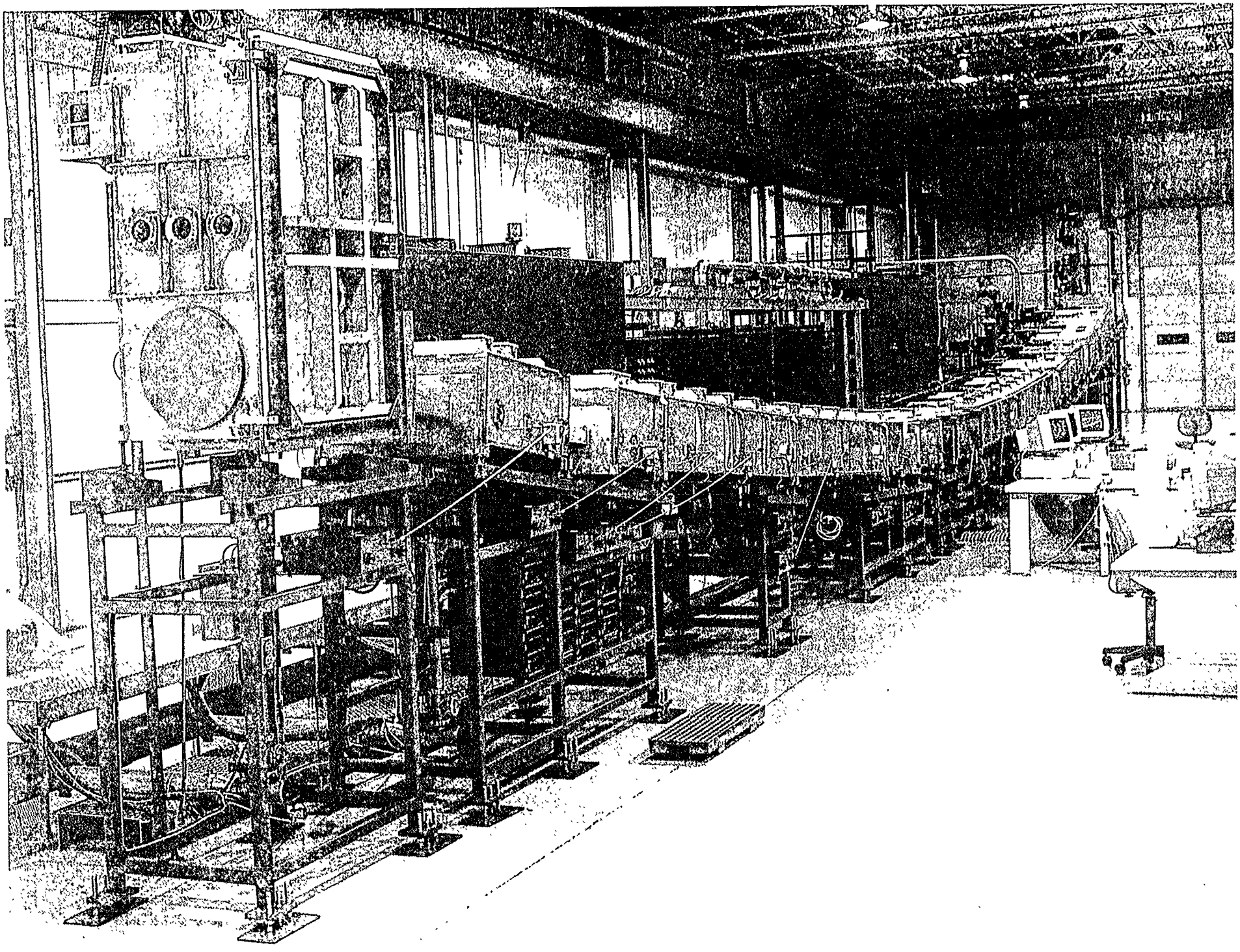

In order to isolate the strip cells electrically, we scribe the TCO layer using a semi-automatic screen printing process. The TCO etching paste is screen printed in a selected pattern and the etch process is activated by heating. After the etch is completed, remnants of the etching paste are removed by rinsing in an agitated aqueous cleaning bath.

4. Short Passivation

Defects in the solar cell that could give rise to electrical shorts on the coated web are electrically isolated by electrolytically converting the transparent conductor into an insulator at the defect sites through a proprietary process. This short passivation operation involves treating the web with electrolyte solution and subjecting the cell to reverse electrical bias. After short passivation, the residual electrolyte is rinsed off with deionized water, and the web is dried with hot air.

5. Screen Print Grid Pattern

To aid current collection, a silver grid pattern is screen printed on the cell. This is followed by an IR curing step.

6. Final Assembly

- Cell Cutting: The slabs are sheared into strips, and qualified for their performance.
- Cell Interconnect: Cells are interconnected to make the cell block assembly. Suitable fixtures are provided to ease the assembly process.
- Laminating: The finished cell block is laminated in a vacuum laminator between two polymer sheets. The polymer sheets are chosen to provide a clear front cover and a pigmented back cover. Tefzel and EVA are used for the front cover.
- Module Finishing: The laminated cell block is trimmed to size and a junction box is attached. Other framing and connector details are added for specific products.
- Testing and Packaging: The module is finally tested in a solar simulator that measures the I-V curve of the finished modules under simulated AM 1.5 conditions, providing a printout of the I-V characteristics. Modules are then packaged, ready for shipment.

ECD's New Continuous Roll-to-Roll Multi-purpose a-Si Deposition Machine

We have designed and constructed, at ECD's expense, a new, improved 200 kW continuous roll-to-roll multi-purpose deposition machine that incorporates improvements necessary to further advance the performance of PV modules. A picture of the machine is shown in Figure 6.

The machine has a left-hand drive assembly, an n-deposition chamber, a serpentine vertical i-deposition chamber, a horizontal i-deposition chamber, a p-deposition chamber, a sputtering chamber, and a right-hand drive assembly. Steering and web tensions are controlled in both forward and reverse directions of web travel. This provides bi-directional deposition of material.

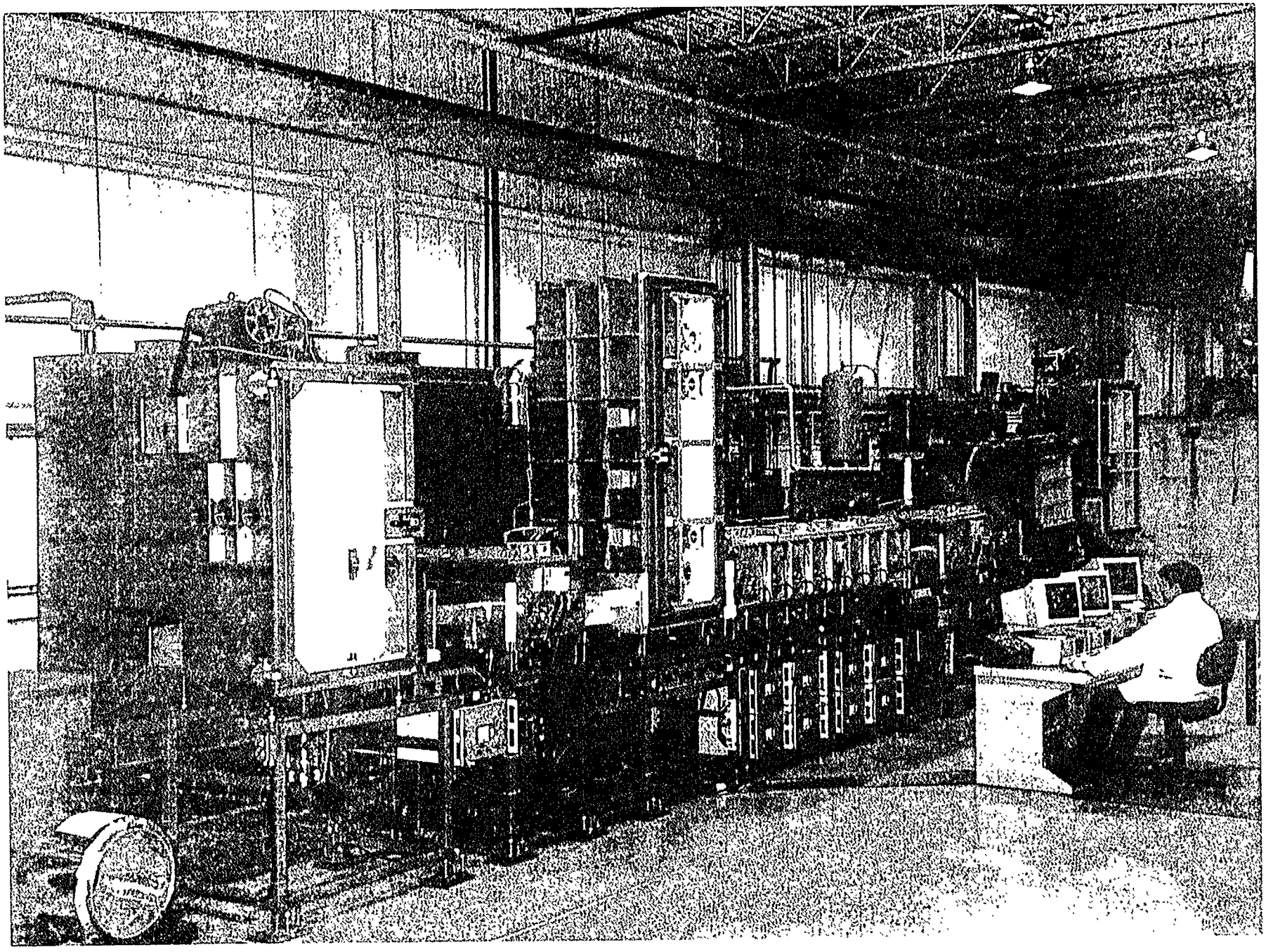

Figure 6 **ECD's multipurpose continuous roll-to-roll a-Si alloy solar cell deposition machine.**

The machine is capable of producing n-i-p solar cells in a single pass and triple-junction cells in three passes. The i chamber has a specially designed proprietary gas distribution manifold and multiple cathodes, and is capable of continuously depositing profiled a-SiGe alloy material in roll-to-roll operation.

This design combines, in one machine, sputtering for the back-reflector and top conductor with RF plasma CVD for the a-Si solar cell.
We utilized this machine to further improve the performance of PV modules produced in a continuous roll-to-roll process.

Continuous Roll-to-Roll Serpentine Deposition Technology

To further advance PV manufacturing technology toward achieving higher production throughput, higher stable module efficiency and lower manufacturing cost, we have designed and constructed, at ECD's expense, a deposition chamber using a continuous roll-to-roll serpentine web configuration. In this serpentine deposition chamber, the web travels vertically while deposition takes place on both sides of a vertically mounted, perforated RF power cathode. As a consequence, we can achieve maximized throughput for a high volume production plant, reduced machine cost, improved gas utilization, reduced power consumption, and improved material stability.

Task I: Optimization of Back-Reflector System

Incorporating textured Ag/ZnO back-reflector into continuous roll-to-roll production line

In our earlier manufacturing process, a textured Al alloy was used as a back-reflector. The high efficiency, small-area device (on which we have demonstrated 13.7% initial active-area efficiency, the world-record efficiency for a-Si alloy solar cell) utilized textured Ag/ZnO back-reflector that had a substantially higher reflectance and diffusivity than the Al alloy back-reflector, resulting in an enhancement of J_{sc} in our laboratory cells.[5] However, initial attempts to transfer this high performance back-reflector technology to a manufacturing process had not been successful due to low yields.

Material and process optimizations were carried out using a 2 MW continuous roll-to-roll back-reflector production machine. The machine is equipped with eight DC magnetron sputtering cathodes. An upward sputtering configuration is used so that particulates do not accumulate on the web surface. Typically, two metal targets and six ZnO targets are loaded in the machine. The back-reflectors (Ag and ZnO) were deposited sequentially at a speed of 1 ft./min on a stainless steel roll that has a dimension of about 2500 ft. long, 14 in. wide, 5 mil thick.

Causes for the low yield using the double-layered back-reflector system Ag/ZnO have been investigated by structural/morphological/chemical analyses of the sites that caused shorts. We have determined that the shorts are caused by defects in the layer structure due to mechanical damage and foreign materials incorporated in the deposited layer during processing.

We incorporated several new designs for the production machine to improve the back-reflector by reducing the mechanical damage such as dimples and scratches. A new bearing design has been incorporated that can transport the web in vacuum at high temperatures (300°C) without contaminating the deposition. The improved bearing design prevented roller seizure and eliminated the loss in yield due to scratches caused by failed rollers. We have identified that most dimples on the stainless steel substrate are caused by the particulates accumulated on the back side of the web. The particulates are collected in the take-up chamber by the roller that applies tension to the web and causes dimples on the web. A wiper is installed in the take-up chamber before the tension applying roller that effectively removes the particulates from the back-side of the web.

With the above improvements, we have effectively reduced the creation of shorts and shunts, and obtained high production yield for the high performance Ag/ZnO back-reflector system. For a 2500 ft. production run, we have achieved an average subcell yield of 99.7%.

Deposition conditions were further adjusted for each layer of the Ag/ZnO system to optimize the back-reflector performance. Deposition temperature, thickness of the Ag and ZnO layers, as well as the rate of sputtering, were found to affect film quality. We have studied the dependence of solar cell current on the Ag layer thickness. The current improves with Ag thickness, presumably due to enhanced internal reflection from a rougher morphology. However, we begin to see a drop in subcell yield for thicker Ag layers. We adjusted the deposition condition to achieve improvements in the following four areas:

1. higher reflectance of Ag layer
2. better texture of Ag layer
3. less absorption in the ZnO layer
4. higher yield

Figure 7 is a quantum efficiency curve of a triple-junction a-Si alloy solar cell on an earlier Ag/ZnO back-reflector. The quantum efficiency in the long wave length region (700nm - 800nm) reflects the performance of back-reflector. After process optimization, we have improved the back-reflector quality as is shown in Figure 8. The quantum efficiency curve on the improved back-reflector shows less evident interference fringes due to diffuse reflection, resulting in higher bottom cell current. For the same a-SiGe bottom cell, the improved Ag/ZnO back-reflector gives 7.43 mA/cm^2 in the bottom cell, compared to 6.78 mA/cm^2 for the initial Ag/ZnO back-reflector.

In summary, the high performance Ag/ZnO back-reflector system has, for the first time, been successfully incorporated in a continuous roll-to-roll production line. We have achieved a 99.7% average subcell yield for the 2500 ft. long production run.

Development of Back-Reflector Evaluation Techniques

Although the Ag/ZnO back-reflector produced in ECD's production machine has demonstrated high current in solar cells, there is room for further improvement. We identified some optical loss in the current back-reflector and note that the degree of texture, which is necessary for light trapping, can be further optimized. There are still interference fringes in the Quantum Efficiency (QE) curve of the cell, which indicate that the degree of texture is not optimum.

To further improve solar cell current, we developed evaluation techniques to accurately measure the performance of back-reflector systems and we conducted a research program to develop high performance back-reflectors using R&D batch deposition machines.

In order to evaluate the performance of the back-reflector, we developed a technique to measure the optical losses of reflective layers on stainless steel substrates. We also used angular dependence of reflection, and Scanning Electron Microscope (SEM) to study the texture. The QE response for standard solar cells deposited on the back-reflector is used as the final criteria for back-reflector performance evaluation.

We modified Photothermal Deflection Spectroscopy (PDS) for use as an important measurement technique for back-reflector performance evaluations. PDS has demonstrated advantages in the measurement of optical loss, especially for highly reflective and textured surfaces, because, unlike conventional reflectance measurements, PDS measures the fraction of the light that is converted to heat.

In current back-reflector research, we use PDS to detect the low absorption signal of highly reflective surfaces such as Ag. The majority of light is specularly reflected, or, in the case of textured surfaces, scattered and does not contribute to the signal that PDS measures. Therefore, with appropriate calibration, PDS is a powerful tool in measuring the light absorption loss in highly reflective and highly textured surfaces.

The PDS signal for different wavelengths is calibrated with a Perkin-Elmer 330 Spectrophotometer using plain specular stainless steel. Table 1 lists the PDS signal and reflectance measured with a Perkin-Elmer Spectrophotometer, as well as the method we use to obtain the calibration factor (C), which is the ratio of PDS absorption (A_{pds}) to PDS signal (V_{pds}). When we measure other samples with PDS, we obtain the absorption loss by multiplying V_{pds} with the calibration factor A_{pds}/V_{pds} , which should be the same for all back-reflector samples on stainless steel substrate. Table 2 lists the data from the absorption measurement of specular Ag sample (BR13) and the reference sample (OBR83) using PDS and using the calibration factor we obtained above. We have found that the optical loss at 827 nm using the existing back-reflector (OBR83) is 7.0%.

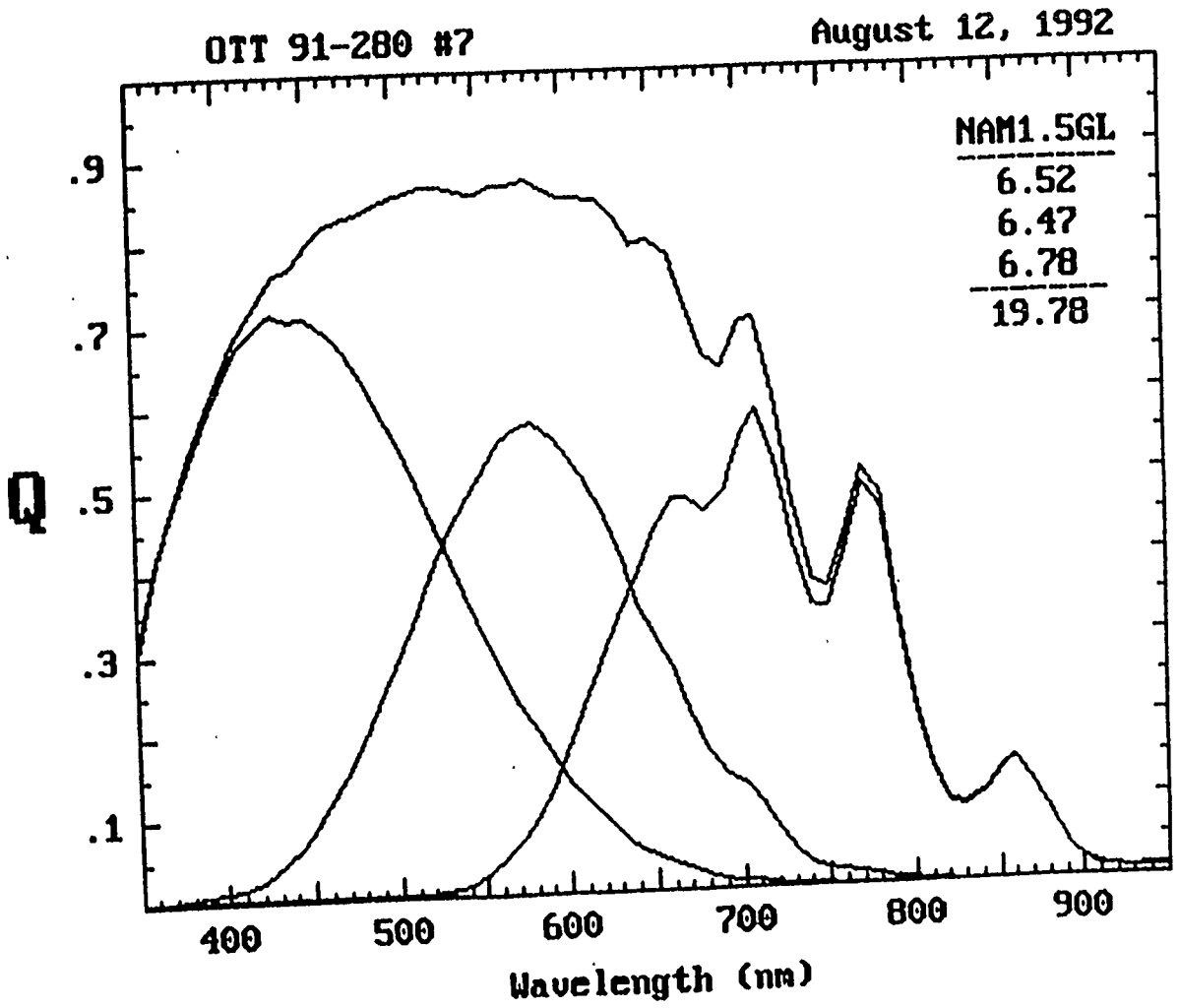

textured back-reflector

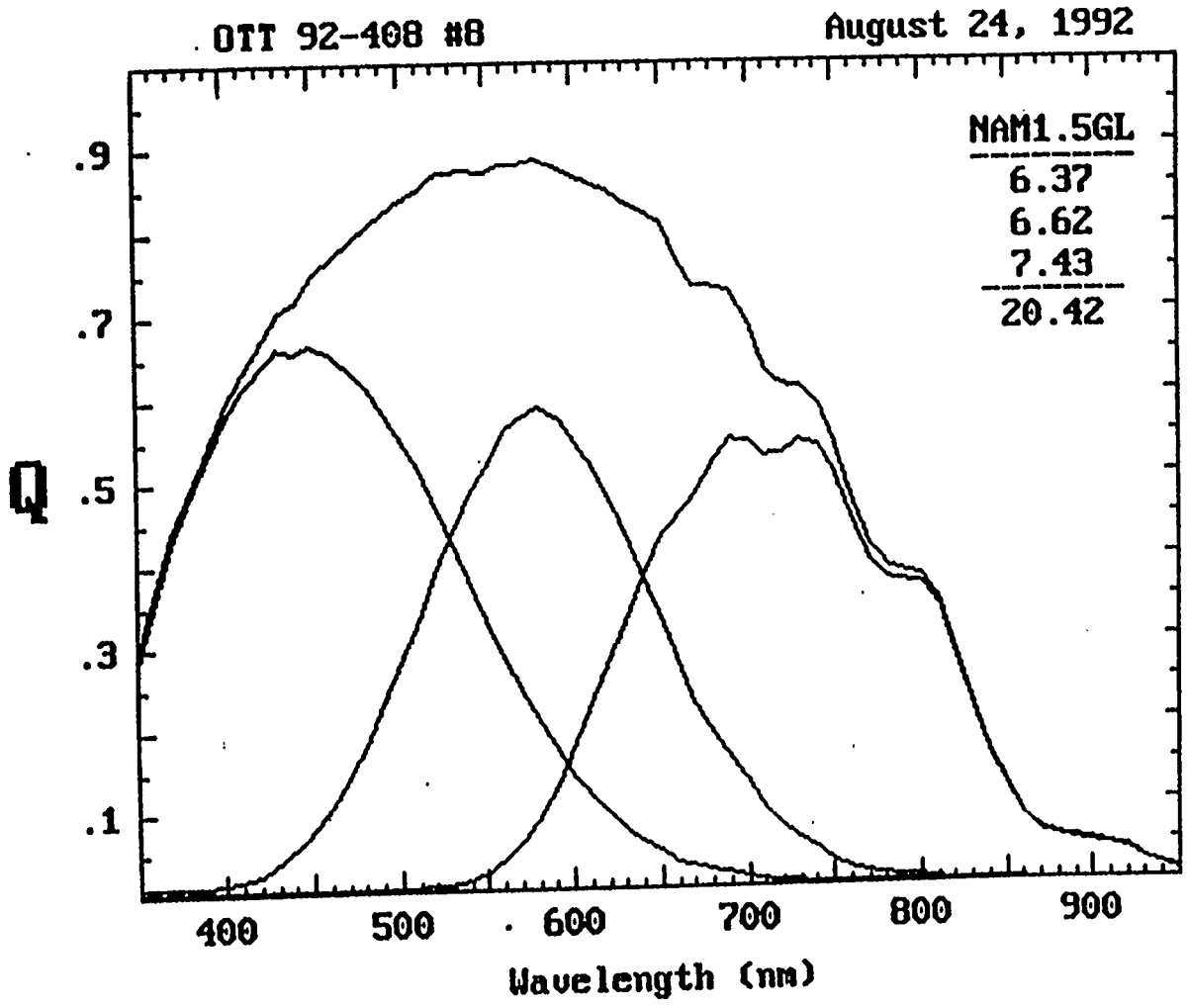

Figure 8. **Quantum efficiency curve of a triple-junction solar cell having more textured back-reflector**

Table 1: Calibration of PDS signal Perkin-Elmer 330 spectrophotometer.

hν(eV)	Photon energy	2.1	1.9	1.7	1.5	1.3	1.1
λ(nm)	Wavelength	590	653	729	827	954	1127
V_{pds}(mV)	Lock-in output	1.32	2.8	4.04	4.69	8.3	9.3
V_{tp}(mV)	Thermopile output	0.0271	0.0578	0.0832	0.101	0.192	0.266
V_{pds}/V_{tp}	Relative absorption	48.7	48.4	48.6	46.4	43.2	35.0
R_{pe}	Reflection from Perkin-Elmer	64.5%	65.5%	67.0%	69%	-----	-----
A_{pe}	$=1-R_{pe}$	35.5%	34.5%	33%	31%		
F	$A_{pe}/(V_{pds}/V_{tp})$	7.29×10^{-3}	7.13×10^{-3}	6.79×10^{-3}	6.68×10^{-3}		
F_{av}	average of F			7.0×10^{-3}			
c	calibration factor $A_{pds}/V_{pds}=F_{av}/V_{tp}$	0.259	0.121	0.084	0.069	0.0365	0.0263

Table 2: PDS measurement of optical loss of specular Ag (BR13) and reference back-reflector (OBR83).

Sample	Type		Wavelength (nm)					
			590	653	729	827	954	1127
BR13	Specular Ag on SS	V_{pds}(mV)	0.09	0.18	0.23	0.23	0.39	0.41
		Phase (degree)	55	61	61	59	61	59
		Reflection loss	2.3%	2.2%	1.9%	1.6%	1.4%	1.1%
OBR83	Textured Ag/ZnO	V_{pds}(mV)	0.57	1.00	1.03	1.02	1.57	1.5
	on SS	Phase (degree)	55	58	58	56	56	54
		Reflection loss	14.8%	12.1%	8.7%	7.0%	5.7%	3.9%

We routinely check the system reproducibility of the PDS setup by measuring the reference sample OBR83. The measurement on this sample has always been reproducible within a few percent. The absolute PDS signal calibration depends, to some extent, on the surface conditions of the sample to be measured. We are in the process of gaining further understanding and obtaining more reliable and accurate calibration.

PDS can be used to measure the light loss of different solar cell layers without complete cell structure. In Table 3, we list the PDS measurement of SS, SS/Ag, SS/Ag/ZnO, SS/Ag/ZnO/n^+.

Development of New Back-Reflector

After identifying the optical losses and the lack of ideal texture in our existing back-reflector, we directed our effort to developing a new back-reflector. The research was focused on obtaining: 1) higher reflectance, and 2) better texture for more enhanced light trapping.

Different back-reflector systems have been systematically explored. We developed a new back-reflector Ag (hot)/Ag (cold)/ ZnO system which demonstrated 0.2 mA/cm^2 - 0.4 mA/cm^2 improvement in short circuit current (J_{ph}) of solar cells grown on these back-reflectors over those on previous back-reflectors (OBR83). The improvement in J_{ph} is mainly due to improved texture.

Since the reflection loss was found to increase when texture increases for high temperature evaporated Ag (hot Ag), an additional Ag layer was deposited at lower temperature (cold Ag) to cover the hot Ag to enhance the reflectance and to preserve the texture. This Ag (hot)/Ag (cold) structure can be easily incorporated in our existing continuous roll-to-roll manufacturing line.

Table 4 (a), Table 4 (b) and Table 4 (c) show the deposition conditions, PDS spectrum, and angular dependence of reflectance, respectively, for a standard Ag/Ag back-reflector. The light loss measured from PDS is much smaller than that of just the hot Ag layer. The light loss at 1.5 eV photons is 5.7%, which is still higher than the cold Ag layer alone. It is likely that this 5.7% loss is due to the texture, since for a textured surface, the normal incident light is no longer normal to the surface microscopically, so the reflectance decreases.

Figure 9 shows the SEM photographs of a Ag/Ag sample (BR48). The first graph on the left-hand side was taken with normal electron beam incidence and at a relatively low magnification of 10,000x. The second graph on the right-hand side was taken at a 60° angle and a 40,000x magnification. The size of the grains is around 0.4 μm, which is believed to be appropriate for the red light scattering.

We prepared a series of solar cells on the Ag/Ag back-reflectors together with reference OBR83. In Table 5, we list the deposition conditions of four Ag/Ag samples and the QE data of the solar cell on these back-reflectors. The QE curve of these samples are shown in Figure 10. Comparing the QE curve of Ag/Ag back-reflector with those on OBR83, we see, on the average, 0.2 mA/cm^2 higher current density. The increase in the current is in two wavelength regions: in the red and in the blue. The increase in the red is mainly due to the improvement in the enhanced texture, as evidenced by the lack of interference fringes in the cells on Ag/Ag back-reflectors. The increase in the blue is probably due to the decrease in the reflection loss of the ITO coating when the surface is textured, since: 1) normal incident light enters the ITO at a non-normal incident angle microscopically; and 2) the ITO is effectively thinner. These result in a lower reflection loss at the front surface, thus enhancing the QE in the blue.

Table 3: Reflection loss of various layers measured by PDS.

Sample		Wavelength (nm)					
		590	653	727	827	954	1127
SS	V_{pds} Reflection loss	1.32 34.1%	2.8 33.9%	4.04 33.9%	4.67 32.3%	8.3 30.3%	9.3 24.4%
SS/Ag(specular) BR13	V_{pds} Reflection loss	0.09 2.3%	0.18 2.2%	0.23 1.9%	0.23 1.6%	0.39 1.4%	0.41 1.1%
SS/Ag(textured) BR66	V_{pds} Reflection loss	0.33 8.5%	0.607 7.3%	0.76 6.4%	0.83 5.7%	1.63 5.9%	2.00 5.3%
SS/Ag(specular)/ZnO SS/BR23/ZnO38	V_{pds} Reflection loss	0.17 8.5%	0.40 4.8%	0.517 4.3%	0.371 2.6%	0.67 2.4%	0.91 2.4%
SS/Ag(specular)/ZnO/thin n^+ SS/BR42/ZnO54/LL563	V_{pds} Reflection loss	1.25 32%	1.82 22%	1.84 15.4%	1.92 13.2%	3.22 11.8%	3.05 8.0%

Table 4. **Deposition conditions, PDS results and angular dependence of reflectance for standard Ag/Ag back-reflector (BR66).**

(a) deposition parameter (BR66)

Ag (bottom layer):	Ts	=	400°C
	Thickness	=	1000 Å
	Dep. Rate	=	1.3 Å/sec.
Ag (top layer)	Ts	=	RT
	Thickness	=	1500 Å
	Dep. Rate	=	15 Å/sec.

(b) PDS results (BR66)

	Wavelength (nm)					
	590	653	727	827	954	1127
V_{pds} (mV)	0.33	0.607	0.76	0.83	1.63	2.00
Loss (%)	8.5	7.3	6.4	5.7	5.9	5.3

(c) Angular dependence

Detector output:
Incident beam: 2.5 mA
Reflector beam: 0.366mA at $\theta = 0°$
1.17×10^{-3} mA at $\theta = 30°$
0.645×10^{-3} mA at $\theta = 60°$

Percentage of specular reflected light: 14..6%
Percentage of scattered reflected light: 80%

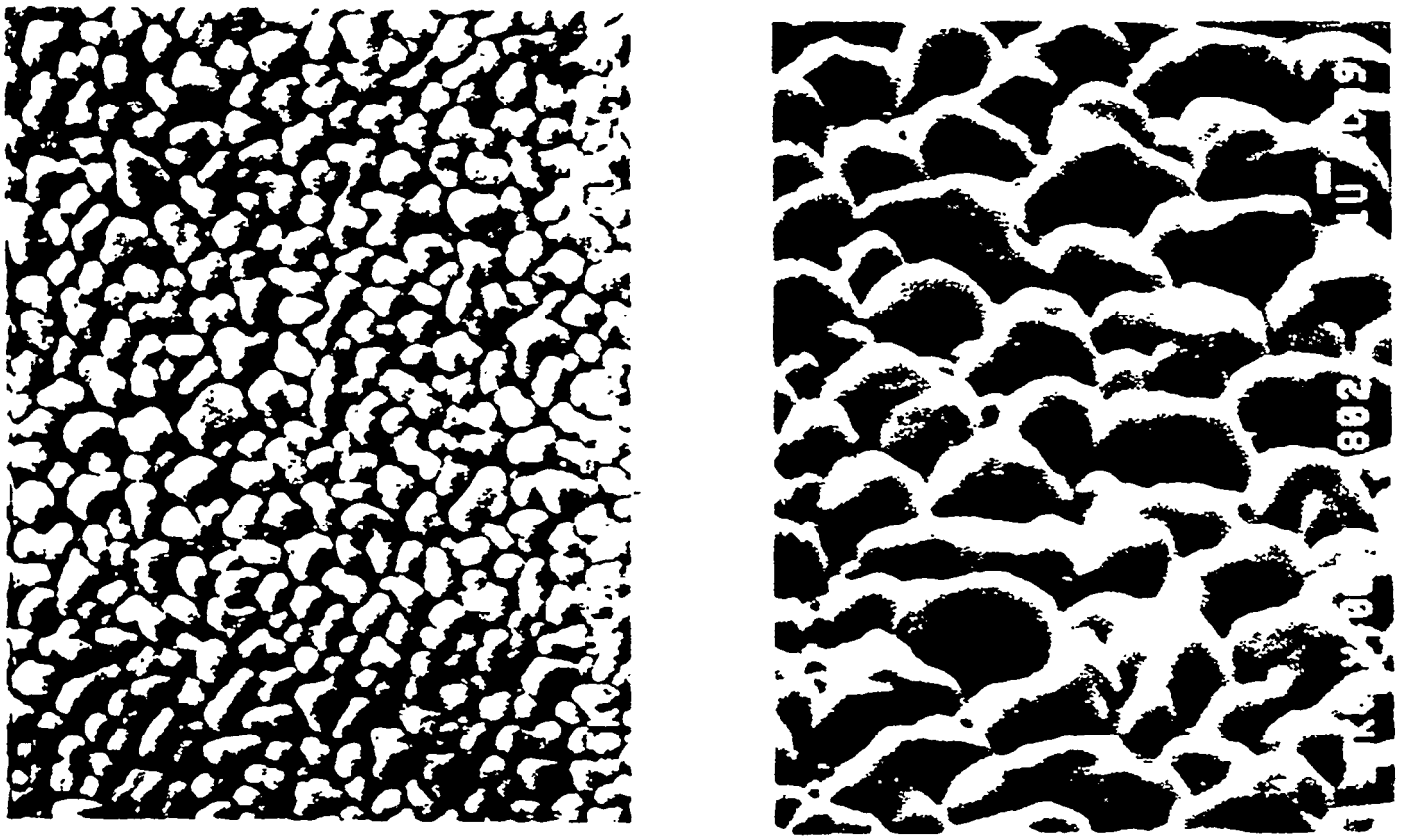

Figure 9 SEM photographs of a Ag/Ag back-reflector.

Table 5. **Deposition conditions of Ag/Ag back-reflector and the QE data of solar cells on these back-reflectors and on reference back-reflector.**

Sample #	Ag (bottom)			Ag (top)				QE of cells on Ag/Ag back-reflector				QE of cells on OBR 83			
	Ts (°C)	d (Å)	Rate Å/sec	Ts (°C)	d (Å)	Rate Å/sec	Solar cellrun#	Jph	Q400	Q590	Q700	Jph	Q400	Q590	Q700
BR34	350	1000	1.3	RT	1500	2.0	LL562	16.87	0.60	0.86	0.47	16.67	0.57	0.87	0.455
BR48	400	1000	0.5	RT	1500	15	LL565	16.69	0.65	0.85	0.42	16.49	0.64	0.86	0.34
BR49	350	1500	1.3	RT	1700	15	LL566	16.95	0.64	0.856	0.47	16.64	0.59	0.87	0.39
BR50	450	1000	0.5	RT	1500	15	LL567	17.00	0.63	0.87	0.47	16.77	0.60	0.88	0.41

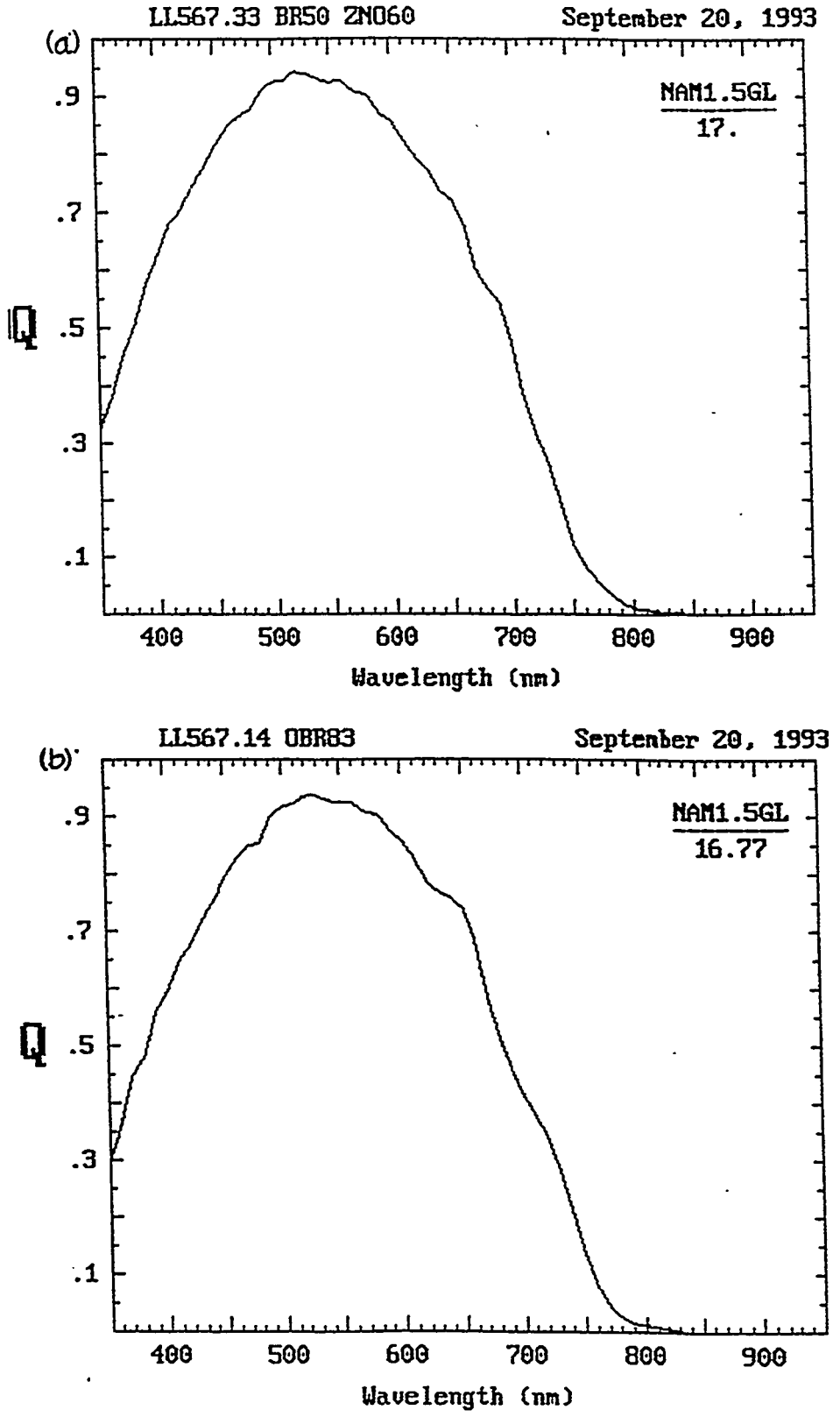

Figure 10. QE curves of solar cells on Ag/Ag back-reflectors (a) and on OBR83 (b).

Figure 11 shows a QE curve with QE=73% at 400 nm for an a-Si n-i-p solar cell. This high blue QE is mainly due to the enhancement from texturing.

Figure 12 shows the QE of an n-i-p cell with the same i layer thickness as other n-i-p samples. The J_{ph} of this sample is 17.2 mA/cm^2 while similar n-i-p cells deposited on previous back-reflector shows J_{ph} of 16.8 - 17.0 mA/cm^2. The lack of interference fringes and the enhancement in the red response indicate good light trapping from this texture.

Back-Reflector Optimization of New Pilot Machine

The sputtering chamber in the pilot deposition machine is equipped with four DC magnetron sputtering targets. An upward sputtering configuration is used so that particulates do not accumulate on the web surface. Typically, we install one Ag target, two ZnO targets for the Ag/ZnO back-reflector deposition and one ITO target for the deposition of the top conductive layer. We can also install two metal targets for the deposition of multiple metal layer back-reflectors and install an ITO target only when the machine is needed for ITO deposition.

A diffusion pump is installed in the sputter chamber to maintain an Ar background pressure of around 2 mTorr during sputtering.

The gas gates on both sides of the sputter chamber are designed such that the sputter chamber is well isolated from the gaseous environment existing in RF plasma CVD chambers, pressure gradation is properly maintained and the low deposition pressure can be maintained with the existing pumping system.

In order to improve the transmission of the ZnO layer, we incorporated a small amount of O_2 into the sputtering gas. Experimental results revealed that the extra O_2 in the sputtering gas was indeed effective in improving the transmission of the ZnO layer, and hence the light enhancement from this back-reflector. Even though the added O_2 in the sputter gas reduced the conductivity of ZnO by reducing the oxygen deficiency, the contribution to series resistance from the ZnO layer remained orders of magnitude lower than that from the rest of the solar cells.

Figure 13 (a) and 13 (b) are SEM pictures of the Ag/ZnO back-reflector after optimization, taken at different incidence angles, showing a high degree of texture. Figure 14 shows the quantum efficiency curves of a triple-junction solar cell deposited on the improved back-reflector. The response in the red is high, indicating a good back-reflector performance.

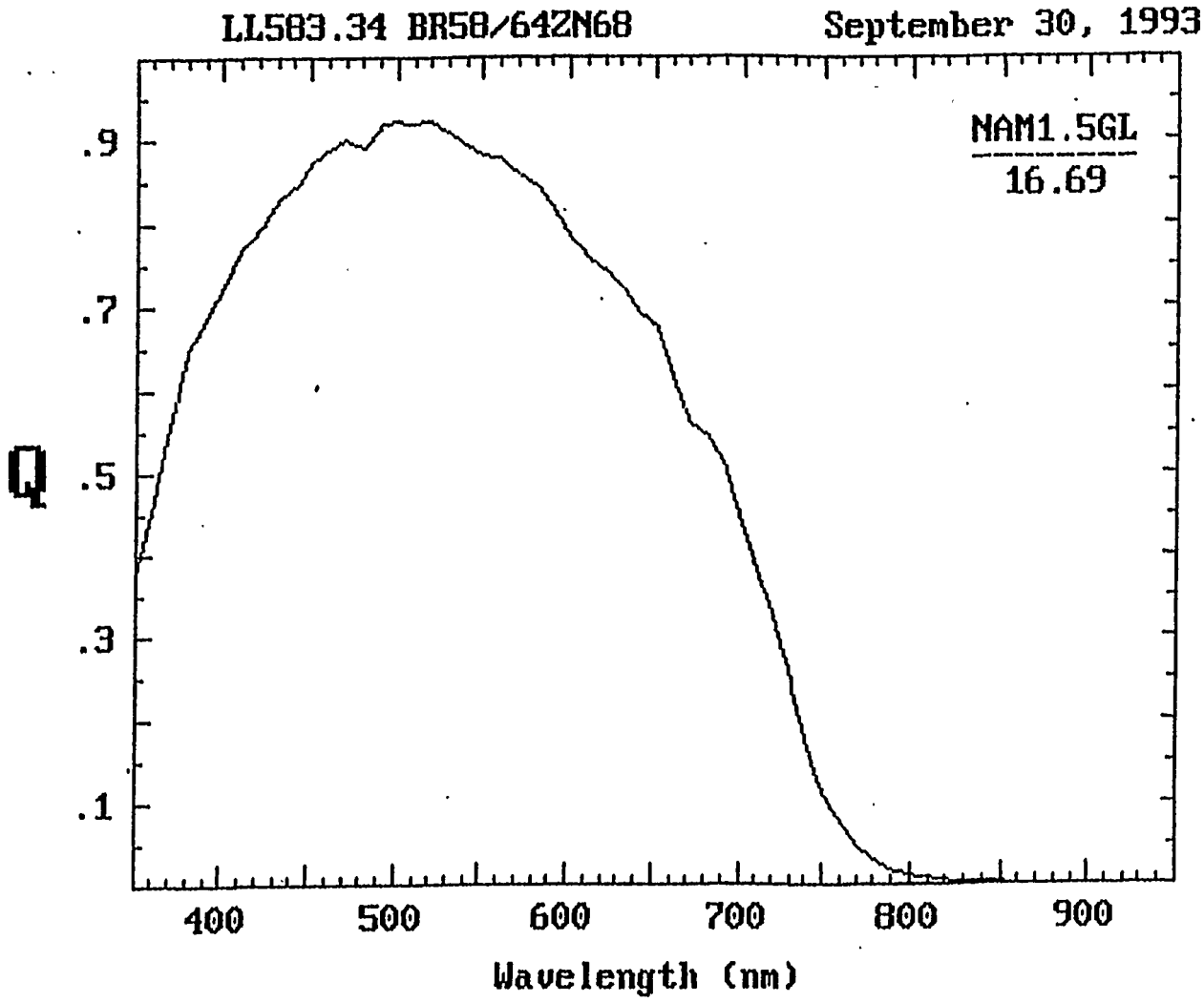

Figure 11. QE curve of a solar cell on textured Ag/Ag back-reflector showing QE=73% at 400nm.

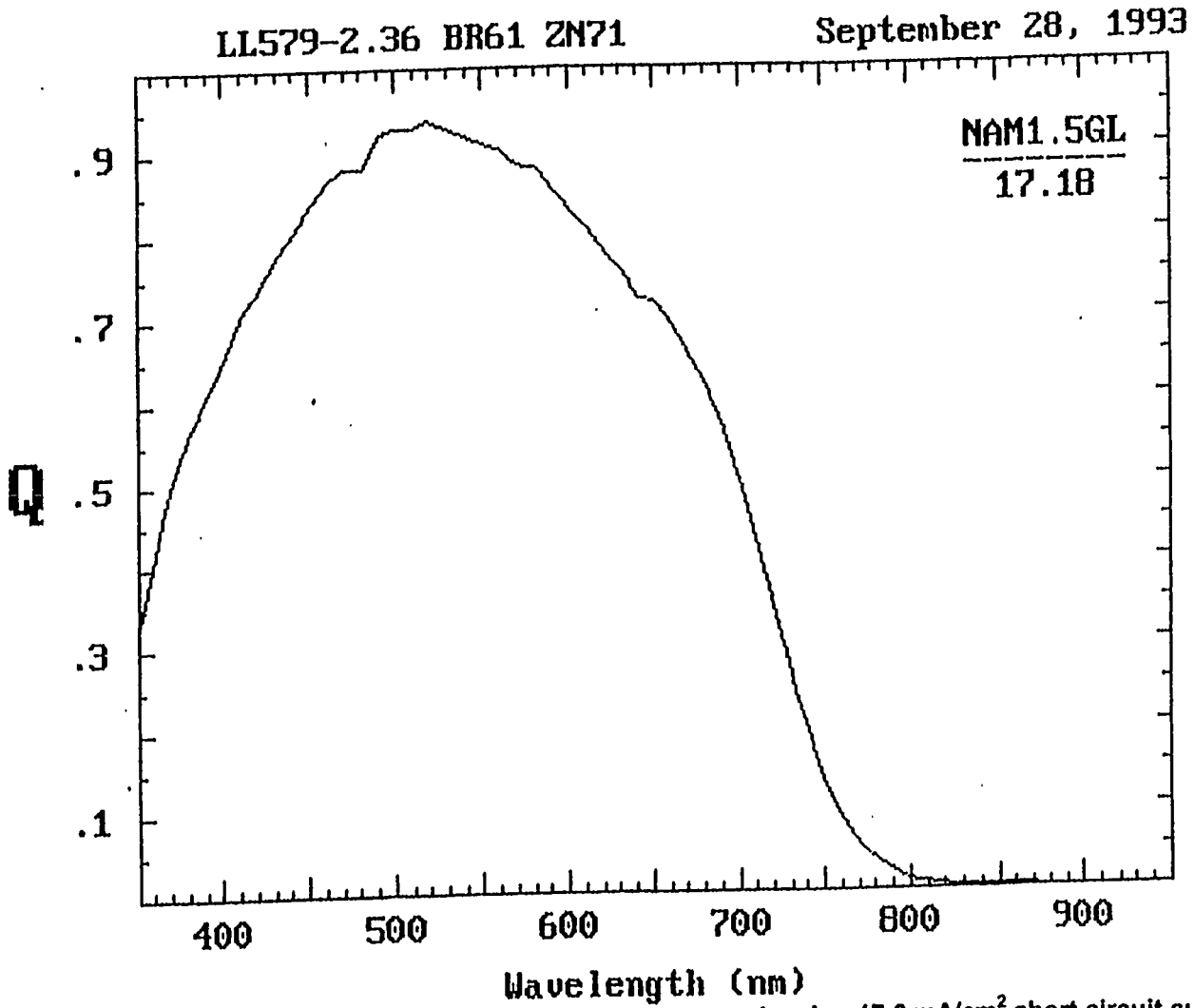

Figure 12. QE curve of an n-i-p solar cell on Ag/Ag back-reflector showing 17.2 mA/cm^2 short circuit current.

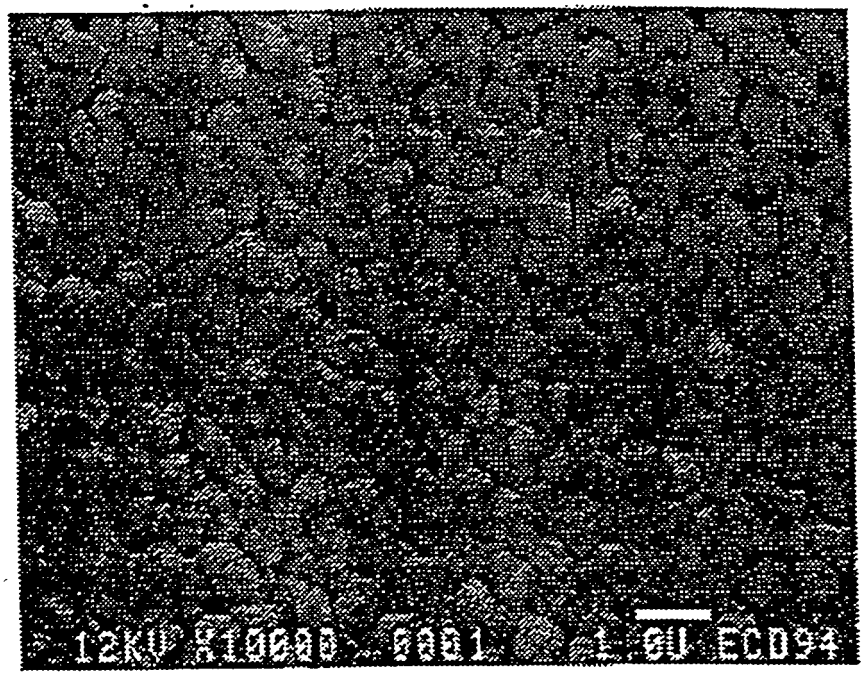

Figure 13a. SEM photo of Ag/ZnO back-reflector at normal electron incidence.

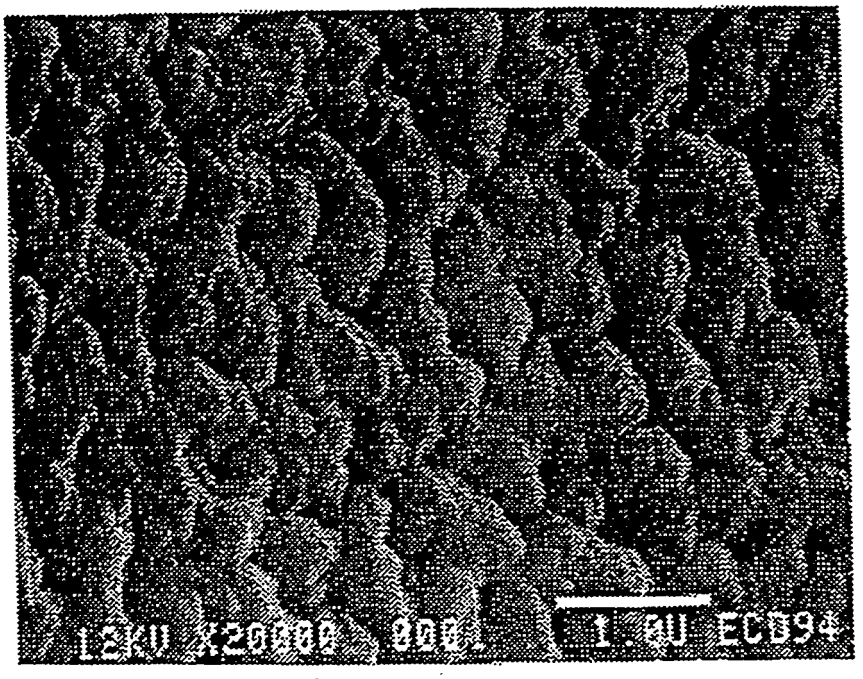

Figure 13b. SEM photo of Ag/ZnO back-reflector at 60° incidence angle.

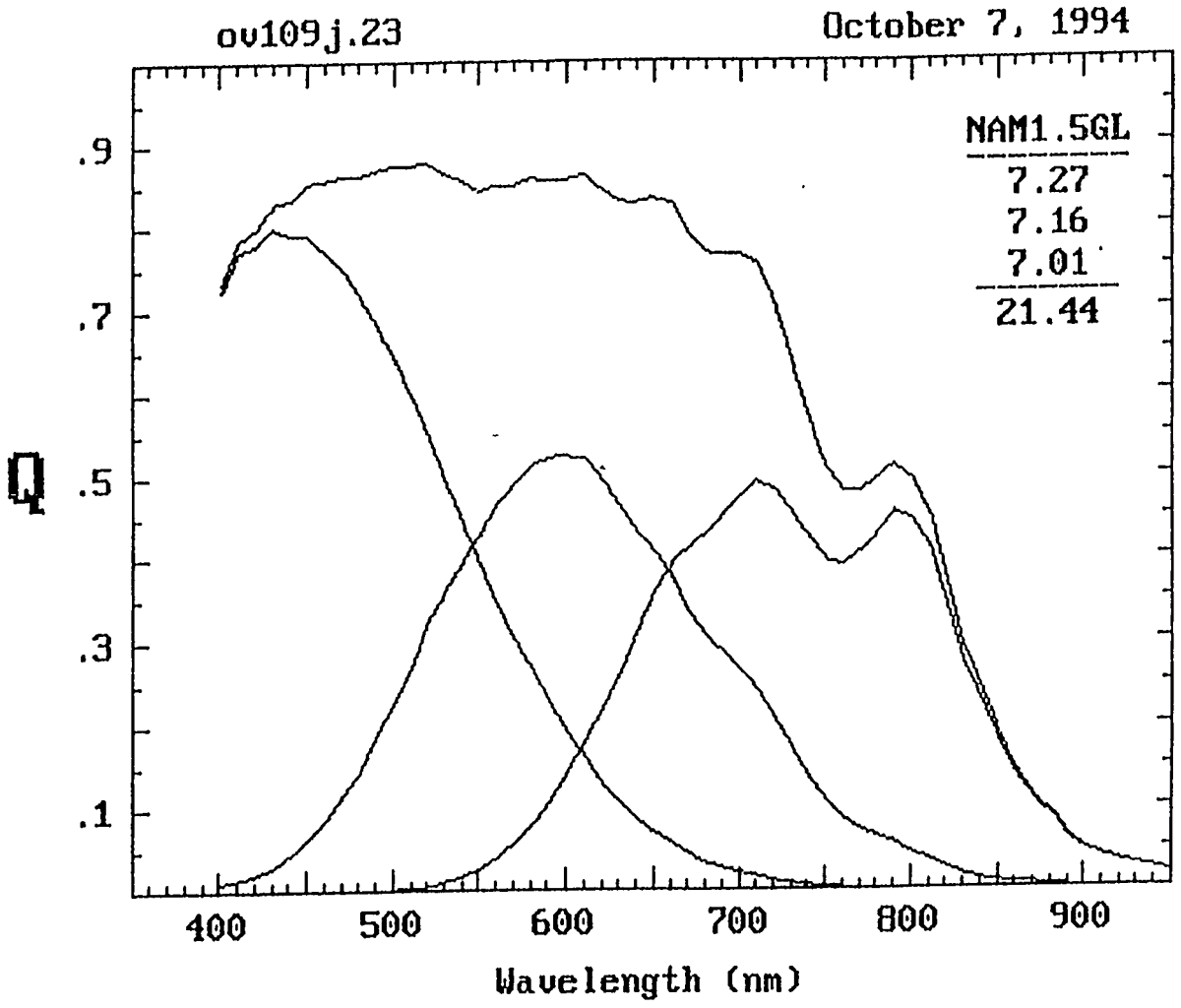

Figure 14. Quantum efficiency curves of a triple-junction solar cell.

Task II: Optimization of the Si-Ge Narrow Bandgap Solar Cell

ECD's roll-to-roll a-Si alloy deposition machine, shown in Figure 5, produces a triple-junction two bandgap solar cell structure with a-SiGe as the bottom cell intrinsic layer. This is the first time that a narrow bandgap cell has been incorporated into a continuous roll-to-roll production process. We have used this machine to optimize the a-SiGe narrow bandgap solar cell. The bottom cell section of the roll-to-roll process machine consists of three RF glow discharge CVD deposition chambers: an n1 chamber for the n^+ a-Si layer; an i1 chamber for the a-SiGe layer; and a p1 chamber for the p^+ microcrystalline Si layer.
Bandgap profiling is an important tool for achieving higher efficiency as has been shown in earlier investigations at ECD[14]. In order to incorporate bandgap profiling capability in the continuous roll-to-roll machine, a proprietary gas distribution manifold and cathode configuration was designed and incorporated in the roll-to-roll machine.

This gas distribution manifold delivers gas mixtures containing different amounts of GeH_4 into different parts of the i1 chamber. The bandgap profiling is designed such that relatively higher Ge content is on the side of i layer closer to the p^+ layer. With such a profiled bandgap, more light is absorbed near the p^+ junction to minimize the distance holes must travel to be collected. Also, the graded bandgap profiling induces an internal field to aid holes traveling toward the p^+. a-SiGe narrow bandgap cell with such a profiled bandgap shows much better fill factor. Figure 15 shows the Ge concentration of films deposited at different parts of the i1 chamber, which corresponds to different depths in the i1 layer thickness. The left hand side is close to the p+ layer. The calculated curve is obtained by estimating the Ge composition from the delivered gas mixture. The measured Ge composition was obtained from Auger sputtering depth profile. The calculated curve closely matches the measured curve, as is shown in Figure 15. This result demonstrates that our machine design for incorporating the bandgap profile is effective.

The a-Si interface layer between i1 and p1 has also been optimized. A proprietary interface layer enhanced the V_{oc} and fill factor.

The performance of the a-SiGe bottom-cell depends on the Ge content, the bandgap profile and the i layer thickness. We investigated such relations systematically using a-SiGe single cell structure deposited in our roll-to-roll machine. We deposited a set of such cells with the same Ge content in the i layer but with different degrees of profiling. The fill factor of the cell increased as the profile became steeper. Especially important is the increase in the fill factor measured under red light, which is the light that a-SiGe cell sees as the bottom cell of a triple cell. When we further increased the degree of profiling, a loss in V_{oc} became significant. We also studied the dependence of the bottom cell on the Ge content with a fixed profile. We varied the bandgap from 1.4eV to 1.6 eV. When the Ge content was increased, J_{sc} increased due to the smaller bandgap. However, the losses in V_{oc} and fill-factor became significantly large at a high Ge content. The loss in fill-factor is due to the increased defect density in the a-SiGe alloy at a high Ge content.

We have studied the dependence of cell performance on the Ge content, bandgap profiling, and thickness inside a triple-junction solar cell structure. In Figures 16 and 17, we show the J-V characteristics of two triple-junction cells with identical structures except that the bottom cell i layers have different Ge content, bandgap profiling, and thickness. Sample 1, having a bottom cell i layer containing more Ge and with a steeper profile, shows a higher fill factor due to higher current density from the bottom component cell under AM1.5 illumination, which resulted in a higher current mismatch. Sample 2, having a bottom cell i layer containing less Ge, with less profile and being thicker, shows higher Voc . The efficiencies of these two cells are the same, indicating that there is a trade-off between J_{sc} and Voc. In Figure 18 and Figure 19, we show the quantum efficiency curves of Sample 1 and Sample 2. Although the bottom cell of Sample 1

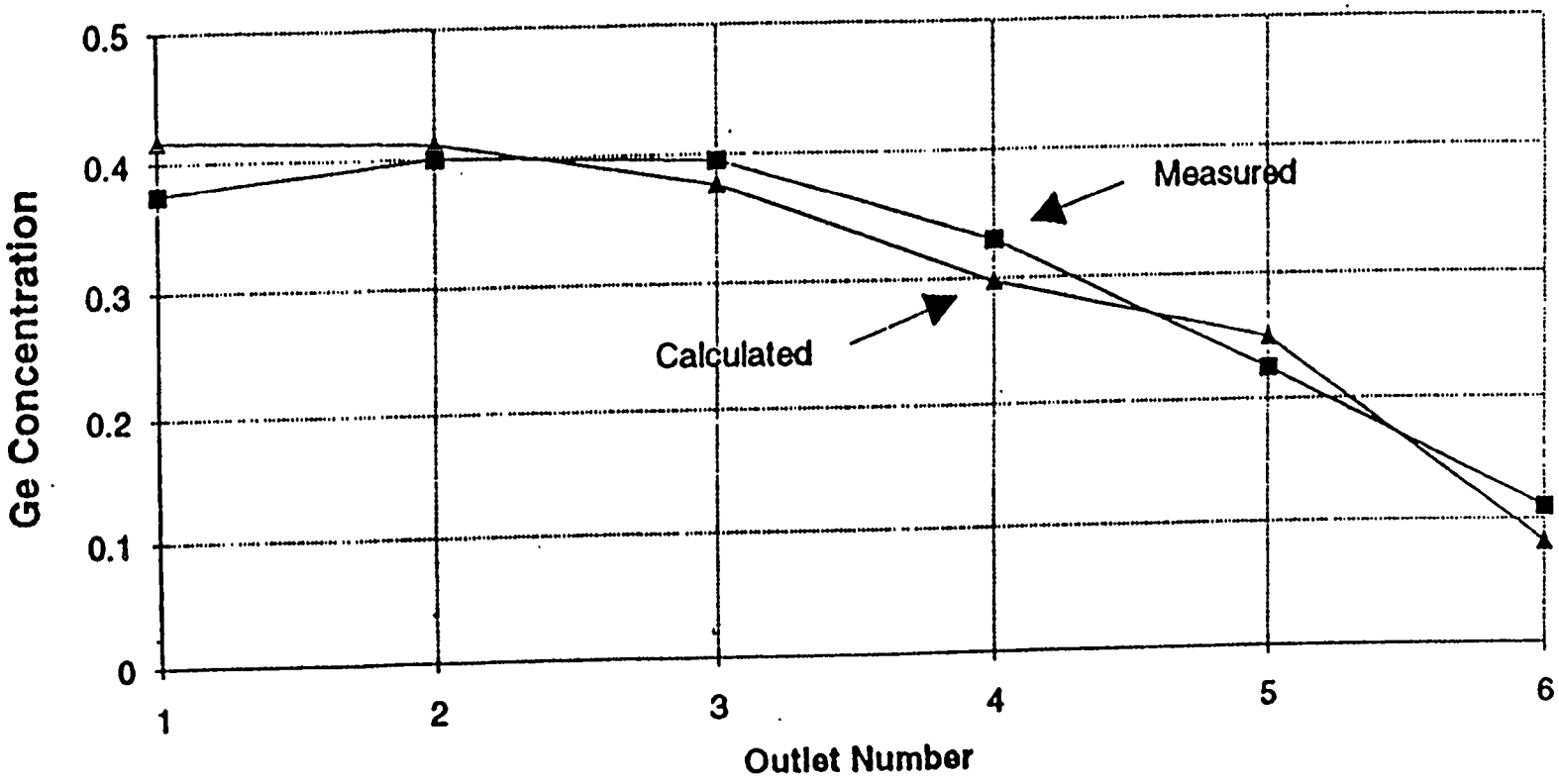
0.5
0.4
0.3
0.2
0.1
0
Ge Concentration
Measured
Calculated
1
2
3
4
5
6
Outlet Number

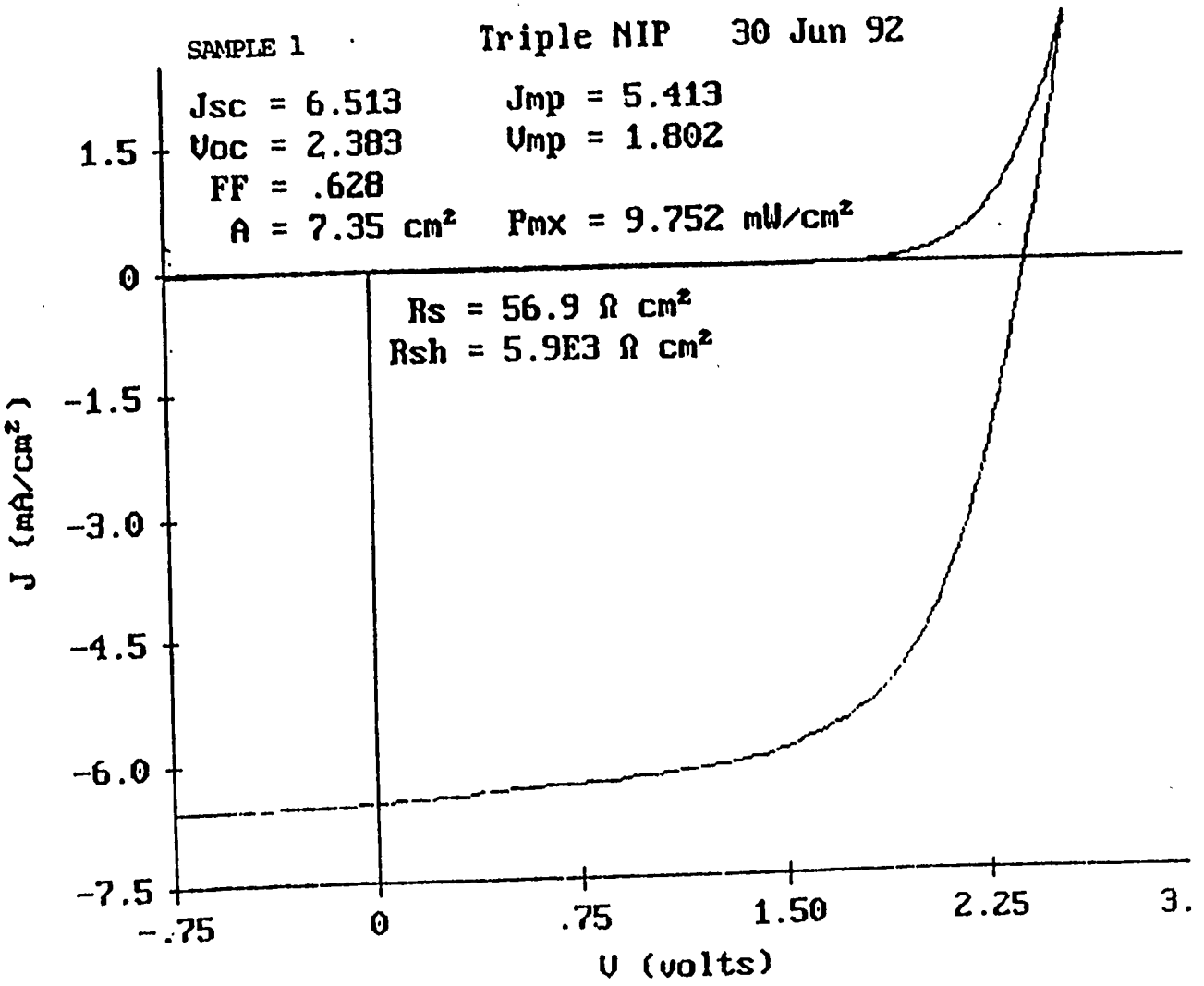
SAMPLE 1
Triple NIP 30 Jun 92
Jsc = 6.513
Voc = 2.383
FF = .628
A = 7.35 cm²
Jmp = 5.413
Vmp = 1.802
Pmx = 9.752 mW/cm²
Rs = 56.9 Ω cm²
Rsh = 5.9E3 Ω cm²
J (mA/cm²)
1.5
0
-1.5
-3.0
-4.5
-6.0
-7.5
-.75
0
.75
1.50
2.25
3.
V (volts)

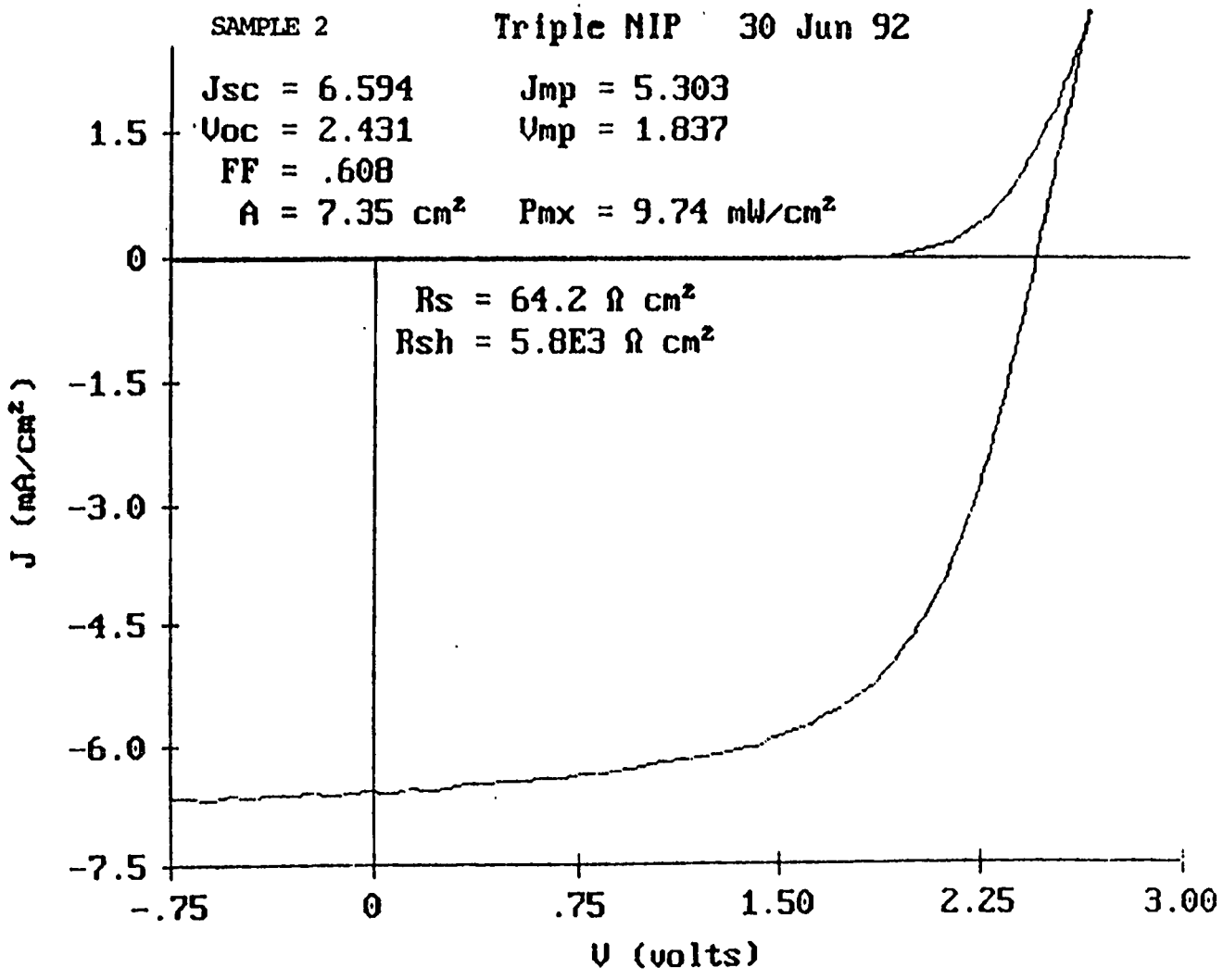
SAMPLE 2
Triple NIP 30 Jun 92
Jsc = 6.594
Voc = 2.431
FF = .608
A = 7.35 cm²
Jmp = 5.303
Vmp = 1.837
Pmx = 9.74 mW/cm²
Rs = 64.2 Ω cm²
Rsh = 5.8E3 Ω cm²
J (mA/cm²)
1.5
0
-1.5
-3.0
-4.5
-6.0
-7.5
-.75
0
.75
1.50
2.25
3.00
V (volts)

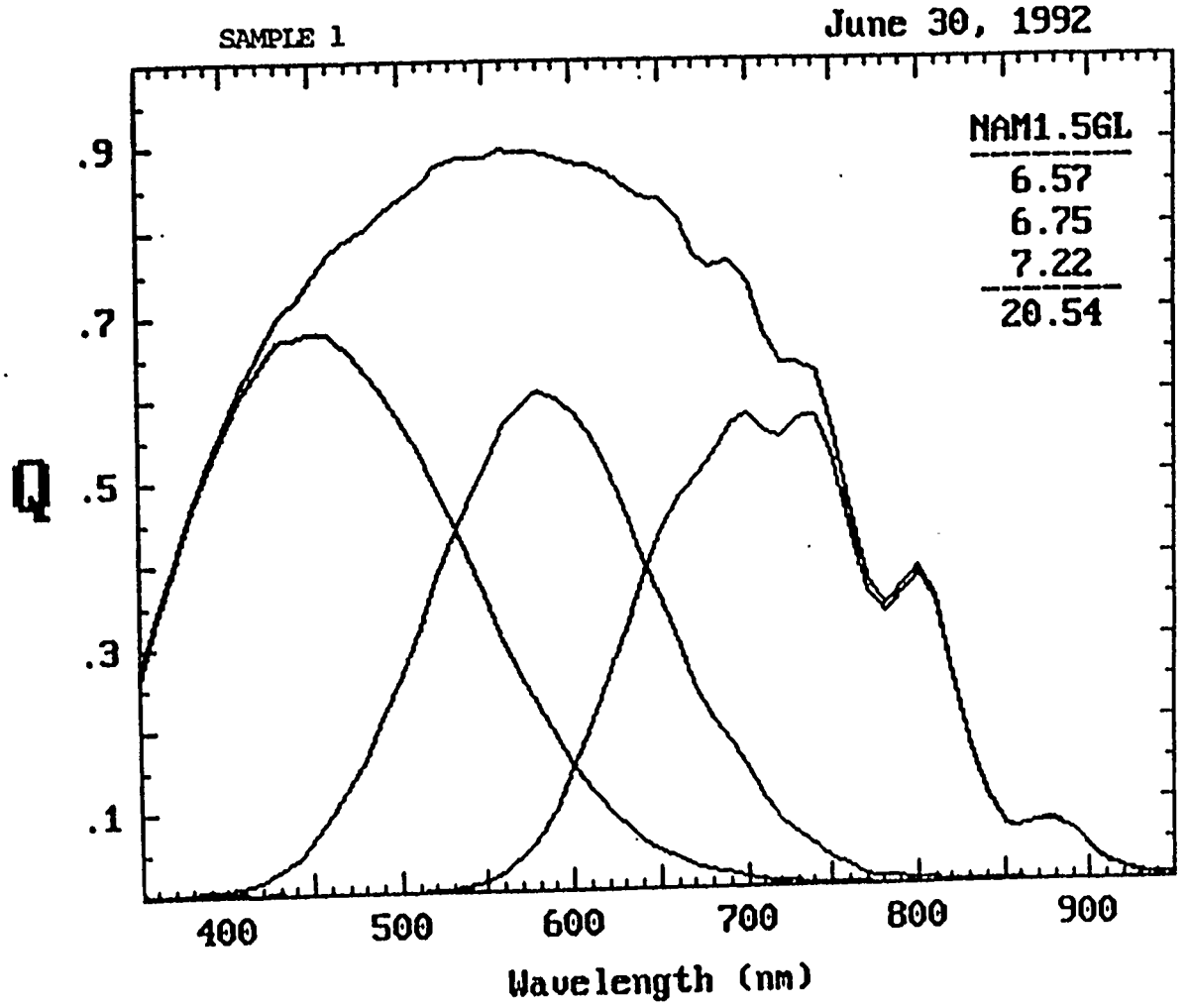

Figure 18. **Quantum efficiency curve of sample 1 triple-cell**

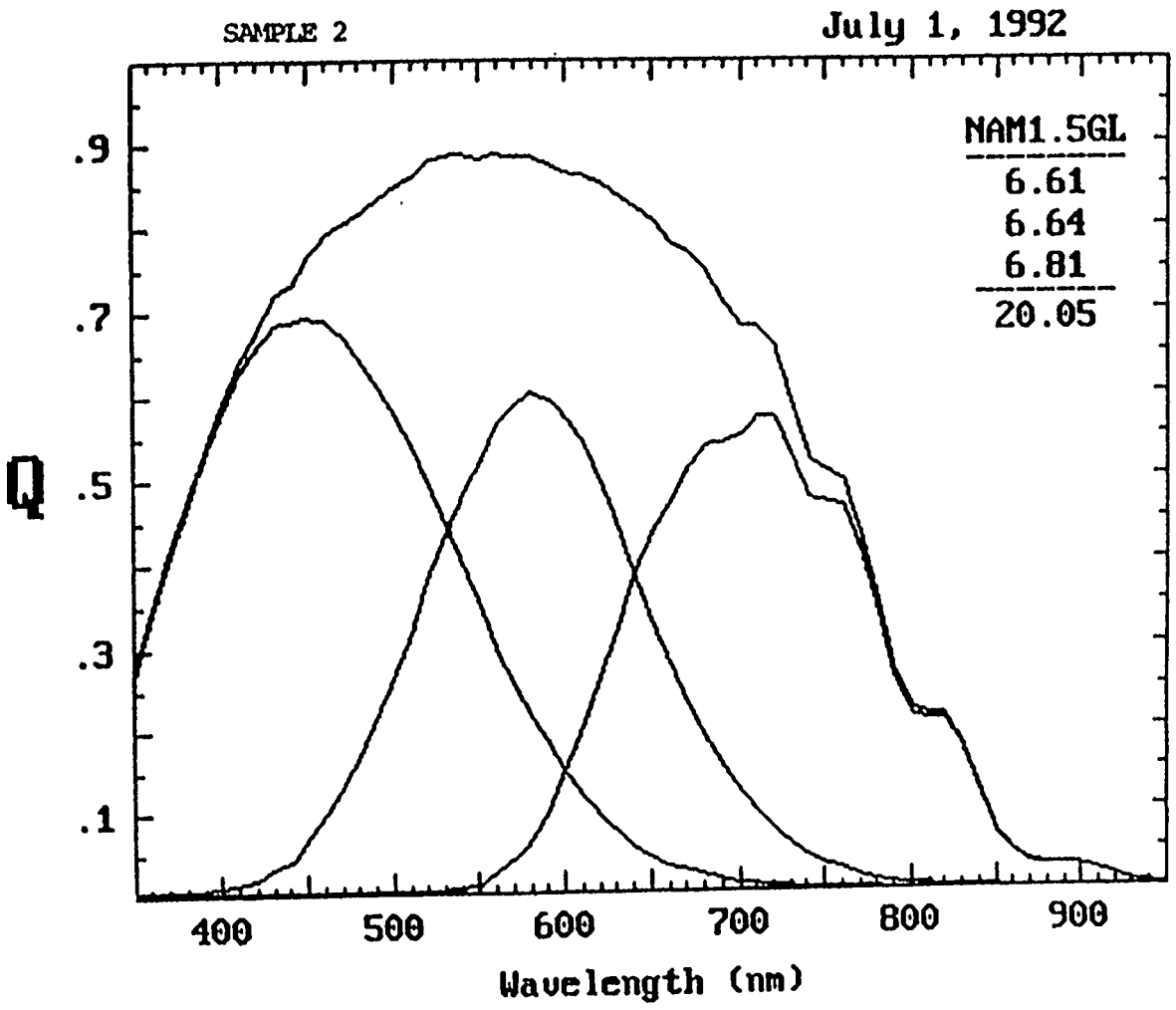
SAMPLE 2
July 1, 1992
NAM1.5GL
6.61
6.64
6.81
20.05
Q
.9
.7
.5
.3
.1
400
500
600
700
800
900
Wavelength (nm)

contributes relatively less V_{oc} compared to that of Sample 2, it absorbs more light in the red and also has a better fill factor, hence it increases the overall fill factor of the triple cell.

We optimized the Ge content, degree of bandgap profiling, and the thickness of the bottom cell i layer, based on the response of the cell under red illumination. Figure 20 shows the J-V characteristics of a typical single-junction a-SiGe cell deposited on Ag/ZnO back-reflector. Figure 21 shows the J-V curves measured under filtered blue and red light. The red fill factor of this Si-Ge cell was 59%, as is seen in Figure 21. Figure 22 shows the quantum efficiency curve of this same cell. The relatively high red fill factor and high response to the red suggest that this narrow bandgap bottom cell was well suited for use as the bottom cell of triple-junction two bandgap solar cell.

As will be shown in Table 7 in the next section, Task III, we have demonstrated the production of high quality a-SiGe solar cells on 2500 ft. production rolls in a highly uniform and consistent manner in our continuous roll-to-roll amorphous silicon alloy deposition machine.

We designed and constructed, at ECD's expense, the multi-purpose continuous roll-to-roll deposition machine which is capable of producing triple-junction multiple bandgap solar cells. Machine design efforts have focused on improvements that will result in further increases in stable module efficiency.

The i deposition chamber was designed to deposit a-SiGe with a profiled bandgap. We have deposited a-SiGe solar cells with bandgap profiling, as shown in Figure 23(a), and without bandgap profiling, as shown in Figure 23(b). Except for the profiling in bandgap, these two samples were deposited under similar conditions. The V_{oc} is increased from 0.46V to 0.62V, J_{sc} increased from 11.0 to 12.3 mA/cm^2 and FF increased from 0.54 to 0.62 after the bandgap profiling is implemented.

A 10.2% stable efficiency has been recently achieved[17] for a 1 ft.^{2} a-Si alloy solar panel by United Solar Systems Corp., a joint venture company between ECD and Canon. This high efficiency module was produced using a-Si/a-SiGe/a-SiGe triple-junction, triple bandgap structure. The middle cell was prepared with middle bandgap (≈1.6eV) a-SiGe alloy to improve the solar cell stability.[24] When a-SiGe was used as a middle cell, the i layer thickness of the middle cell can be reduced to approximately 2000Å. Thus, the stability of the triple-junction cell will be improved.

To incorporate this triple-junction, three bandgap solar cell design into ECD's continuous roll-to-roll deposition line, we have deposited and studied the a-SiGe alloy solar cells to be used as the bottom and middle cells of the triple bandgap a-Si alloy solar cells.

Figure 24(a) is the J-V curve of a narrow bandgap a-SiGe alloy solar cell, deposited on bare stainless steel, and used as the bottom cell. Figure 24(b) is the J-V curves of this solar cell with weak blue and red illumination. The V_{oc} is 0.6 V and the red FF is 0.64. When a similar cell is deposited on a high performance back-reflector, J_{sc} of around 21 mA/cm^2 is expected.

Figure 25(a) is the J-V curve of a middle bandgap a-SiGe alloy solar cell, deposited on bare stainless steel which is to be used as the middle cell. Since the bandgap is smaller than that of a-Si, the middle cell i layer can be made much thinner, yet maintain the proper current matching. Consequently, the triple-junction cell will have higher stable efficiency. Figure 25(b) is the J-V curves of this middle bandgap a-SiGe solar cell under blue and red illumination. The FF under white and colored lights are high.

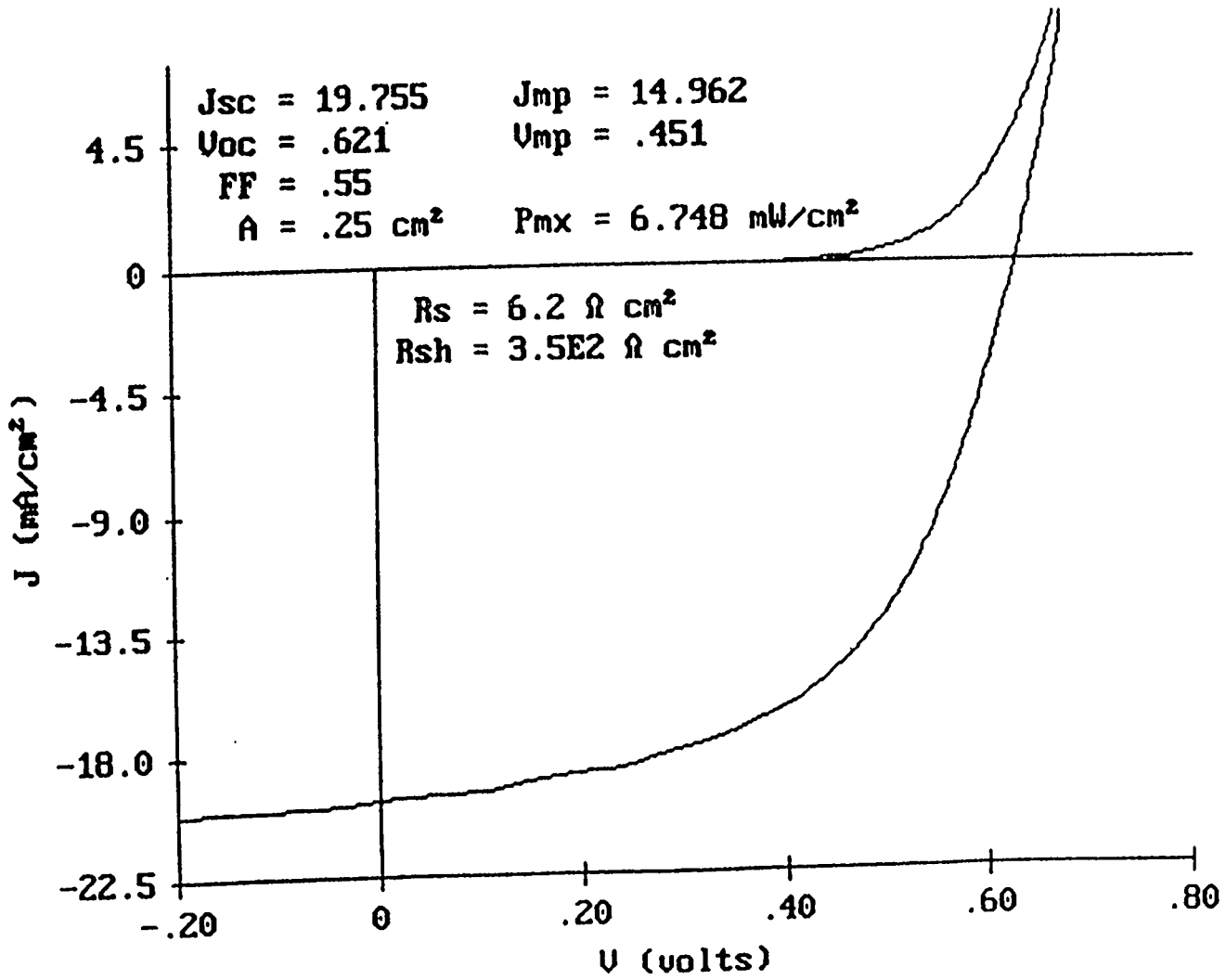
Jsc = 19.755
Voc = .621
FF = .55
A = .25 cm²
Jmp = 14.962
Vmp = .451
Pmx = 6.748 mW/cm²
Rs = 6.2 Ω cm²
Rsh = 3.5E2 Ω cm²
4.5
0
-4.5
-9.0
-13.5
-18.0
-22.5
J (mA/cm²)
-.20
0
.20
.40
.60
.80
V (volts)

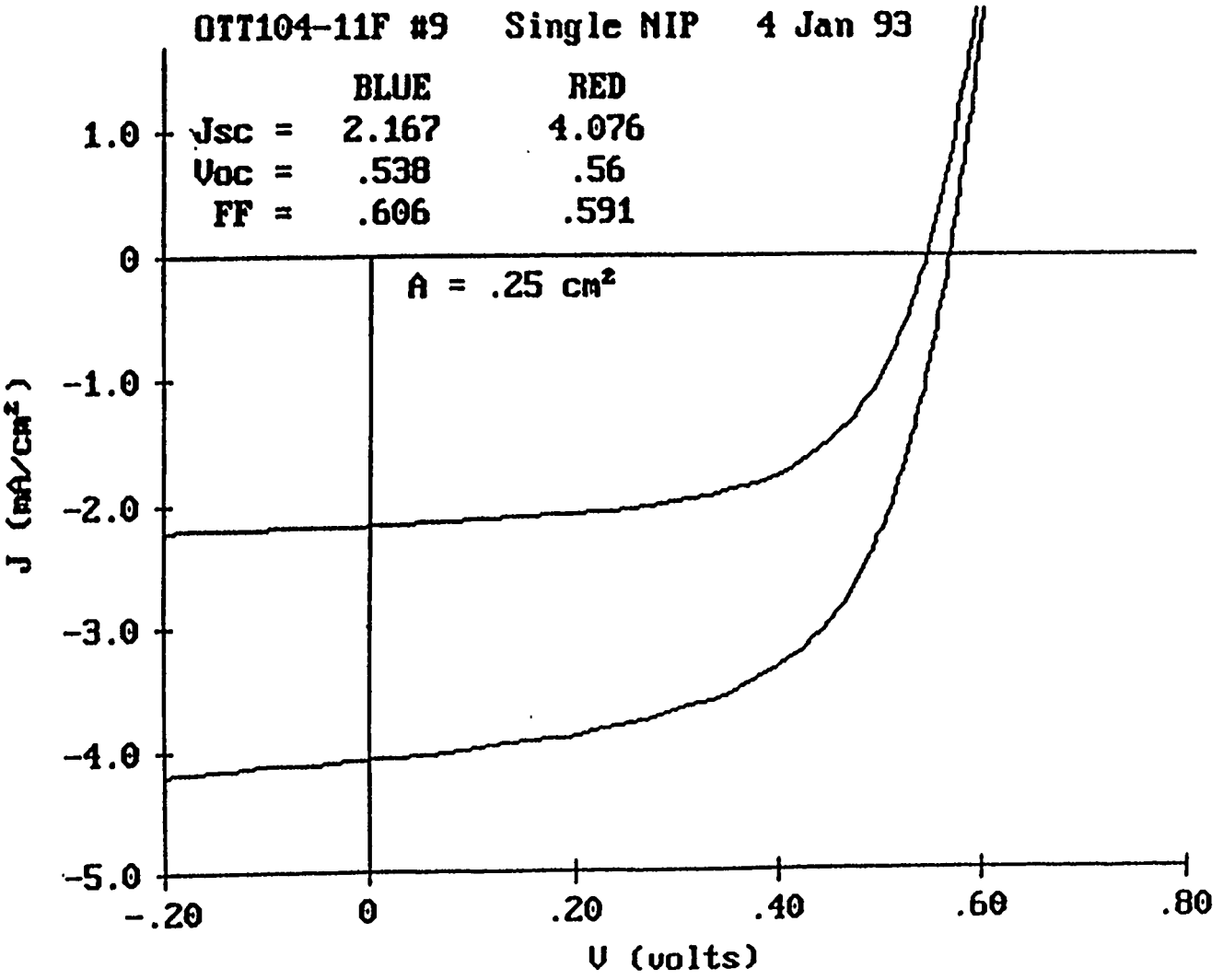
OTT104-11F #9 Single NIP 4 Jan 93
BLUE RED
Jsc = 2.167 4.076
Voc = .538 .56
FF = .606 .591
A = .25 cm²
1.0
0
-1.0
-2.0
-3.0
-4.0
-5.0
J (mA/cm²)
-.20
0
.20
.40
.60
.80
V (volts)

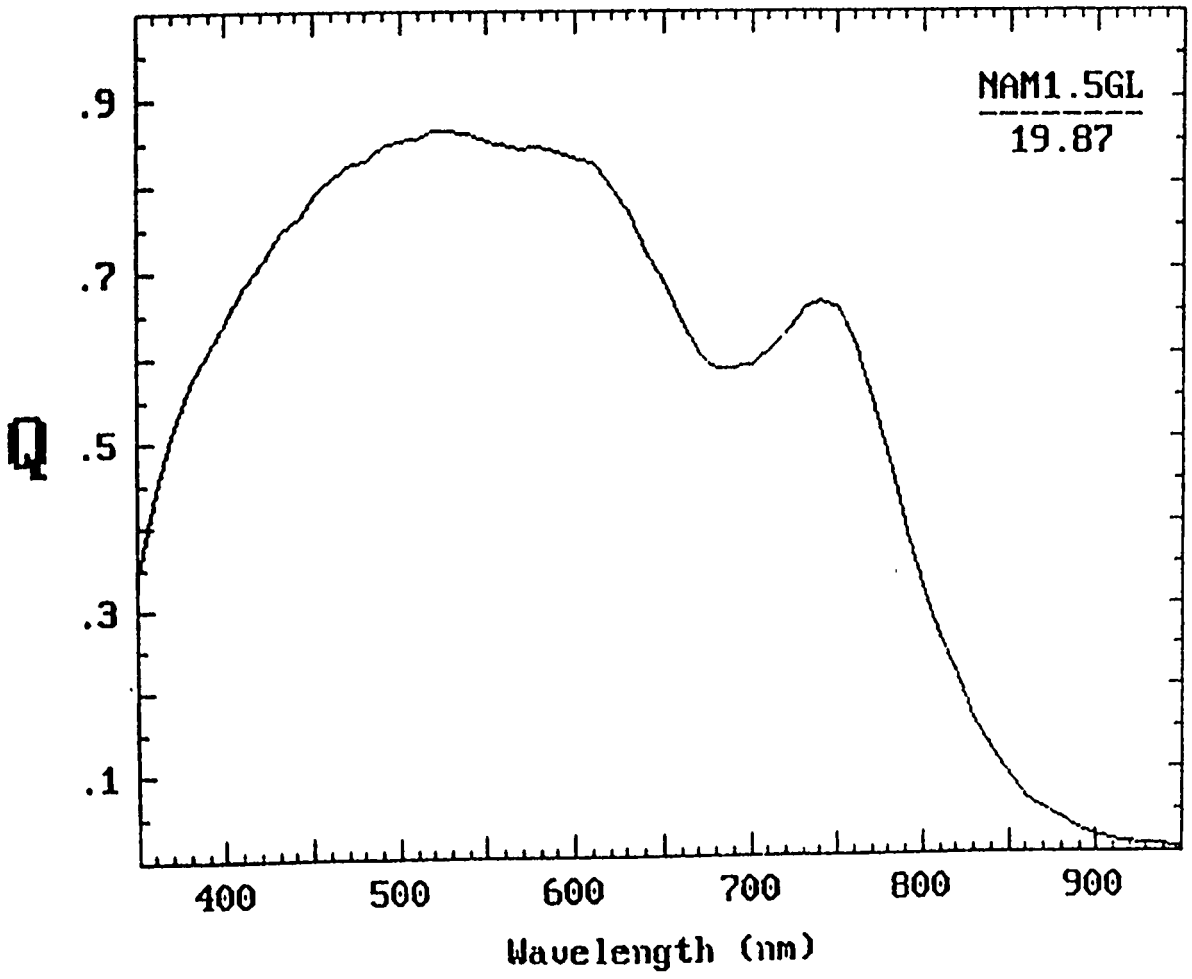
NAM1.5GL
19.87
Q
.9
.7
.5
.3
.1
400
500
600
700
800
900
Wavelength (nm)

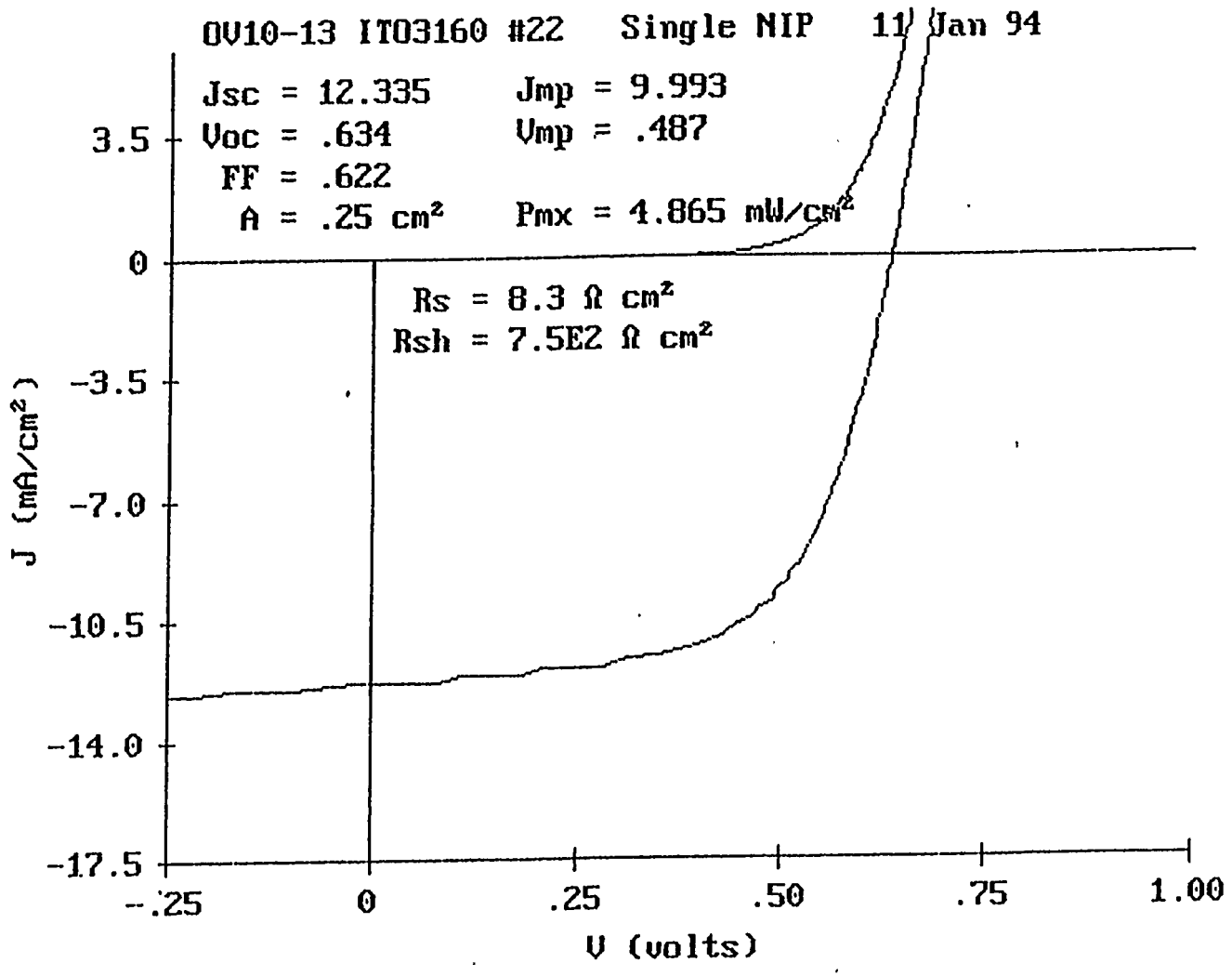

Figure 23a. **J-V curve of a band-gap profiled a-SiGe solar cell deposited on bare stainless steel.**

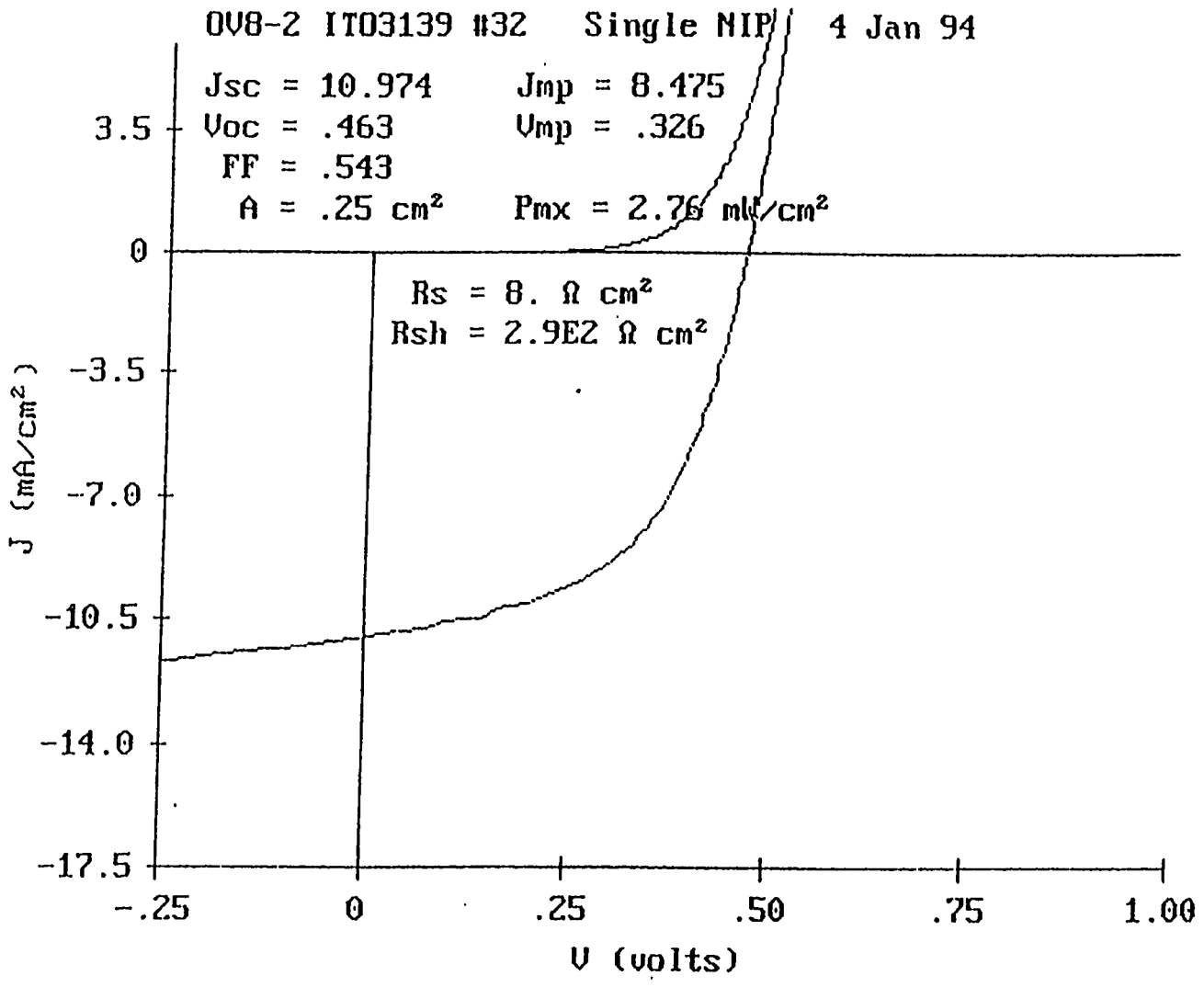

Figure 23b **J-V curve of an a-SiGe solar cell without bandgap profiling.**

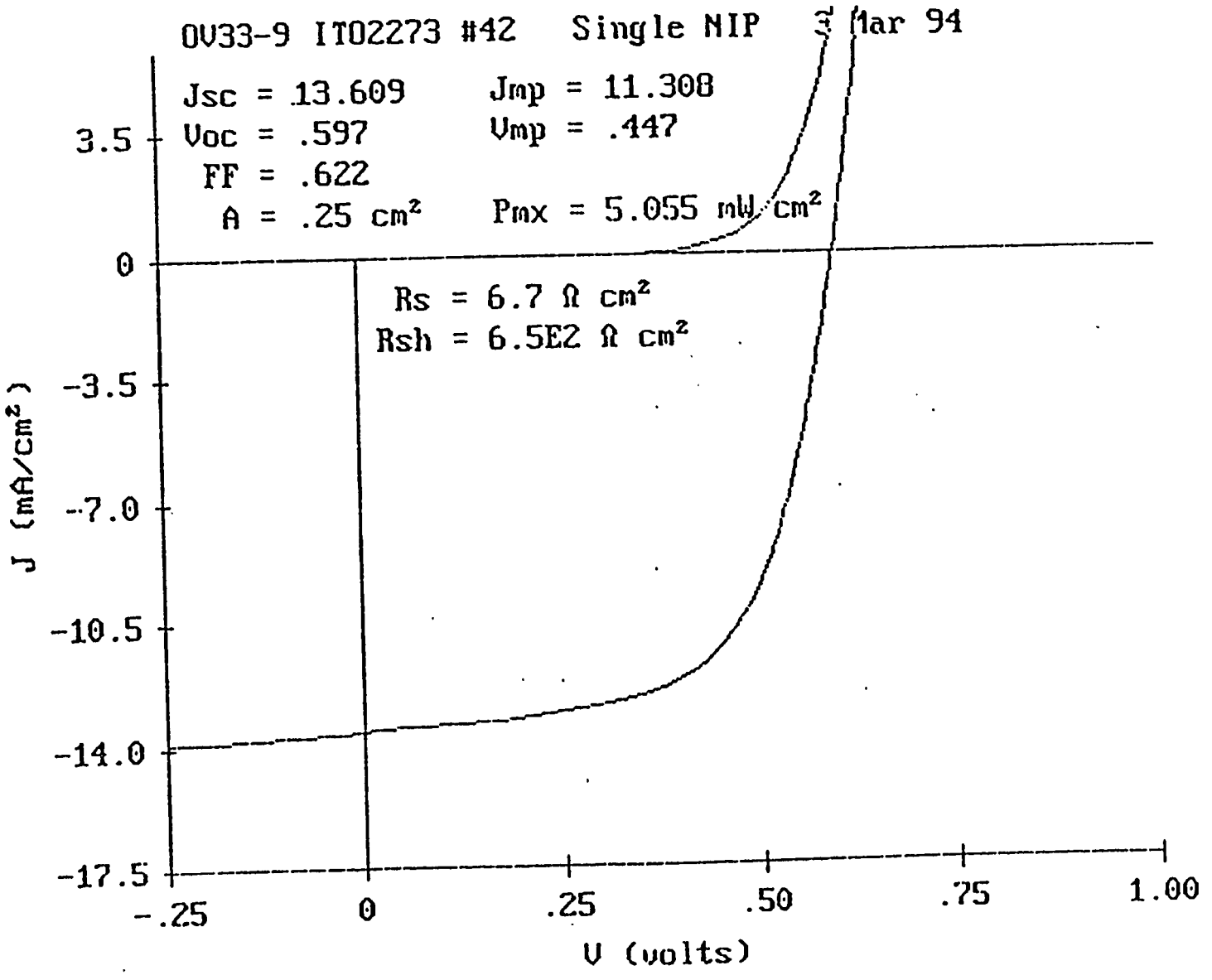

Figure 24a J-V curve of a narrow band-gap a-SiGe solar cell to be used as the bottom cell of triple-junction solar cell.

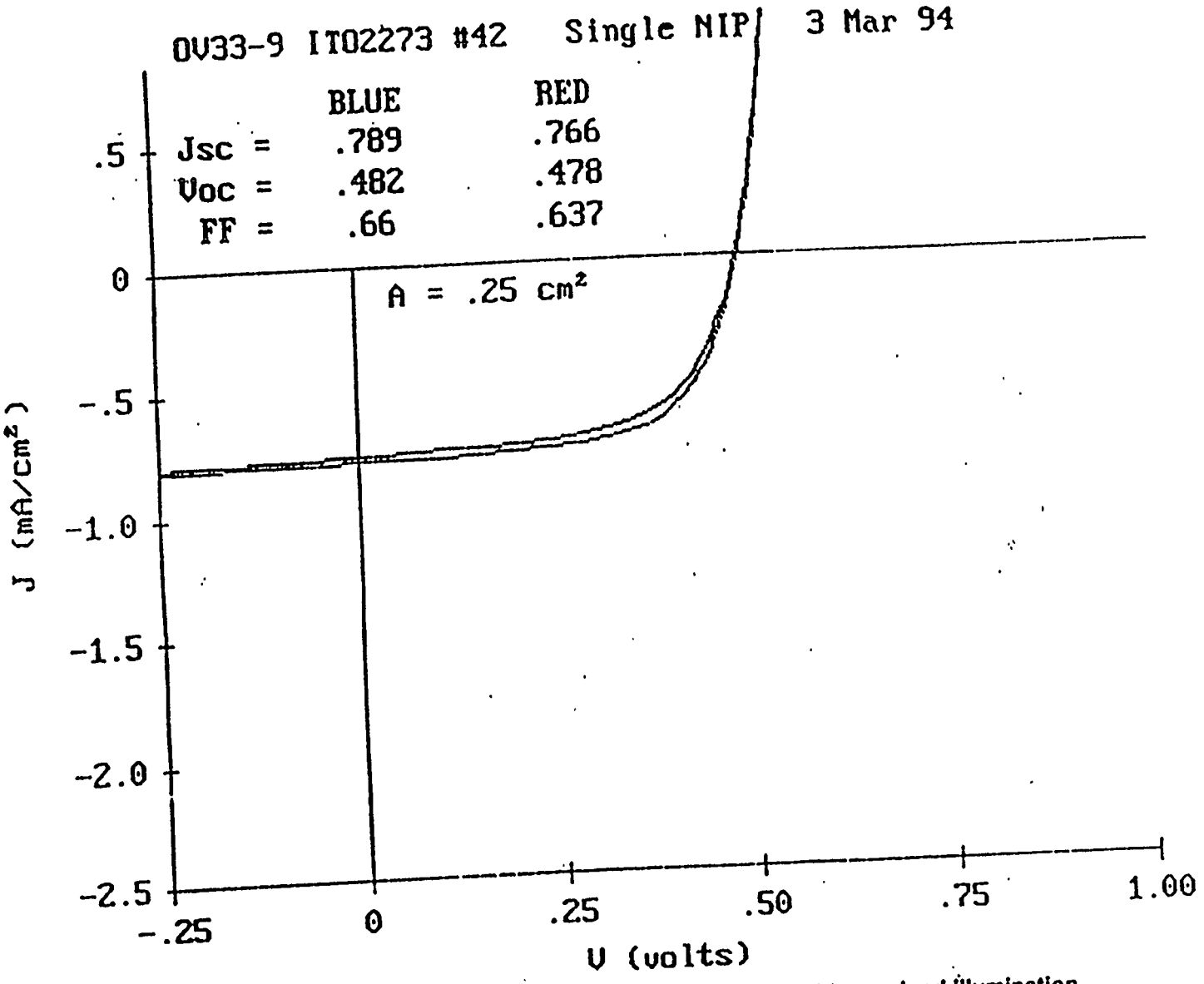

Figure 24b **J-V curve of the narrow band-gap a-SiGe solar cell under blue and red illumination.**

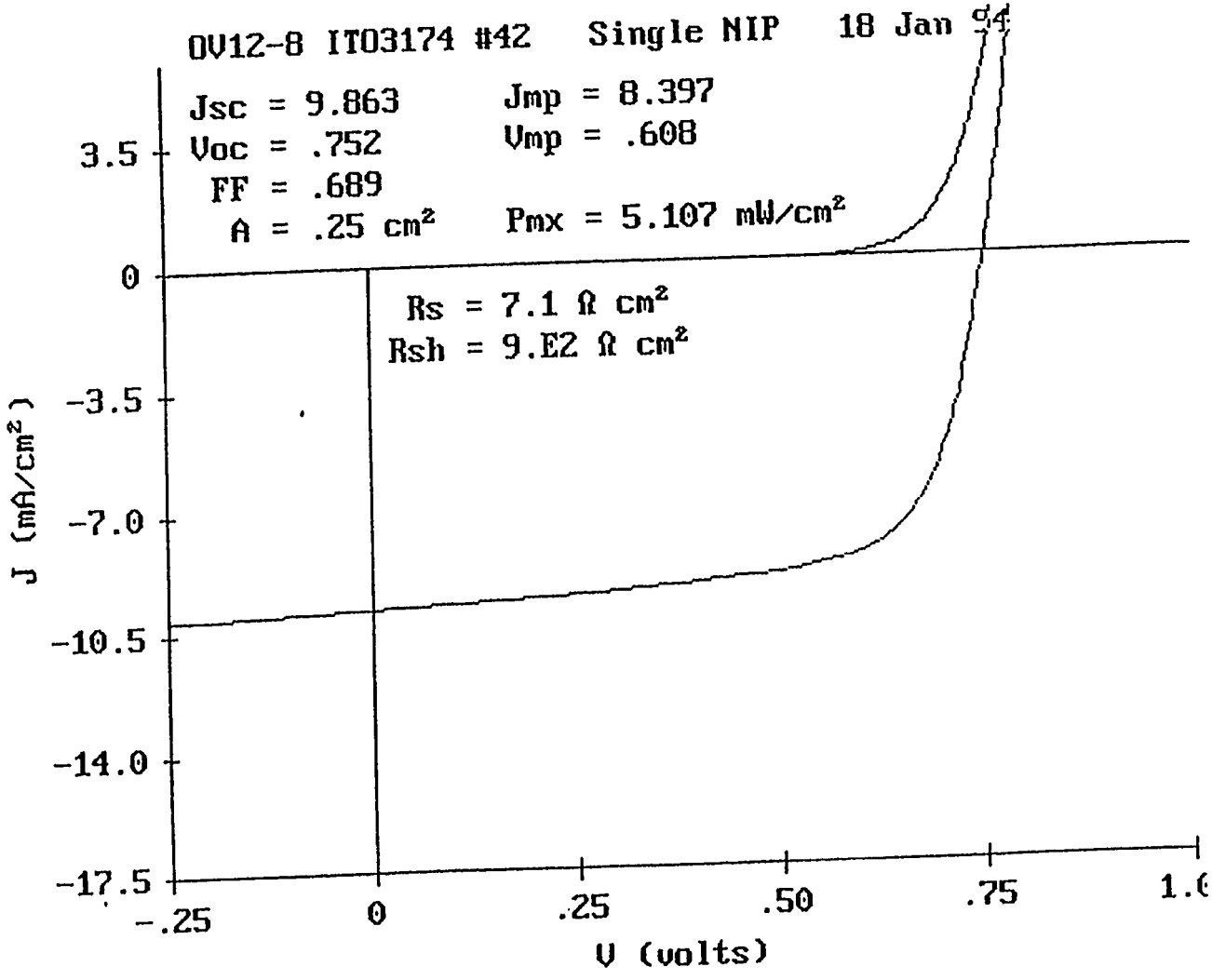

Figure 25(a) **J-V curve of an a-SiGe solar cell to be used as the middle cell.**

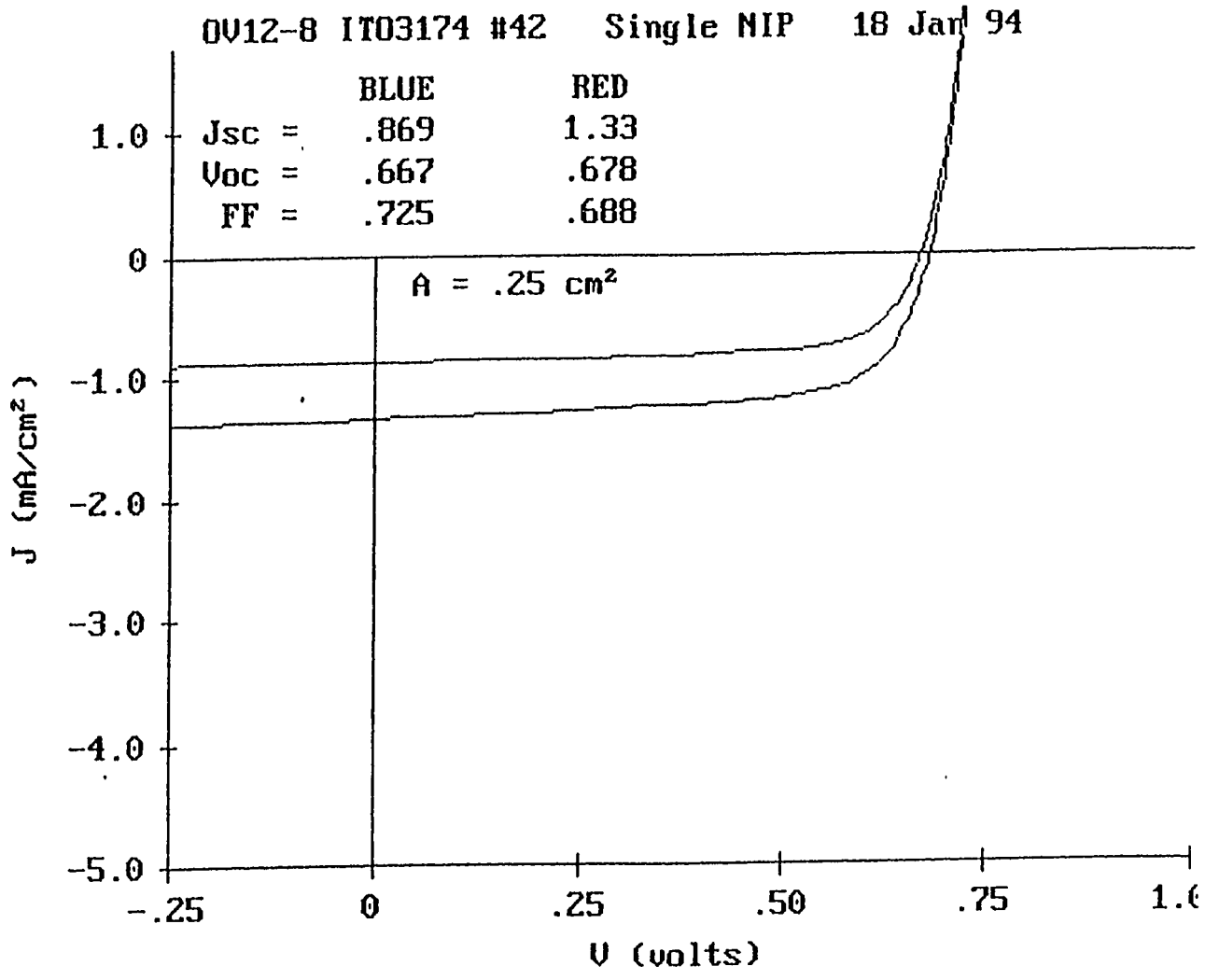

Figure 25(b) **J-V curves of the a-SiGe solar cell to be used as the middle cell under blue and red illumination.**

Task III: Optimization of the Stable Efficiency of Photovoltaic Modules

Introduction

In Task III the entire process, including substrate washing process, back-reflector deposition, a-Si alloy deposition, transparent conducting oxide deposition, and module assembly, was optimized for the high yield, low cost production of high efficiency stable modules. The improvements that resulted in Task I and Task II were incorporated to improve the performance of the solar cell.

Improvement to the Continuous Roll-To-Roll Solar Cell Deposition

We have systematically investigated the dependence of sub-cell efficiency on the thickness of each layer and current matching. The short circuit current densities of the component cells were, for example, 6.6 mA/cm^2, 6.8 mA/cm^2, and 7.2 mA/cm^2 for the top (i3), middle (i2), and the bottom (il) component cells as we see from the quantum efficiency curve in Figure 18. We explored the effect of mismatched current conditions on the efficiency by adjusting the thickness of the il, i2 and i3 layers.

When the i3 layer was thinner, J_{sc} decreased. However, the fill-factor increased because the current limiting thin top cell has a higher fill-factor and also mismatched cells give a higher overall fill-factor. In addition, the top cell limited devices have better stability because the top cell is more stable. Therefore, we designed the device to be top cell limited. Since EVA/Tefzel encapsulation absorbs some light, we produced the top i layer (i3) slightly thicker to compensate the current loss due to EVA/Tefzel absorption and still maintain the proper current matching. The bottom i layer was designed to have the highest current since it is the component cell with a relatively low fill-factor.

We also studied and adjusted the deposition conditions of all n^+ and p^+ layers to achieve the following:

- proper doping and thickness for high V_{oc};
- minimum thickness to reduce the absorption (this is especially important for the p3 layer);
- good tunnel junctions between pl and n2 and between p2 and n3 layers to minimize series resistance.

In addition to the optimization of the deposition conditions for each individual layer, we improved the process and hardware related aspects in order to improve production yields and consistency.

In earlier production runs, bearing seizures caused failure in the transport mechanism. To eliminate the problems that we encountered in the substrate transport mechanism, we incorporated an improved mechanical transport system including the newly designed bearings into the back-reflector system, a-Si alloy deposition system and the transparent conductor evaporation system, to ensure reliable operation. As discussed in Task I, the improved design effectively prevented mechanical failures such as back-side scratches on the web. These improvements resulted in consistently increased production yields.

QA/QC Process

Forty to one hundred QA/QC coupons, 4" long x 14" wide, were uniformly selected from a roll throughout the full production run for quality assurance and quality control testing (QA/QC). Twenty-eight test solar cells of 7.35 cm^2 in area were processed on each coupon by the following procedures:

1) TCO scribing by screen printing of etching paste, heat curing, and rinsing;
2) short and shunt passivation; and
3) screen printing of Ag paste grid.

Figure 26 is a schematic drawing of a QA/QC coupon, with 28 test cells. We measured the J-V characteristics of cells under AM 1.5 Xenon lamp solar simulator. Figure 27 is the J-V curve of a 7.35 cm^2 cell on a QA/QC coupon. The J-V data of 28 cells in a typical coupon is summarized in Table 6. From the table, the efficiencies of all 28 cells are above 10%. The uniformity is excellent. With a subcell yield criterion of fill factor >0.55, the yield of this coupon is 100%. The average V_{oc}, J_{sc} , fill factor, and efficiency are 2.37 V, 6.51 mA/cm^2 , 0.673, and 10.41%, respectively, as is shown in the table.

To further analyze the performance of solar cells, samples are taken after the a-Si alloy deposition machine and before the web is loaded into the roll-to-roll TCO machine. These sample cells are evaluated by evaporating small area ITO and Ag grid patterns on them in batch evaporation systems. Figure 28 is a J-V curve characteristic of a 0.25 cm^2 triple-junction two bandgap solar cell produced in our continuous roll-to-roll a-Si alloy deposition machine in a 2500 ft. production run with improved process conditions. As is seen in Figure 28, 11.1 % initial efficiency was achieved in the a-Si alloy solar cell production machine under production conditions. Figure 29 is the quantum efficiency curve of the 11.1% cell shown in Figure 28.

A Typical 2500 Foot (19 KW) Production Run

As described previously, ECD's PV production process consists of operation through continuous roll-to-roll machines of web washing, back-reflector deposition, a-Si alloy deposition and TCO deposition, followed by module assembly. Ag/ZnO back-reflector, a-Si alloys, and TCO are sequentially deposited on 5 mil. thick, 14 in. wide, and 2500 ft. long stainless steel rolls at a speed of 1 ft./min. A typical 2500 ft. roll is finished within 42 hours. During operation all of the process parameters are controlled, monitored, and recorded through the use of PC computerized data acquisition and process controlling systems.

Out of the total web width of 14", 12.5" is used as the active area in the final module assembly. With a yield of 99% and stable module efficiency of 8%, a 2500 ft. run produces an output of 19.2 kilowatt.

In Table 7, we show the statistical summary of the I-V data of QA/QC coupons throughout an entire production run. A QA/QC coupon has 28 cells and the average was calculated on 28 cells. In each line of this table, we list average V_{oc} , J_{sc} fill factor, and efficiency as well as the yield of a coupon taken at the corresponding slab number. Detailed I-V data for each cell of the coupon at meter mark 417m was shown previously in Table 6. Over the entire run, the average efficiency is 10.21% with a standard deviation of 0.02%. The average subcell yield for this production run is 99.7%.

Figure 3, that we showed earlier, is a three-dimensional plot of cell efficiency for all cells in this run. It shows the efficiency data for 1176 individual cells for the entire production run as a function of the position of sub-cells in the 2500 ft. long, 14 in. wide substrate. Out of 1176 cells plotted in the figure, only three cells failed. Figures 30, 31 and 32 show the three dimensional plot of V_{oc}, J_{sc}, and fill factor, respectively. The solar cell performances are highly uniform throughout the entire run. Production parameters recorded in the computerized data acquisition system showed excellent consistency and uniformity achieved in our continuous roll-to-roll manufacturing process.

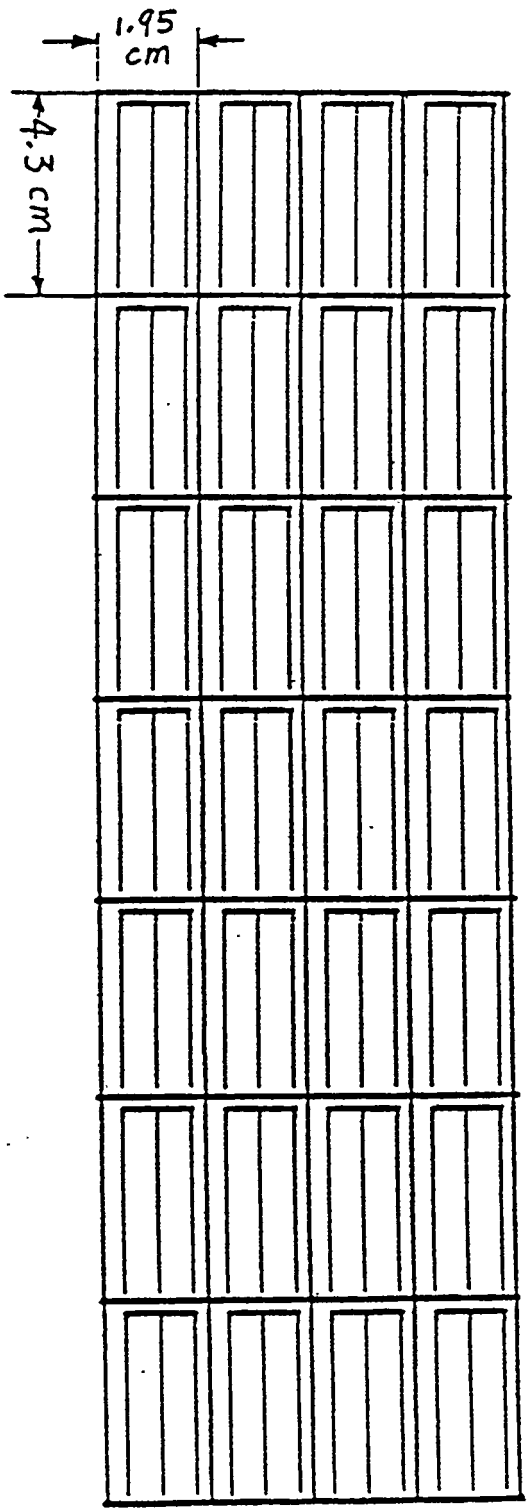

Figure 26. **Schematic drawing of a QA/QC coupon with 28 sub-cells (7.35cm^2 active area)**

Table 6. Statistical data for J-V curves of 28 cells on a QA/QC coupon.

Cell Number	Voc (V)	Jsc (mA/cm2)	FF	Eff. (%)
1	2.38	6.45	0.706	10.49
2	2.38	6.45	0.694	10.64
3	2.37	6.66	0.658	10.37
4	2.37	6.88	0.642	10.46
5	2.37	6.65	0.673	10.59
6	2.38	6.54	0.676	10.52
7	2.38	6.52	0.668	10.36
8	2.39	6.36	0.670	10.19
9	2.38	6.32	0.684	10.29
10	2.37	6.35	0.686	10.30
11	2.37	6.88	0.633	10.31
12	2.37	6.52	0.671	10.36
13	2.38	6.39	0.688	10.45
14	2.39	6.71	0.669	10.72
15	2.38	6.24	0.698	10.36
16	2.38	6.47	0.663	10.20
17	2.37	6.55	0.679	10.54
18	2.37	6.52	0.672	10.39
19	2.37	6.67	0.654	10.33
20	2.38	6.49	0.674	10.40
21	2.39	6.63	0.663	10.50
22	2.38	6.39	0.684	10.39
23	2.37	6.27	0.704	10.47
24	2.37	6.43	0.695	10.59
25	2.37	6.53	0.679	10.50
26	2.37	6.66	0.652	10.30
27	2.38	6.67	0.651	10.34
28	2.38	6.37	0.674	10.21
Average	2.37	6.51	0.673	10.41

Yield for cells with FF>=0.55: 100%

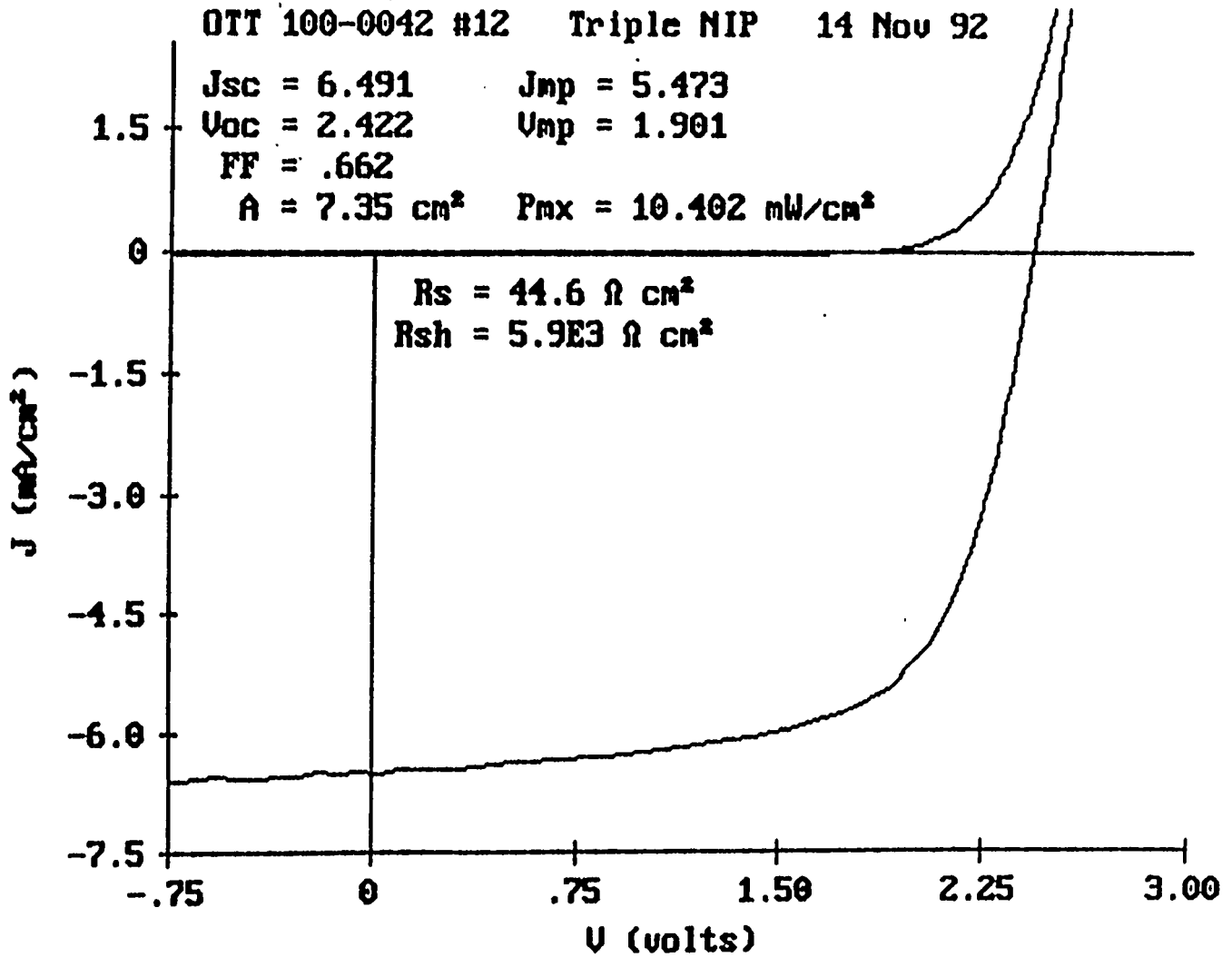

Figure 27. J-V curve of a 7.35cm² triple-junction sub-cell

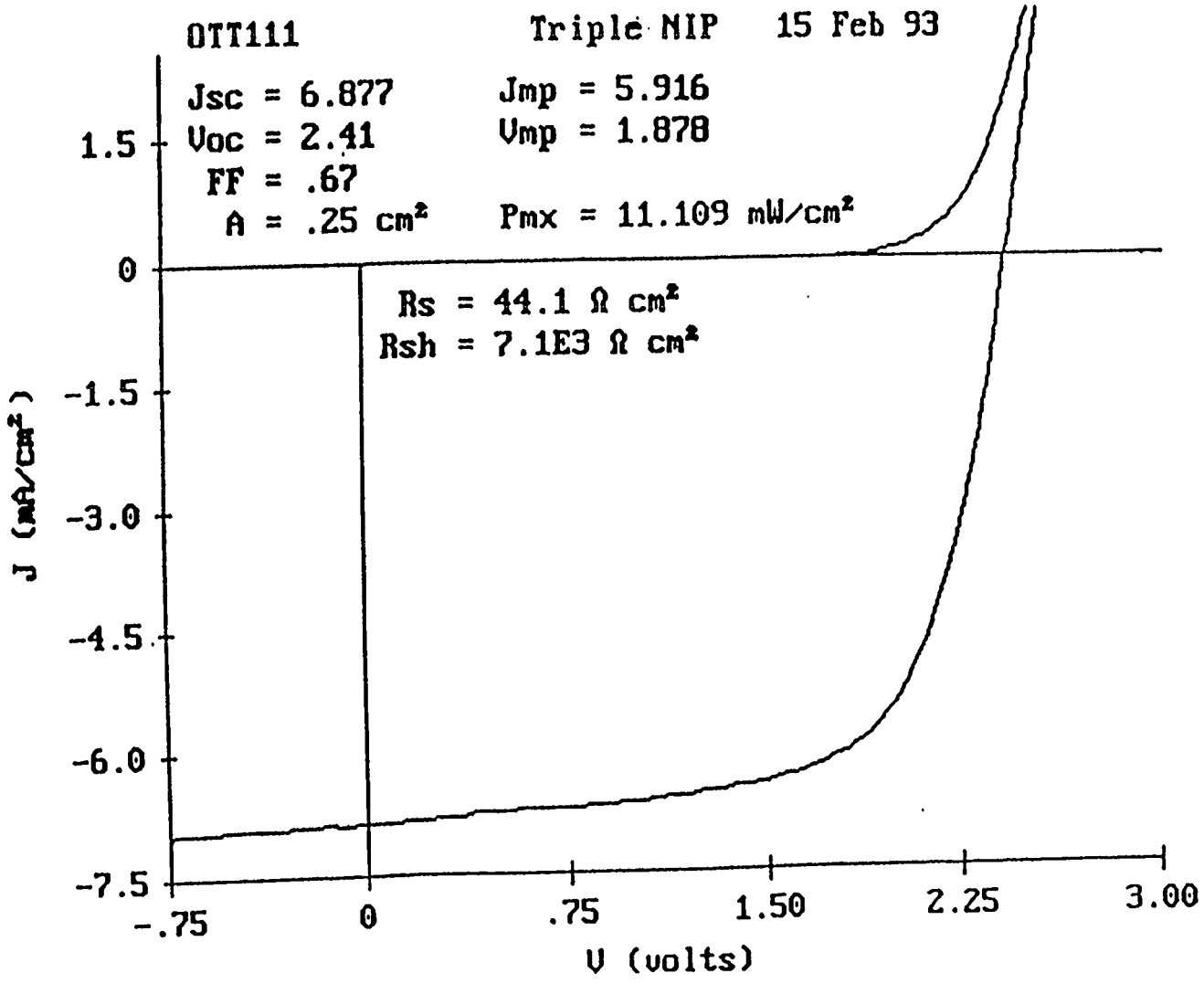
OTT111
Triple NIP 15 Feb 93
Jsc = 6.877
Voc = 2.41
FF = .67
A = .25 cm²
Jmp = 5.916
Vmp = 1.878
Pmx = 11.109 mW/cm²
Rs = 44.1 Ω cm²
Rsh = 7.1E3 Ω cm²
1.5
0
-1.5
-3.0
-4.5
-6.0
-7.5
J (mA/cm²)
-.75
0
.75
1.50
2.25
3.00
V (volts)

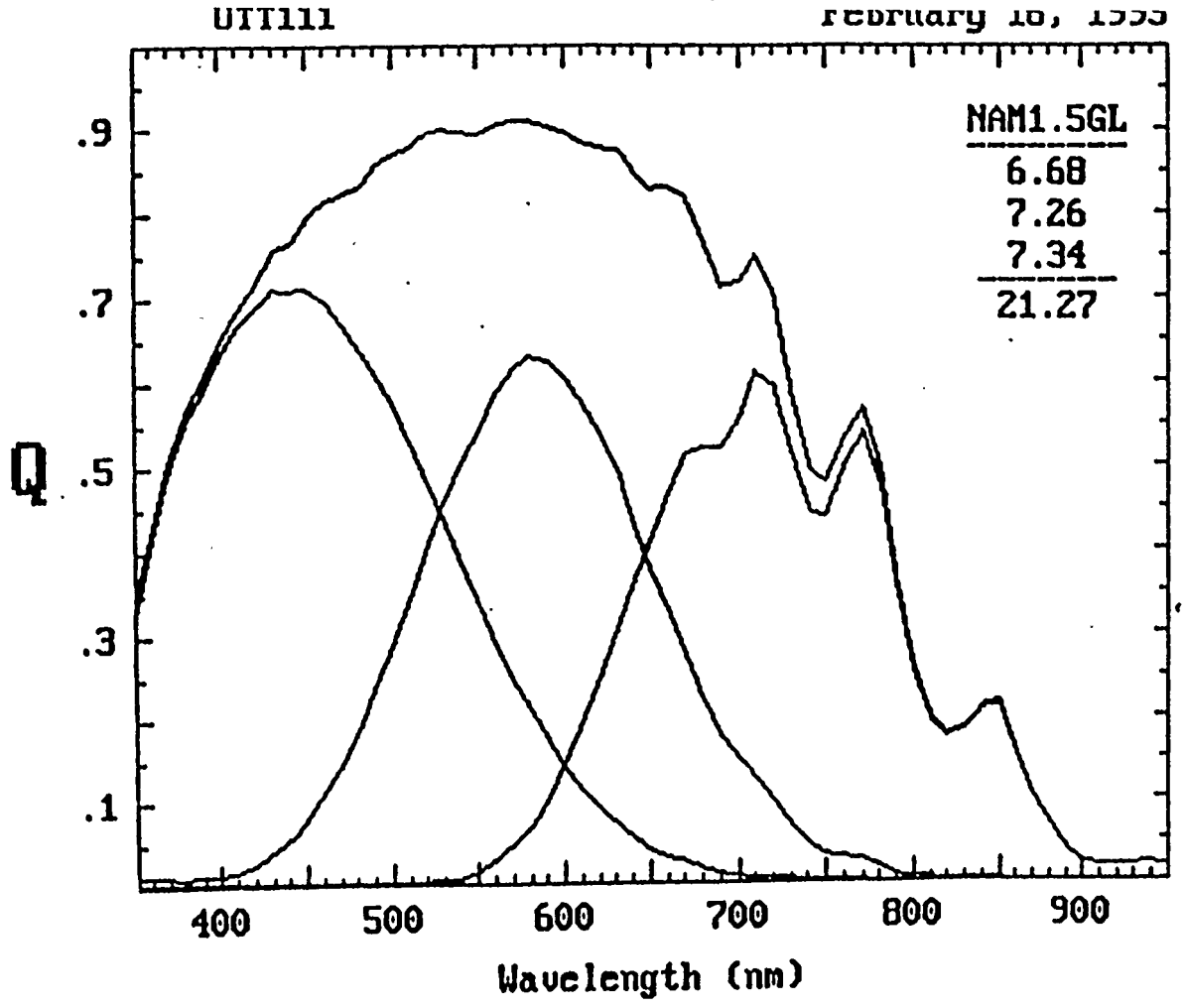

Figure 29. **Quantum efficiency curve for the 0.25cm² triple-junction cell showing 11.1% efficiency**

Table 7. Average cell performance data of coupons throughout an entire run.

Sample Number	Meter Mark (m)	Voc (V)	Jsc (mA/cm2)	FF	Eff. (%)	Yield (%)
1	41	2.35	6.52	0.661	10.15	100
2	62	2.35	6.64	0.658	10.29	100
3	62	2.36	6.53	0.670	10.35	100
4	82	2.35	6.61	0.655	10.20	100
5	103	2.35	6.55	0.655	10.12	100
6	124	2.35	6.43	0.666	10.08	100
7	166	2.35	6.51	0.659	10.10	100
8	166	2.36	6.54	0.669	10.37	100
9	187	2.35	6.55	0.659	10.16	100
10	208	2.38	6.47	0.654	10.07	96
11	229	2.36	6.49	0.662	10.14	96
12	250	2.36	6.33	0.666	09.97	100
13	271	2.36	6.46	0.667	10.20	96
14	271	2.37	6.41	0.671	10.19	100
15	292	2.39	6.40	0.661	10.14	100
16	312	2.36	6.59	0.658	10.25	100
17	334	2.35	6.56	0.662	10.24	100
18	354	2.35	6.42	0.664	10.05	100
19	375	2.35	6.54	0.662	10.22	100
20	375	2.37	6.48	0.669	10.29	100
21	396	2.37	6.54	0.667	10.36	100
22	396	2.37	6.45	0.676	10.36	100
23	417	2.37	6.51	0.673	10.41	100
24	417	2.37	6.56	0.671	10.45	100
25	438	2.37	6.44	0.667	10.20	100
26	438	2.37	6.52	0.665	10.29	100
27	459	2.37	6.39	0.680	10.33	100
28	459	2.37	6.43	0.671	10.26	100
29	480	2.37	6.46	0.675	10.36	100
30	480	2.37	6.45	0.673	10.31	100
31	501	2.37	6.43	0.674	10.30	100
32	501	2.37	6.47	0.667	10.25	100
33	522	2.37	6.32	0.680	10.23	100
34	522	2.37	6.45	0.671	10.26	100
35	543	2.37	6.39	0.680	10.34	100
36	543	2.37	6.48	0.670	10.32	100
37	564	2.38	6.34	0.670	10.15	100
38	564	2.38	6.32	0.669	10.10	100
39	585	2.38	6.35	0.674	10.20	100
40	585	2.38	6.29	0.679	10.19	100
41	595	2.38	6.32	0.671	10.12	100
42	595	2.38	6.40	0.673	10.29	100
Average		2.366	6.46	0.668	10.21	99.7
Std. Deviation		0.002	0.01	0.001	0.02	0.2

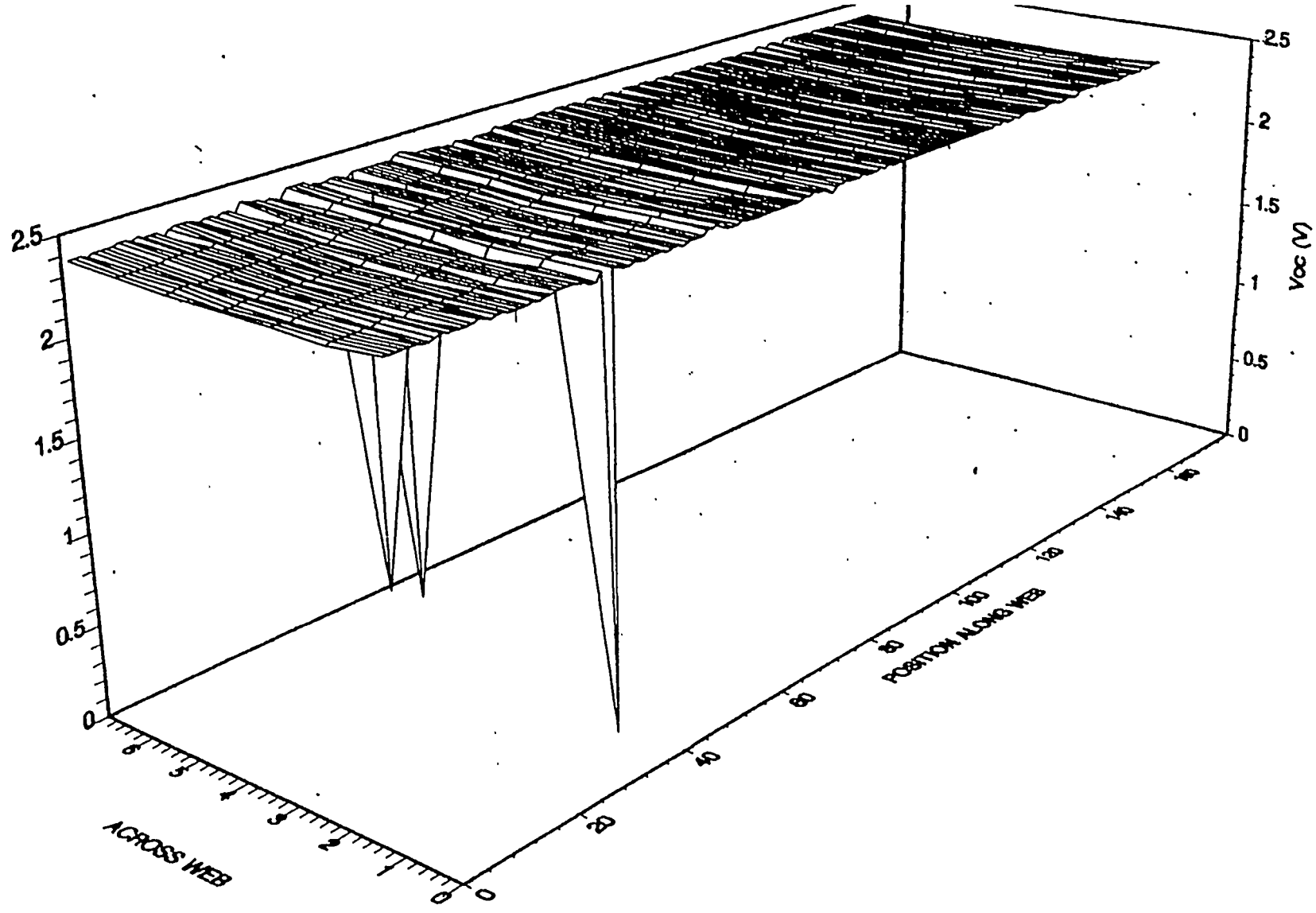

Figure 30. **Open circuit voltage of a 600m production run**

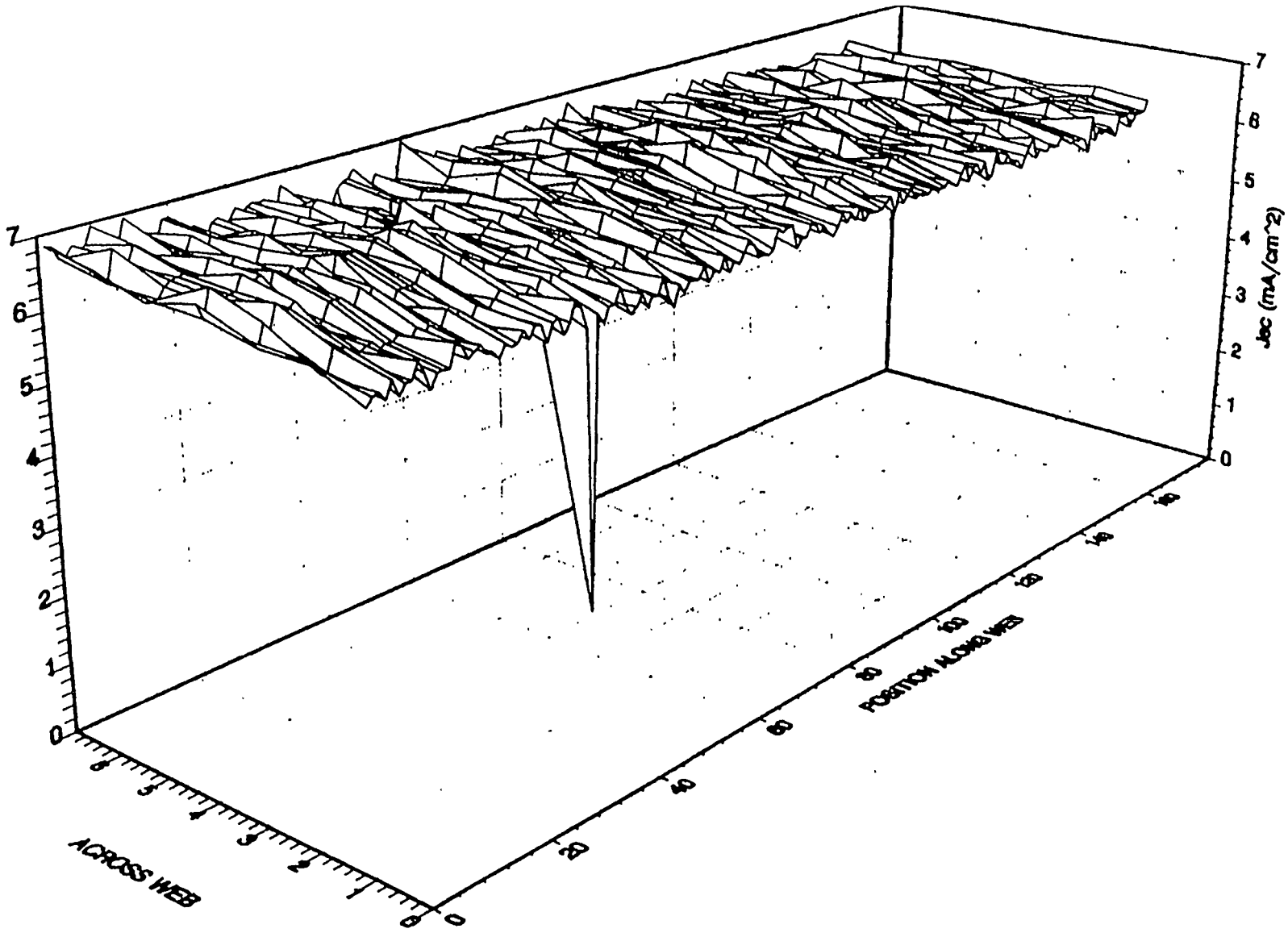

Figure 31. **Short circuit current of a 600m production run**

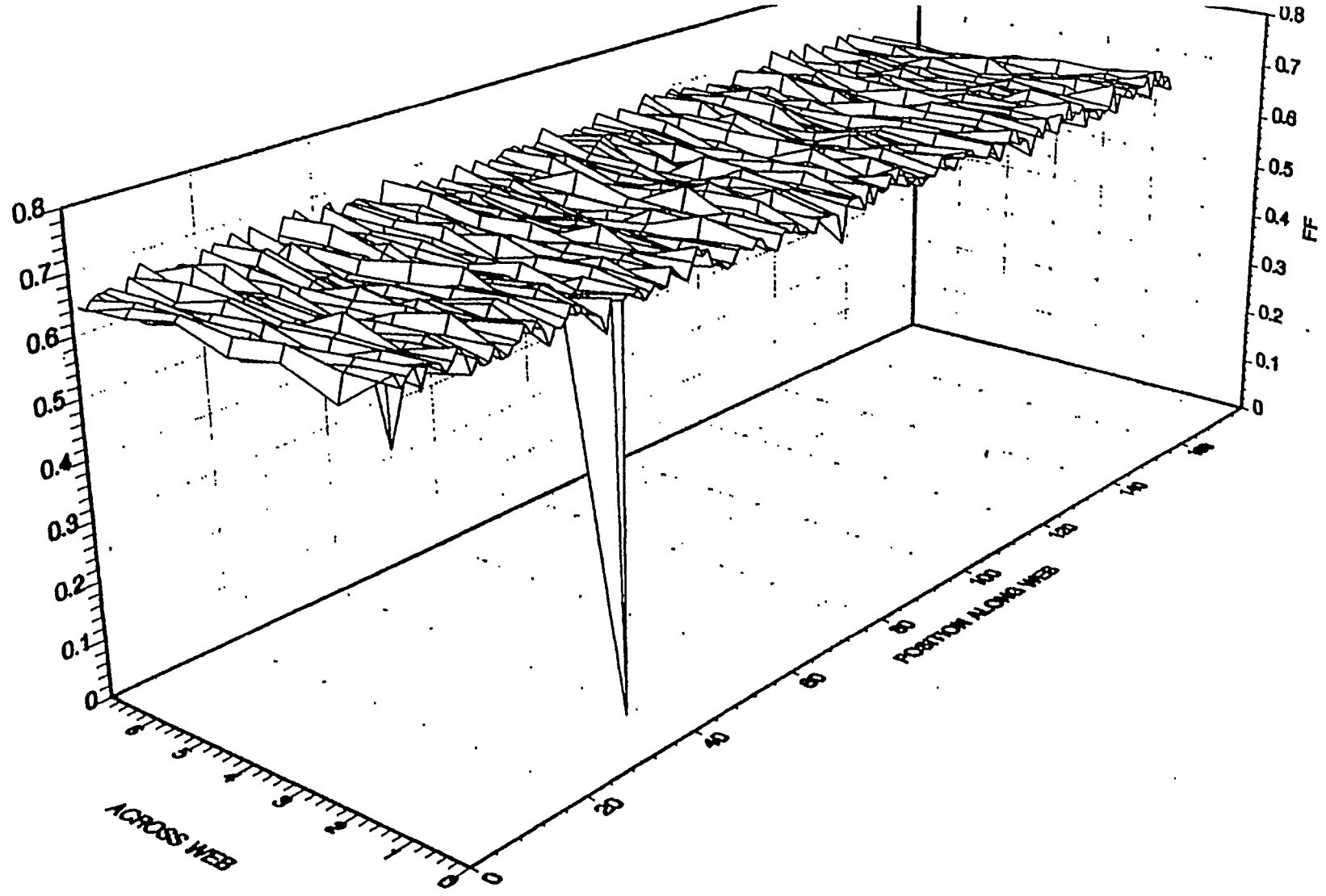

Figure 32. **Fill factor of a 600m production run**

Module Assembly

Strip cells are produced by processing slabs of solar cell material through TCO scribing, short and shunt passivation, and screen printing of Ag paste grid pattern. A strip cell is a single solar cell with an aperture of 12.5" x 5.4". After cutting and busbar installing, nine strip cells are connected together in series, as a module. A diode is connected in parallel with every strip to prevent the strip cell from being reverse biased. The module is then vacuum laminated in a high temperature oven, with Tefzel, EVA and crane glass as the front cover and with layers of EVA, fiberglass, nylon, and metal backing plate as the back cover. An aluminum frame and junction box are installed to finish the module. Figure 33 is a drawing of ECD's 1ft. x 4ft. a-Si alloy production PV module.

ECD's High Efficiency 4 Ft.^{2} Production Module

4 ft.^{2} modules were assembled using triple-junction two bandgap solar cells produced in a continuous roll-to-roll manufacturing line. Figure 34 is the I-V curve of a 4ft.^{2} module measured at NREL. The initial aperture module efficiency is 9.5% and the total power output is 37.01W for a module of 3923 cm^2 aperture area. This efficiency is higher than any reported efficiency for a-Si alloy production modules.

Stable Efficiency Of Modules

To measure the stable efficiency of our modules, light soak stability tests were carried out. Phillip's metal halide 1000/U light bulbs, powered by appropriate ballasts, were used. The light intensity is measured with a Silicon detector filtered with a heat filter so that the quantum efficiency of the detector is close to that of an a-Si alloy solar cell. The light intensity inside the 4ft.^{2} module area is within 20% from 100mW/cm^2 with the average at 100mW/cm^2. Temperature of the modules under light soaking was around 50°C. The temperature was slightly higher at the center of the module where the light intensity is about 20% higher than 100mW/cm^2 . Each module was degraded with a load such that it was operating at its peak power point. Figure 35 is the I-V curve of this module after 2380 hours of degradation. The stable module efficiency after 2380 hours of one sun light soaking at approximately 50°C under load is 7.9%. In Figure 36, we plot the semilog plot of efficiency to light soaking time. Clearly the module efficiency has come to a saturation under light soaking. No further degradation, within measurement accuracy, is found for these modules after prolonged light soaking.

A set of PV modules produced in ECD's continuous roll-to-roll manufacturing line was tested according to NREL's "Interim Qualification Tests and Procedures for Terrestrial Photovoltaic Thin-Film Flat-Plate Modules." Except for some cosmetic microdelamination, these modules have passed the specified 20 humidity-freeze cycling test and 200 thermal cycling tests.

Optimization using new 200 KW pilot machine

In order to incorporate new R&D advances and to further improve the stable module efficiency, we designed and constructed, at ECD's expense, a new multi-purpose continuous roll-to-roll a-Si alloy solar cell deposition machine having 200 kW capacity.

As is shown in Figure 6, the new continuous roll-to-roll multi-purpose deposition machine consists of seven chambers:

1) Chambers at each end for the web loading and unloading, and for web driving and steering systems which can transport the web in both directions during deposition.

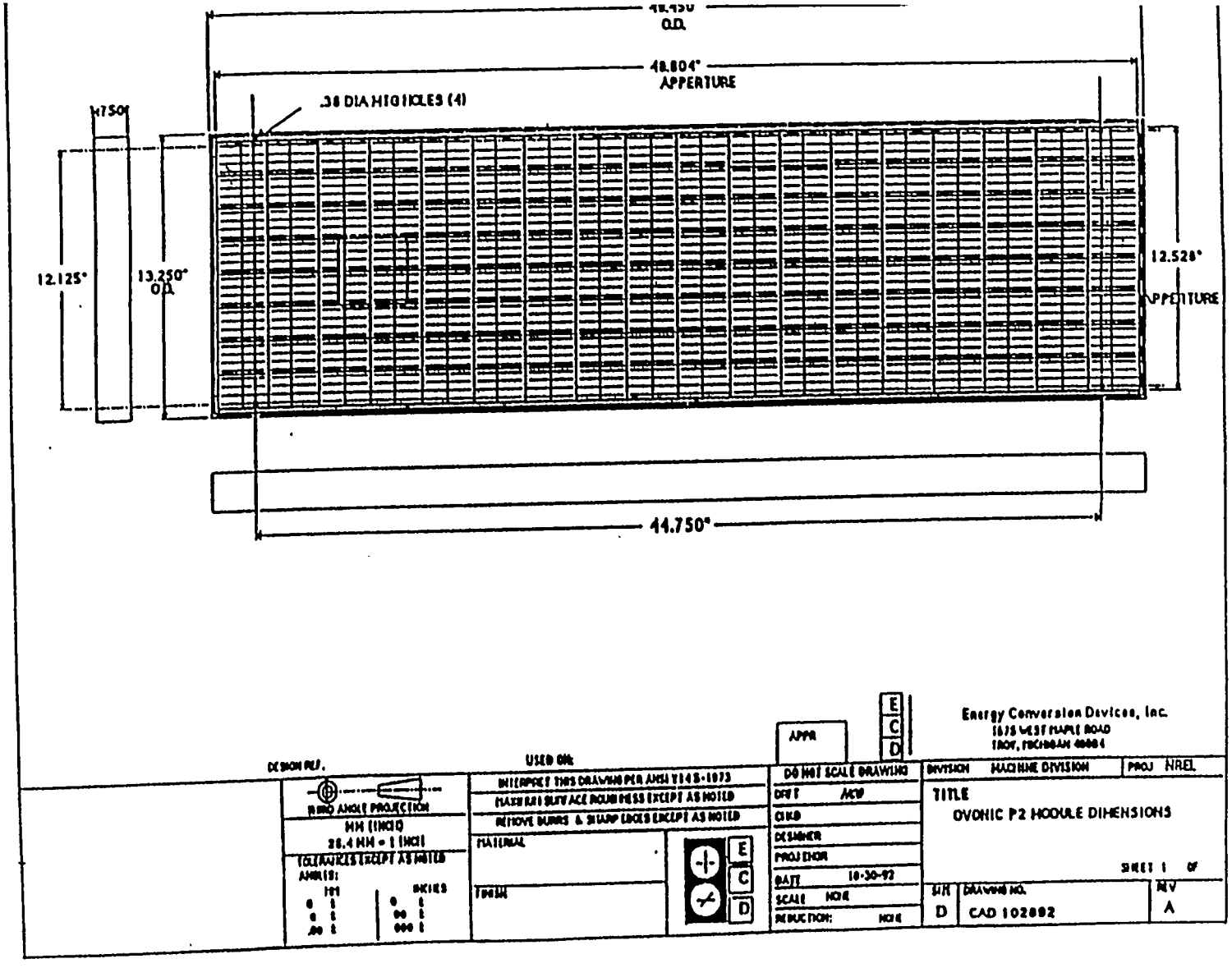

Figure 33. A schematic drawing of a 1 ft x 4 ft module.

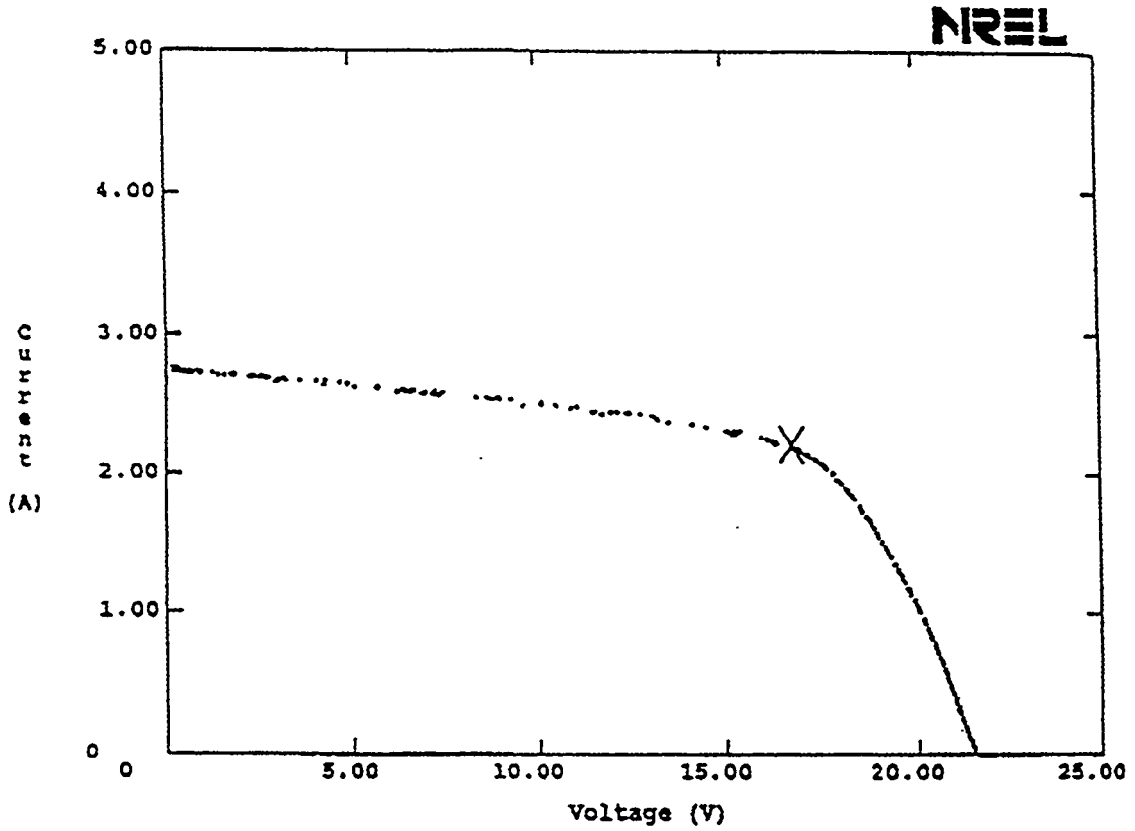

Manufacturer: ECD
Sample Type : a-Si/a-Si/a-Si module
Sample # : 030

Test Date : April 29, 1993
Test Time : 5:51 PM
Spectrum : ASTM E892 Global
File Name : C:\IV\data\IV4162.xy
NREL Spire 240A solar simulator (peak)
Estimated total uncertainty in efficiency is ± 5 %

Total irradiance = 1000 W/m^2
Temperature = 25 °C
Aperature Area = 3906 cm^2

Voc	= 21.51 V
Isc	= 2.743 A
Pmax	= 37.01 W
V at Pmax	= 16.72 V
I at Pmax	= 2.214 A
Fill Factor	= 62.7 %
Efficiency	= 9.47 %

Figure 34. I-V curve of a 4 ft^2 triple-junction a-Si alloy PV module, measured by NREL, showing 9.5% initial module efficiency.

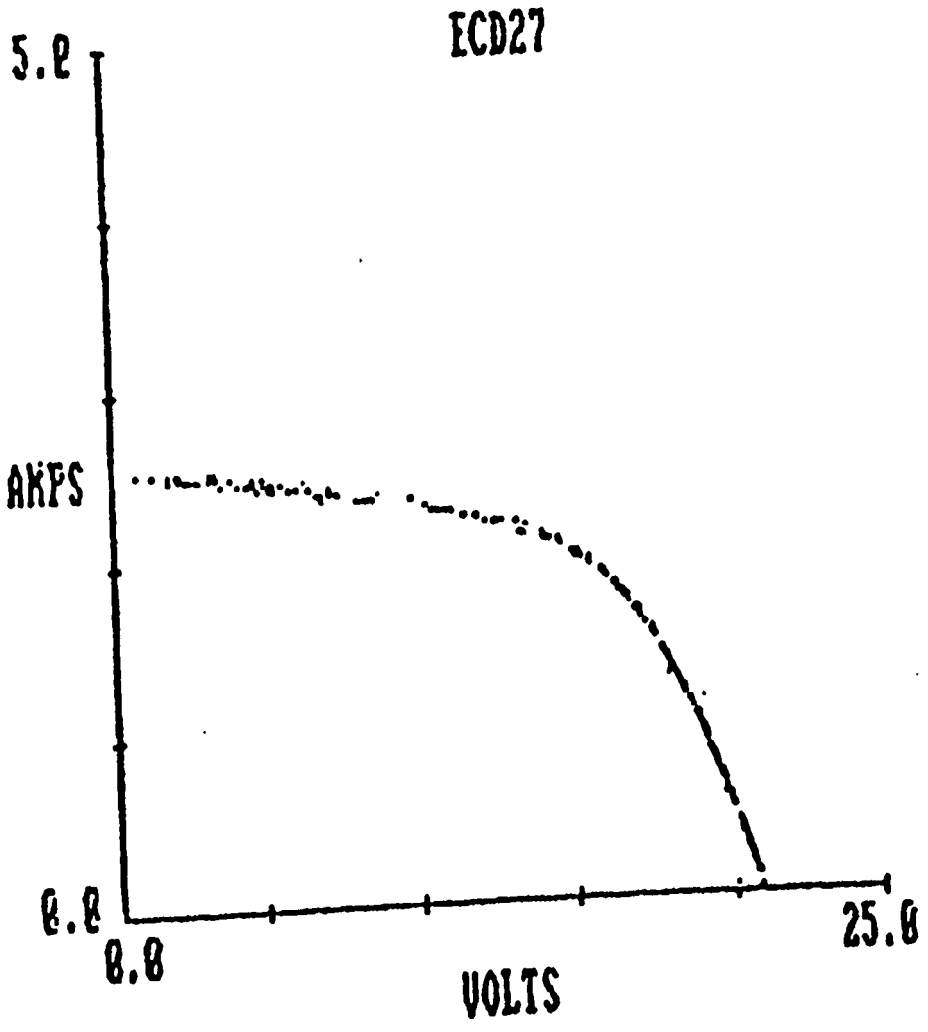

(no filename)
ID. No. M27-2380
02-07-1993, 09:12:54
Sun = 100 mW/cm2
Temp = 23 degC, 23
Voc = 20.90 V
Isc = 2.60 A
Pmax = 30.93 W
Vmp = 15.11 V
Imp = 2.05 A
FF = .57
Rs = 1.83 Ohms
Ef,c = 7.9 %

No. of flashes = 325

Figure 35. I-V curve of ECD's 4 ft² a-Si alloy PV module after 2380 hours of light soaking.

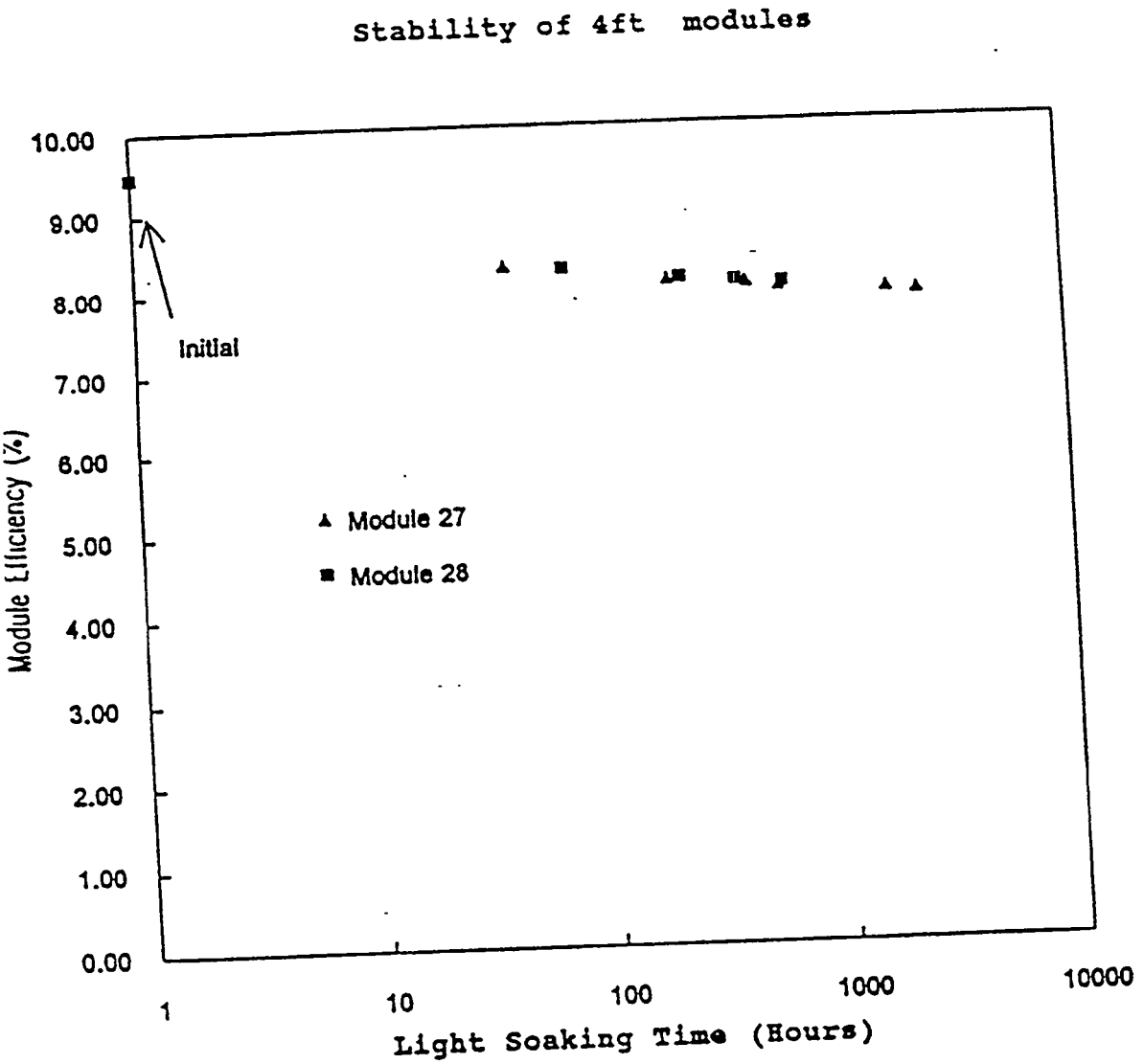

Figure 36. Stability test results of two 4 ft^2 modules

2) n, i, and p RF plasma CVD chambers for the deposition of n, i, and p a-Si alloy layers needed for a single-junction solar cell. A triple-junction solar cell is produced with web passing through the machine three times.

3) A single loop serpentine web deposition chamber for depositing intrinsic a-Si layer in a serpentine configuration.

4) A DC magnetron sputtering chamber for the deposition of Ag/ZnO back-reflector layers and top conductor layer.

This multi-purpose deposition machine is capable of producing complete triple-junction solar cells in a sequential continuous roll-to-roll operation.

We have optimized the operation in the following areas:

- Back-Reflector;
- Top conductor;
- Yield;
- Doped layers; and
- a-Si/a-SiGe/a-SiGe triple cell.

We have adjusted the current matching between different component cells. These fine adjustments include the thickness, and the temperature of the top intrinsic layer; the thickness, Ge content, and bandgap grading of the middle intrinsic layer; and the thickness, Ge content, and bandgap grading of the bottom intrinsic layer. These adjustments were made using quantum efficiency measurements. We measured the quantum efficiency curves of each component cell of the triple cell, and integrated the curve with AM1.5 global spectrum to obtain the short circuit current of each sub-cell. The current of each component subcell was adjusted such that the peak power point of each component cell is at the same current level. After the optimization of the current matching, we produced (0.25 cm^2) a-Si triple cells with 9.5% initial active-area conversion efficiency.

Wire-Grid Module Design

We have developed a new grid/busbar technique to reduce the optical loss, utilizing thin copper wires adhered to the ITO surface with conductive adhesive. Figure 37 shows the sketches of the existing and new grid designs. The detailed analysis indicates that approximately 3 - 4% gain in efficiency is expected for the new design. Figure 38(a) and Figure 38(b) show the J-V curves for a sub-cell with the new wire grids and the previous Ag paste grid. Compared with the same cell using previous screen printed Ag paste grid lines, the fill factor is improved to 0.67 and the series resistance is reduced to 39 Ωcm.

Further progress has been made with a wire grid technique which we expect to eventually replace our standard screen printed grid. Each module contains nine series connected wire-grided strips. The strips were wire-grided by means of a special fixture that can simultaneously lay down four wires at a time. After being affixed to the surface of the strip, the wires were soldered to copper busbars on one side of each strip. The strips were then interconnected using a technique very similar to that used for our standard screen printed strips. The final lamination and framing steps are identical to those used for screen printed strips.

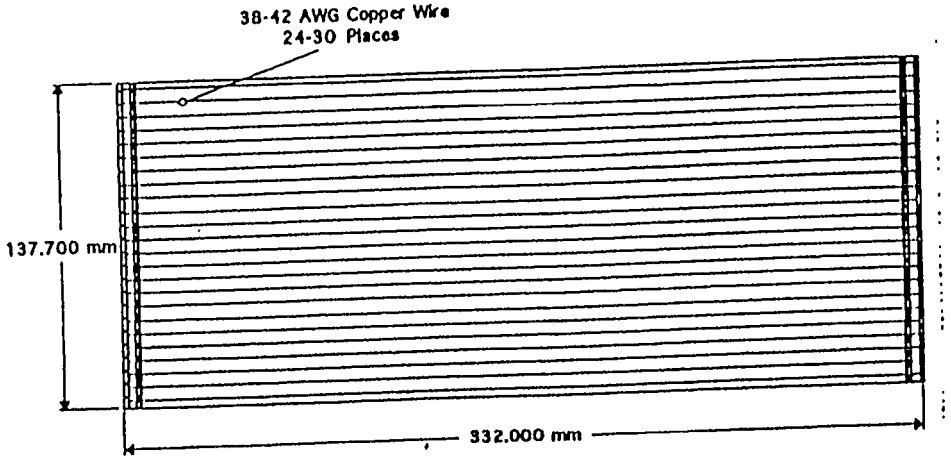

STRIP WITH NEW WIREGRID

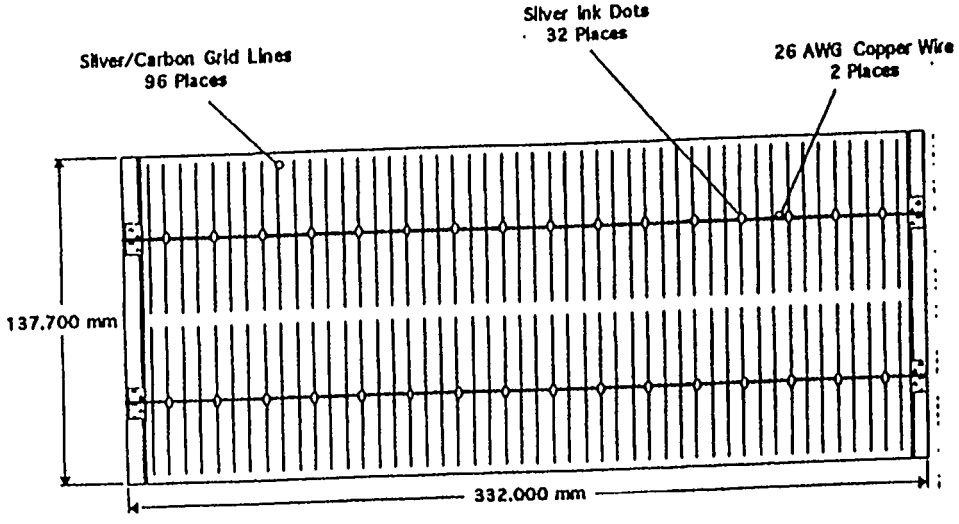

STRIP WITH PRESENT SILVER/CARBON PASTE GRID AND WIRE BUS BARS

Figure 37. A schematic diagram of the new wire grid design, compared with the present grid design.

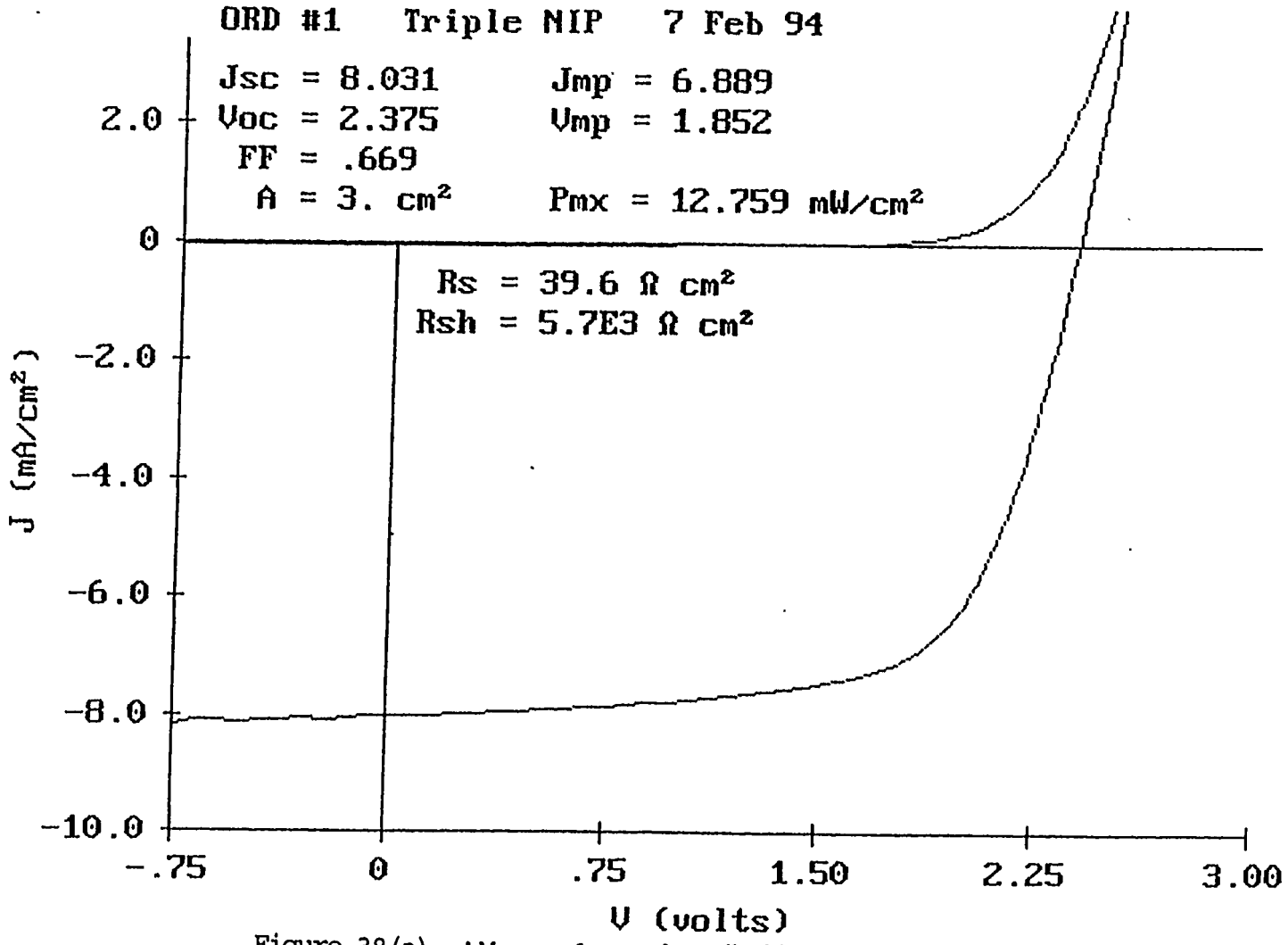

Figure 38(a) **J-V curve for a solar cell with new wire grid.**

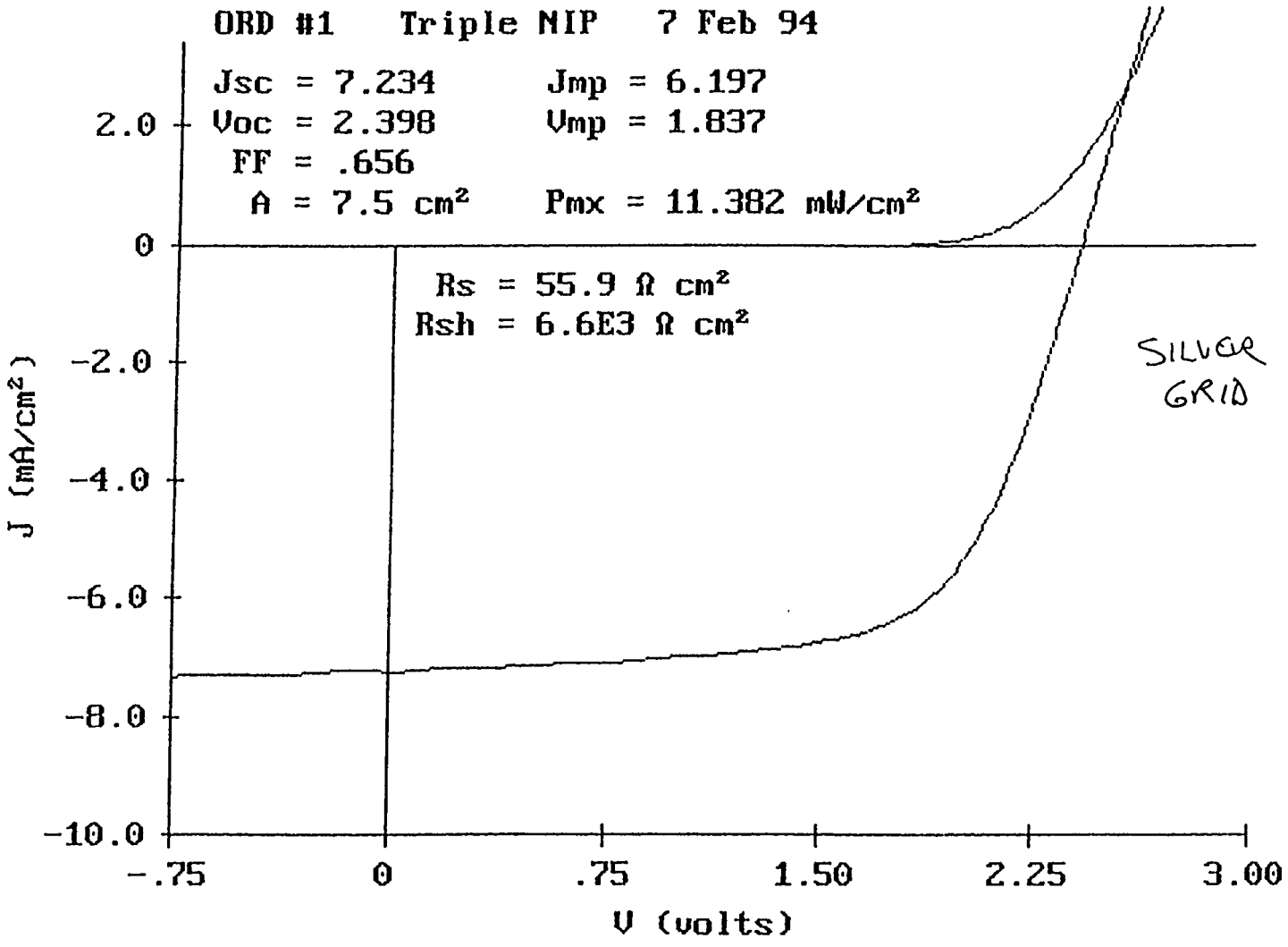

Figure 38(b) J-V curve for a similar solar cell with previous Ag paste grid, for comparison.

Task IV: Demonstration of Serpentine Web Continuous Roll-to-Roll Deposition Technology

A serpentine web configuration has been extensively used in other film processing industries such as the steel industry and photographic film manufacturing to achieve a high throughput for manufacturing processes which require a long reaction time. We have developed a design concept for a serpentine web continuous roll-to-roll amorphous silicon alloy solar cell deposition process to maximize solar cell throughput while keeping the size of individual deposition chambers small.[19]

A schematic diagram for an RF plasma processor for depositing n-i-p/n-i-p/n-i-p amorphous silicon alloy solar cells utilizing a serpentine web roll-to-roll process is shown in Figure 39.

As can be seen in the diagram, deposition takes place on the substrate as it travels vertically through the deposition chamber. This is to be contrasted to the current process in which the substrate travels horizontally. This vertical, roller-guided travel creates a large deposition area using less floor space. In the deposition chamber, a single RF cathode generates a plasma which will simultaneously deposit on regions of the substrate facing both sides of the cathode. Because of the compactness of the serpentine design, substantial cost savings for the equipment will be achieved and heat loss will be substantially reduced, which will reduce electric power consumption. Furthermore, by utilizing a perforated cathode or other open cathode configurations in which the surface area is minimized, gas utilization will be improved as deposition on the cathode is reduced. Cathode heating and dark-space shields are eliminated in the serpentine design which simplifies the internal design.

Due to the serpentine configuration, a slow rate of deposition can be used without reducing throughput and a-Si alloy intrinsic materials can be deposited with a minimum density of microvoids. It has been shown that significant improvement in the stability can be achieved when the a-Si material is deposited at a low rate.[23] We expect that the current 15-18% degradation will be reduced to less than 8%, while reducing the expected gas utilization by at least 25%.

In summary, we anticipate that with the serpentine web roll-to-roll technology, high efficiency stable PV modules can be produced in a high volume production process. A substantial reduction of manufacturing cost will be the consequence of the cost reduction of capital equipment, facilities, gases, energy and factory space.

The benefits of the serpentine design are summarized below:

- Maximized throughput for a high volume production plant;
- Reduced machine cost;
- Improved gas utilization;
- Reduced power consumption; and
- Improved material stability by maintaining low deposition rate.

Detailed engineering and design of a single-loop serpentine web continuous roll-to-roll deposition chamber have been completed. Figure 40 is a picture of the serpentine chamber in the deposition machine.

In the deposition chamber, two deposition zones are separated by a common perforated RF cathode. One deposition zone coats the web as it moves vertically upward and one zone coats the web as it moves downward past the same cathode. A gas manifold that spans the width of the web is placed at the top of the

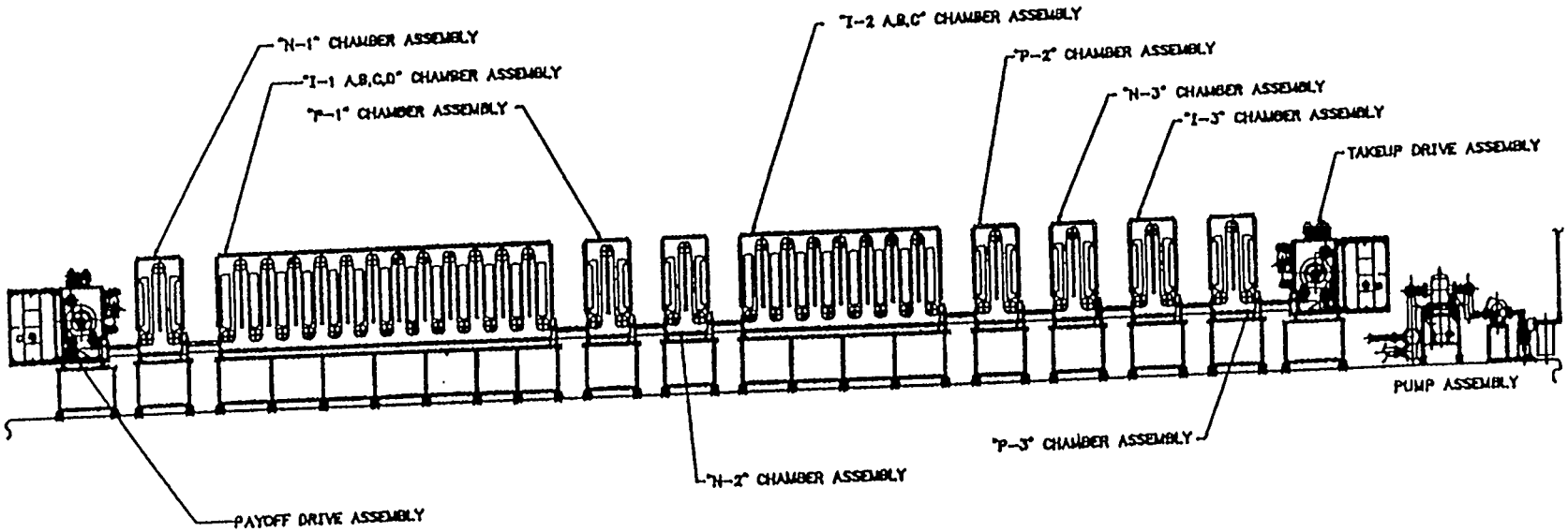

Figure 39. Serpentine web continuous roll-to-roll concept design for triple-junction a-Si cell deposition machine.

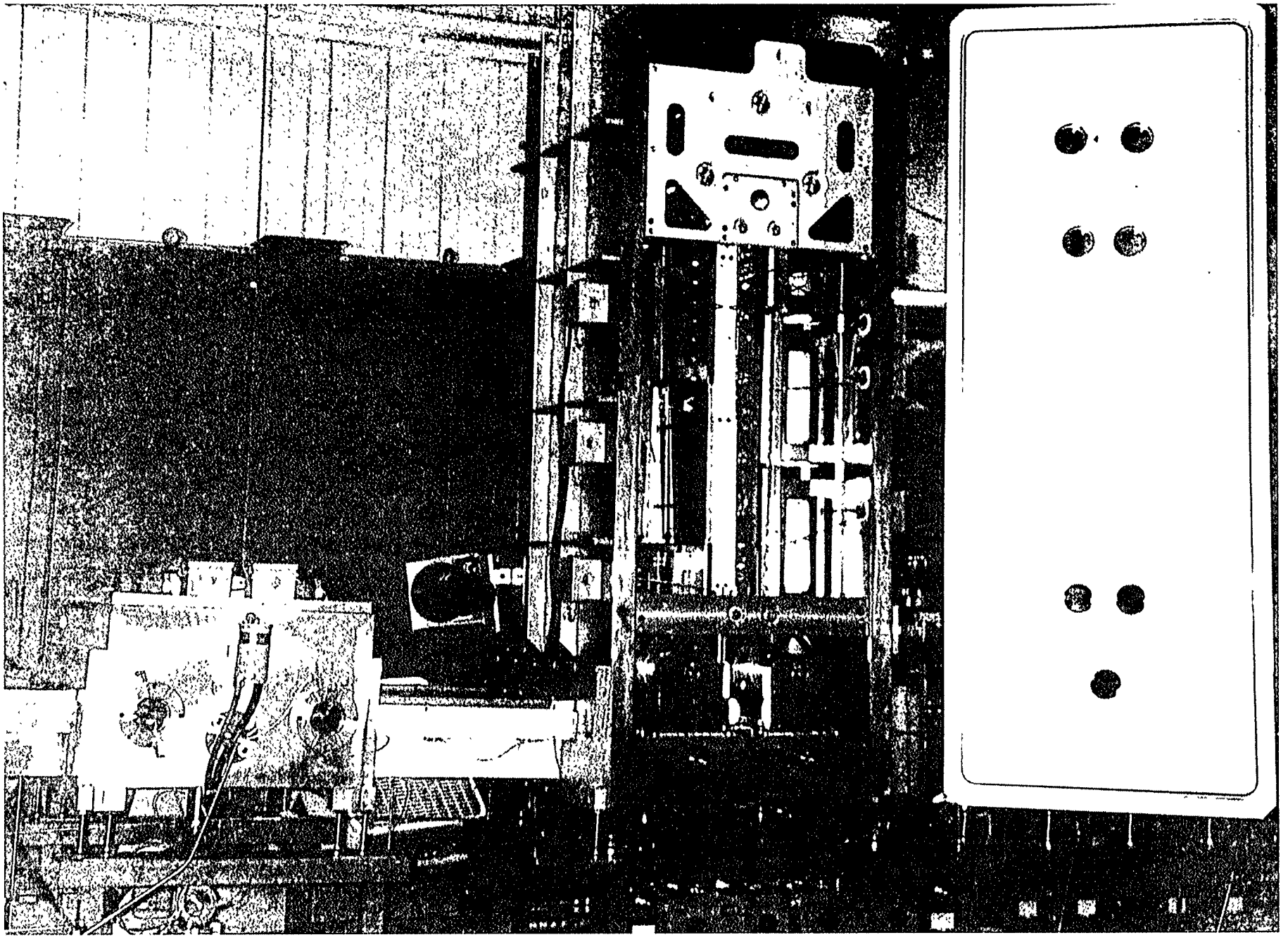

Figure 40. **Picture of the serpentine web continuous roll-to-roll deposition chamber.**

cathode and gas is pumped through a manifold at the bottom. A preheat zone is located before the upward and downward pass of the web across the cathode to insure proper web temperature during deposition.

This chamber has been incorporated into the continuous roll-to-roll multi-purpose deposition machine. a-Si n-i-p solar cells with the intrinsic a-Si layer deposited in the serpentine chamber have been produced.

We performed experiments to optimize the deposition conditions including the gas mixtures, RF power, and substrate temperature. After cleaning and process optimization, we achieved 8.7% initial efficiency for a single-junction serpentine solar cell.

We then incorporated this single junction n-i-p solar cell into a-Si/a-SiGe/a-SiGe triple-junction solar cells. The top cell intrinsic layer of the triple cell was deposited in the serpentine chamber. We optimized the cell current matching between each of the component cells and achieved initial efficiency of 9.5% as is shown in Figure 41.

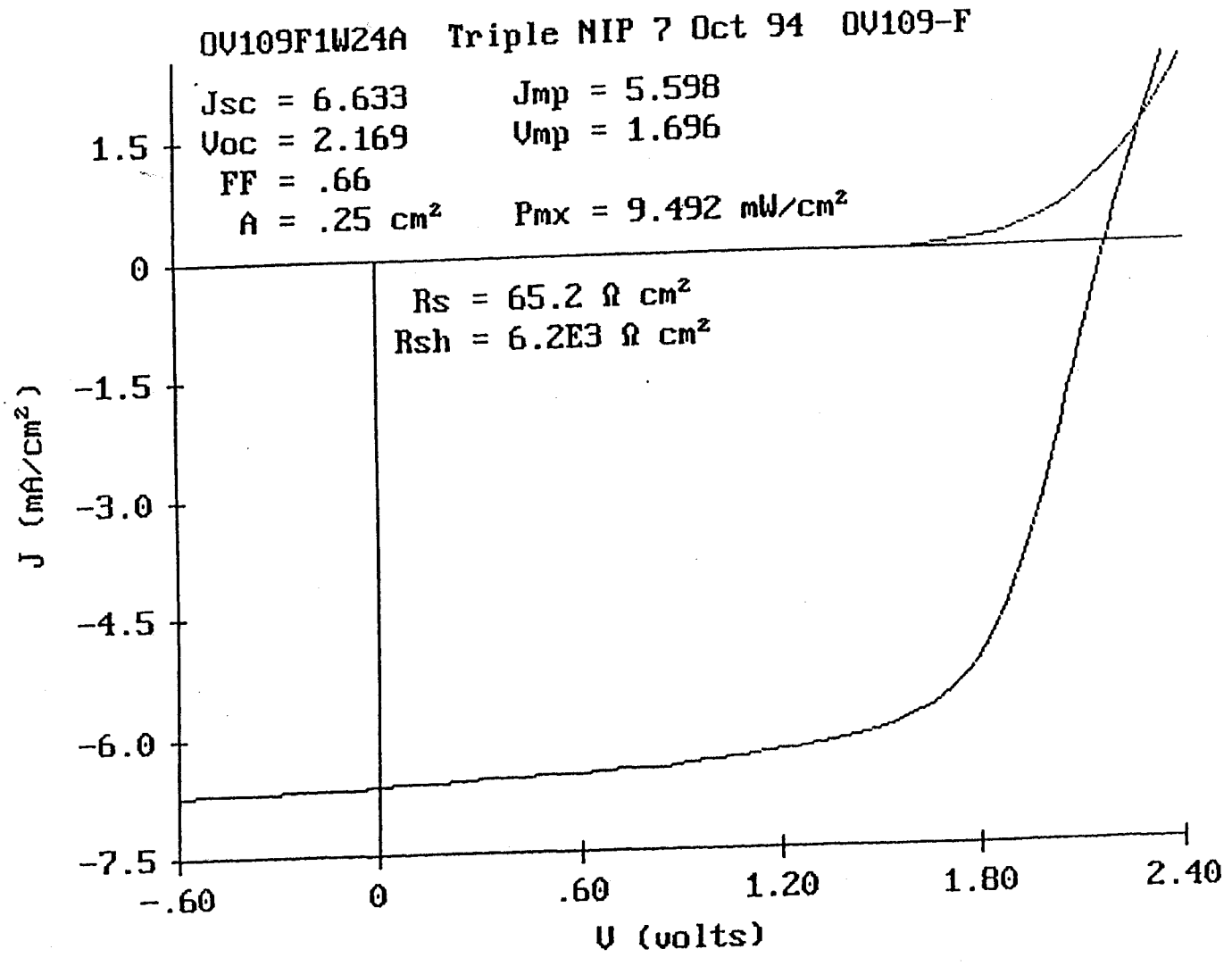

Figure 41. J-V curve of a triple-junction a-SiGe/a-SiGe/a-Si solar cell with the top cell intrinsic layer deposited in the seprentine chamber.

Task V: Material Cost Reduction

We have focused our efforts in two major high material-cost areas:

1. Reduction of germane and disilane costs; and

2. Reduction of module assembly material costs.

One of the highest cost items in the bill of materials for ECD's triple-junction multiple bandgap a-Si alloy solar cell, which consists of a a-Si/a-Si/a-SiGe structure, is germane and disilane. We identified Mitsui Toatsu and Voltaic as the world's largest manufacturers of disilane and germane gases, respectively, and obtained germane and disilane gases at prices which are substantially lower than we previously paid on the world market. We also worked with our Russian joint venture partner, Sovlux, to obtain lower cost gases from Russia. We obtained test quantities of disilane and germane gases produced in Russia. The results of purity analyses of these gases indicated that germane had acceptable purity, whereas disilane had unacceptably high levels of impurities. During this program period, the Russian supplier completed a germane production line and produced 10 Kg of germane. We expect that we can achieve approximately 25% cost reductions for these gases when they are supplied from the Russian supplier.

As the result of process optimization to reduce the layer thickness and to improve gas utilization, 77% material cost reduction for germane and 58% reduction for disilane have been achieved.

As we described previously, the serpentine web continuous roll-to-roll deposition allows us to further improve gas utilization and to reduce the cost for gases. It is calculated that an approximate 40% reduction will be achieved by this approach.

Also a new low-cost module design including wire grids design has been developed to reduce assembly material cost. Specifically, we refined the new improved module design with wire grids. This design will improve the module efficiency by 3-4% by reducing grid coverage and reduce the grid/busbar material costs by approximately 50% by eliminating expensive Ag paste materials. The strip cells prepared with these processes exhibited high fill factors indicating that the wire grids effectively collected the current. We have constructed a tool for producing 1 ft. x 4 ft. modules with wire grids, refined the tool, and assembled a number of 4 $ft.^2$ modules. These modules demonstrated high fill factors and reduced grid coverage.

We developed a concept design for large-area flexible, frameless PV modules to further reduce the manufacturing cost. Material cost is reduced by eliminating the frame and by reducing the cost of other components such as the junction box. The details of the module design is described in Task VI.

It is expected that a combination of these cost reductions will result in a cumulative material cost reduction of 71%.

Task VI: Improving the Module Assembly Process

Our major goal for this program period is to develop advanced a-Si alloy PV module manufacturing technology with the capability of producing modules with stable 10% efficiency in high volume at a cost of approximately $1.00 per peak Watt. Major market segments for the low-cost PV modules produced in high volume will be building-integrated roof-top systems and large-scale solar farms for utility applications.

ECD has developed an improved concept design for large-scale module manufacturing process based on optimizing the manufacturing steps driven by the requirements of the finished product installed in the field and also by cost effectiveness.

Based on what is stated above, a concept module designed to suit this application is large-area, light weight, relatively flexible, and easily mounted to a low-cost mounting structure.

A new module design, nominally 24 ft. x 1.5 ft., with a total weight of 40 lbs., and a total power output of 216 W, has been developed specifically for large scale roof-top and solar farm applications and high volume manufacturing. The strip cells that will be used to assemble these modules will be produced from 3 ft. wide stainless steel rolls. The increased width of the stainless steel rolls increases the throughput of the machine, and results in significant cost reductions due to the economies of scale.

During this program period, we have also developed a concept design for an automated 100 MW plant for the production of the low-cost large-area PV modules. The concept design incorporates all the technical advances achieved in this program. The concept design for a plant with 100 MW annual capacity is shown in Figures 42-45.

The following is a description of ECD's improved low-cost manufacturing process for the products described above:

Operation 1: Roll-to-Roll Substrate Washing Machine

This machine removes all the particulates as well as all the remnants of lubricating and protective oils or other liquids that were part of the rolling, annealing, and rerolling manufacturing process of the 430 BA stainless steel that becomes the substrate for our thin film solar cell. The machine will wash a 3 ft. wide, .005 inch thick, 13,500 foot long coil in 40 hours' continuous operation. The web is subjected to hot pressurized detergent, rotary brushing, ultrasonic powered hot detergent, hot DI water rinsing, drying in IR lamp clean air tunnel and finally re-rolled in a clean air takeup chamber. The web is processed at 16 ft./min.

Operation 2: Roll-to-Roll Back-Reflector Deposition Machine

This machine deposits textured silver, zinc oxide back-reflector layers on the washed substrate by sputtering vacuum deposition process. The machine processes coils of stainless steel substrate from the washing machine at the same production rate as the washing machine. The coil from the washing machine is loaded in the left hand payoff chamber and the web passes through the deposition chamber into the takeup chamber and rewound with protective Interleaf at 16 ft./min.

Operation 3: Serpentine Roll-to-Roll Amorphous Silicon Alloy Triple-Junction Deposition Machine

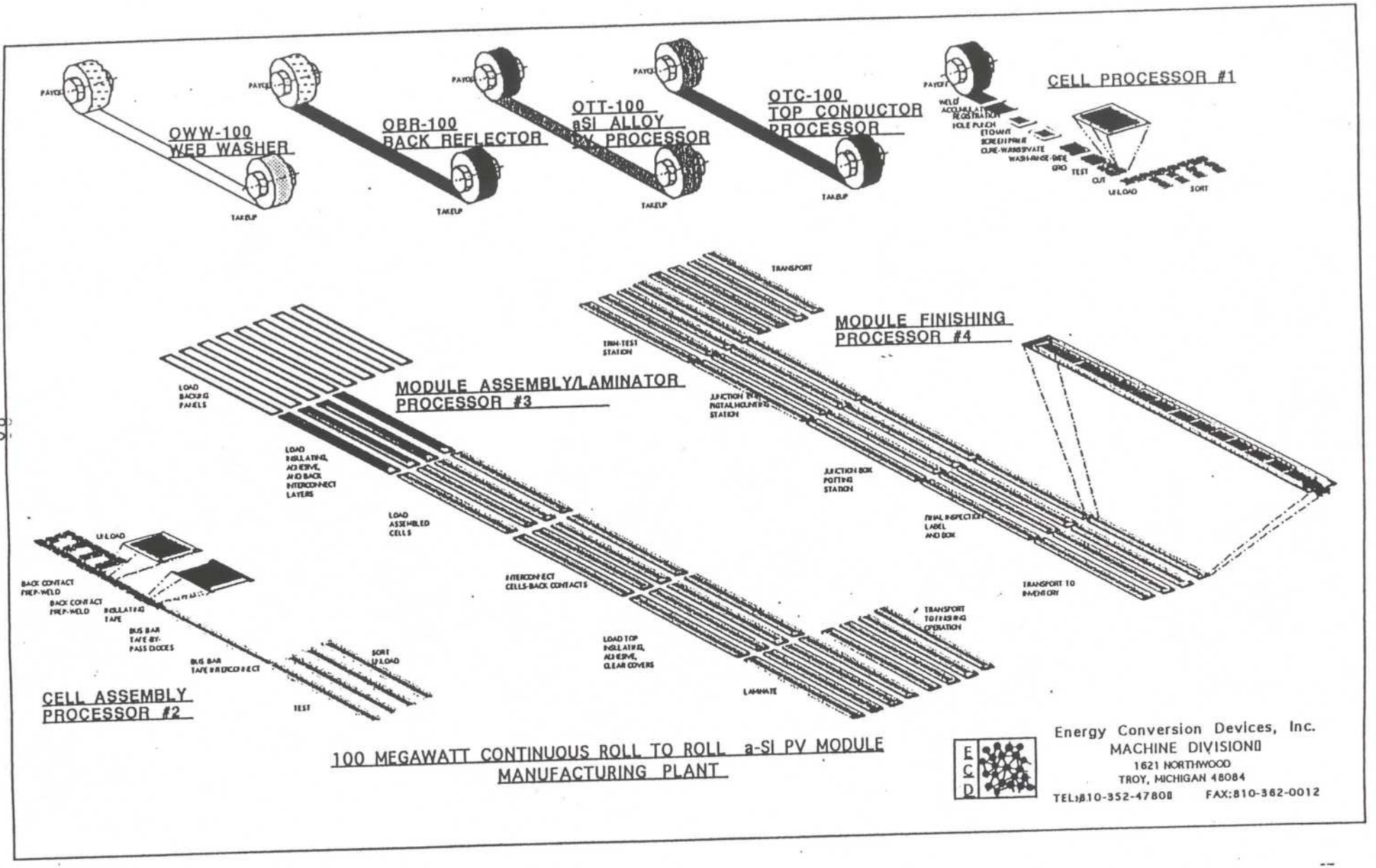

Figure 42. 100 MegaWatt continuous roll-to-roll a-Si PV module manufacturing plant.

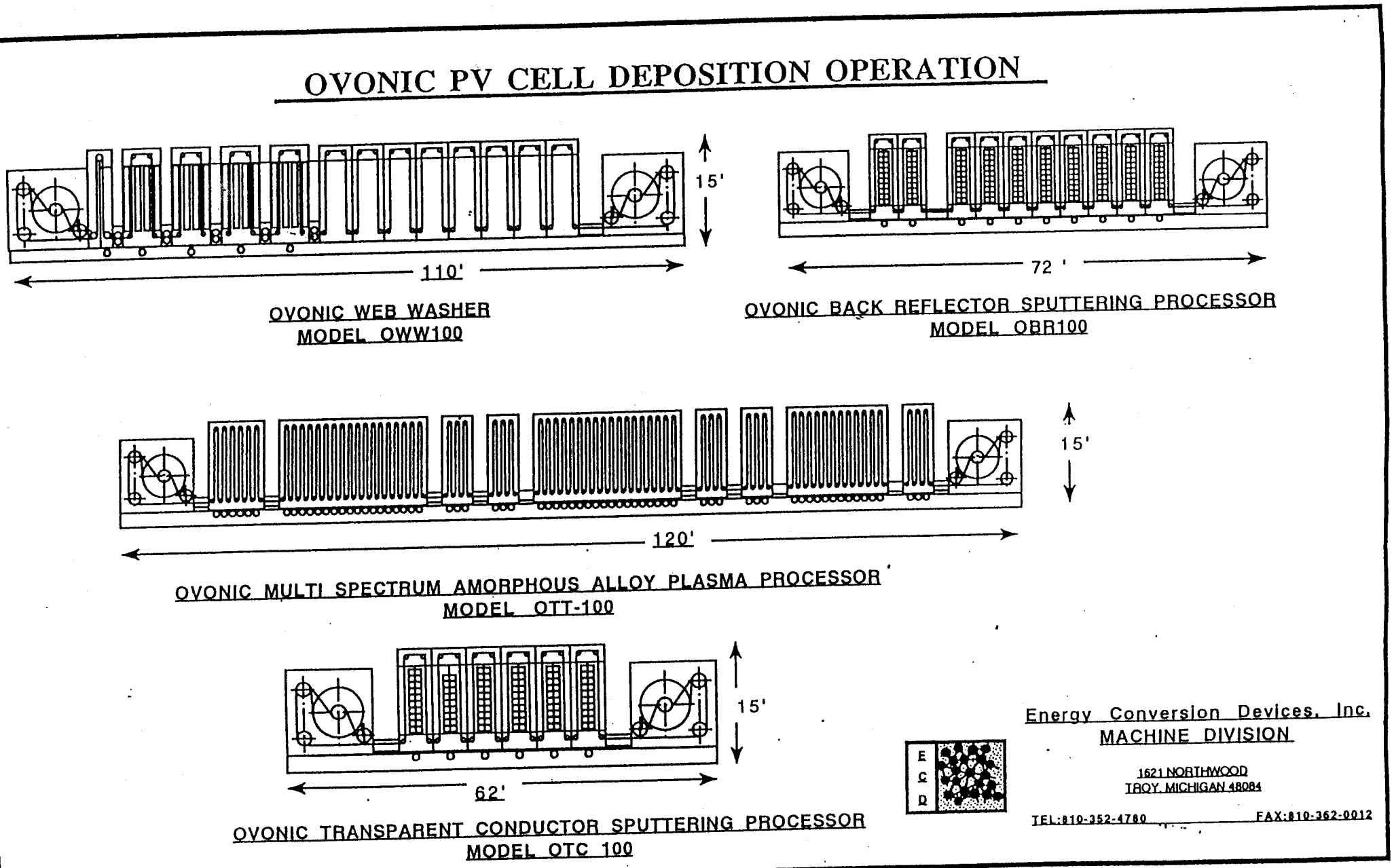

Figure 43. Ovonic PV cell deposition operation.

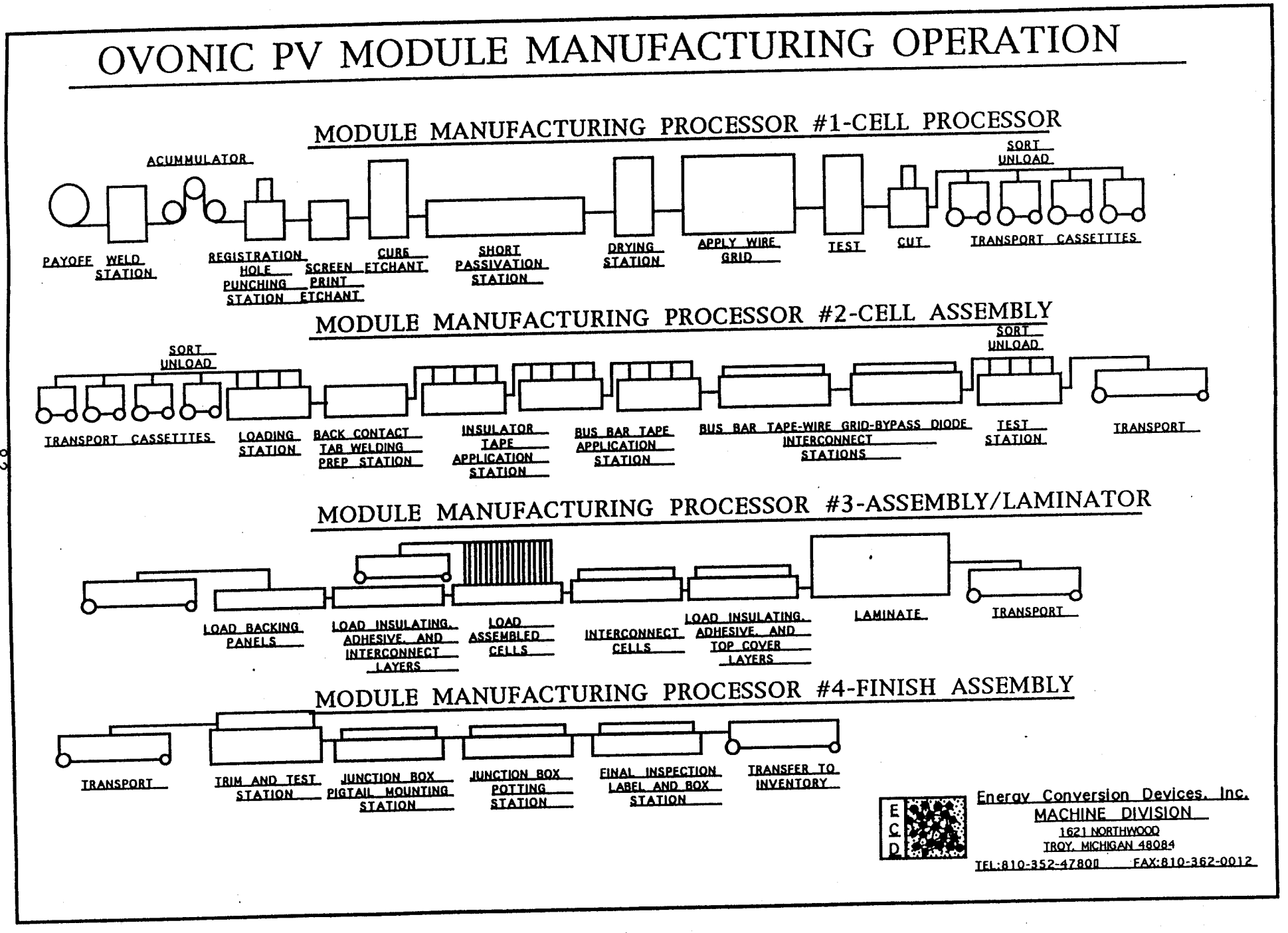

Figure 44. Ovonic PV module manufacturing operation.

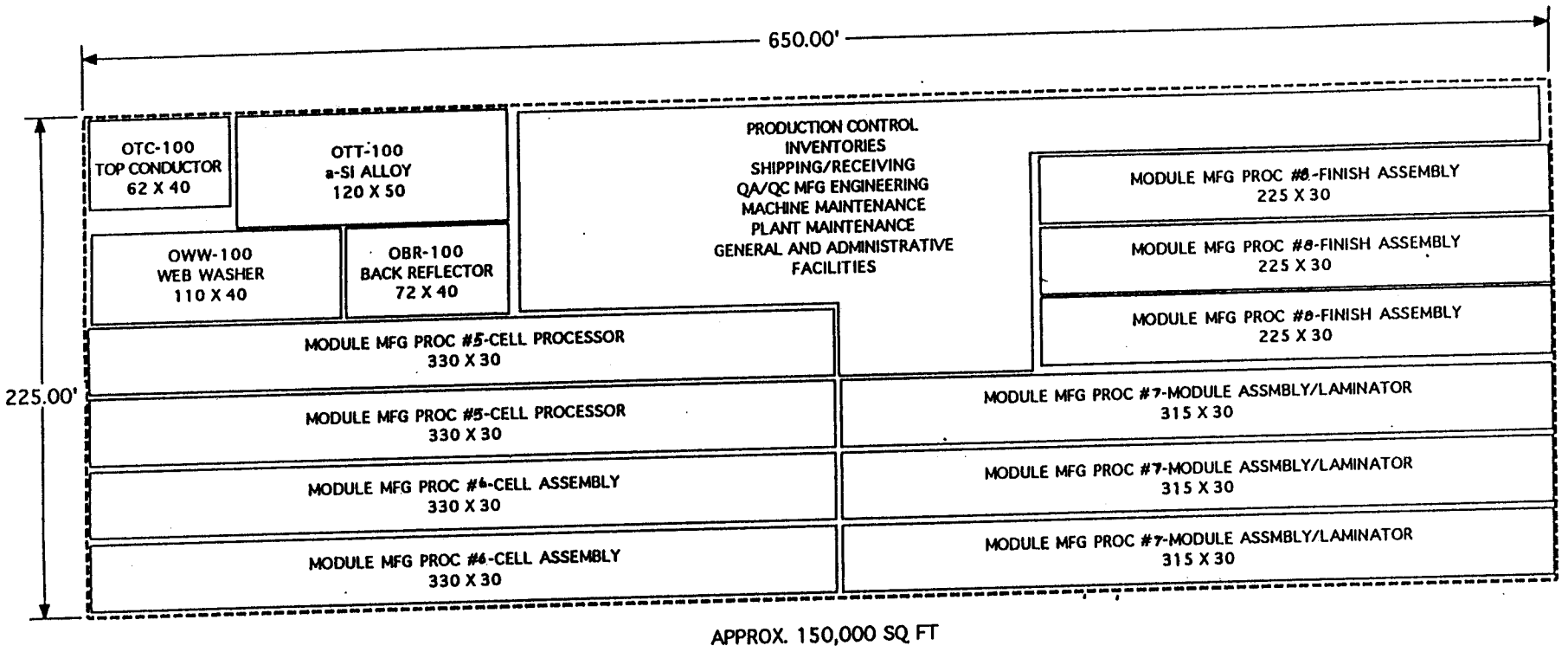

OVONIC 100 MW PV MANUFACTURING PLANT
IDEALIZED FLOOR PLAN

Energy Conversion Devices, Inc.
MACHINE DIVISION
1621 NORTHWOOD
TROY, MICHIGAN 48084
TEL:810-352-47800 FAX:810-362-0012

Figure 45. Ovonic 100 MW PV manufacturing plant -- idealized floor plan.

HCO 5-16-95

This machine deposits nine layers of doped and undoped amorphous silicon alloy thin film material which becomes the active photovoltaic semiconductor material that convert the sun's energy to electrical power. The nine layers are deposited by the RF Plasma CVD vacuum deposition process in separate chambers with isolation "gas gates" that prevent cross contamination of deposition materials. To avoid large machine footprints and allow for proper deposition rates, the web is exposed to RF plasma in ECD's unique serpentine design pass line. Coils from the back-reflector machine are processed at 16 ft./min. Protective interleaf is removed from the coil in the left-hand payoff chamber and new interleaf is re-introduced in the right-hand takeup chamber.

Operation 4: Roll-to-Roll Top Conductor Deposition Machine

This machine deposits a transparent thin conductive layer of indium tin alloy by the reactive DC sputtering vacuum deposition process. Coils from the a-Si alloy deposition machine are loaded in the left-hand payoff chamber and unloaded from the right-hand takeup chamber. The process speed is 16 ft./min. Interleaf is removed from the payoff coil as the coil unwinds and new protective interleaf is introduced in takeup chamber as the processed coil is rewound.

Operation 5: Roll to Process Step and Repeat Solar Cell Processor

This machine takes a full coil of deposited substrate from Operation 4 and performs the following processes in a step and repeat manner with exact tensioning and position controlled at each station (two machines are used for 100 MW operation).

A: Payoff into weld station;
B: Punch station punches accurately place location holes for positioning the web in downstream stations;
C: Screen print etchant paste, defines borders of each cell;
D: Cure etchant paste in serpentine drying station;
E: Rinse etchant in running water dip tank;
F: Immerse etchant and perform proprietary passivation operation, to eliminate all micro and macro shorts and shunts that have developed during deposition process;
G: Rinse passivation fluid;
H: Dry in serpentine drying station;
I: Grind small area in outer edge of substrate (for later weld attachment of interconnect tape);
J: Probe cell and test for PV function-store and record data by position;
K: Code cells from data from previous test station;
L: Cut cells; and
M: Load sorted cells by code onto coded cassette carts.

Operation 6: Module Assembly and Finishing Operations

Two machines are used for the 100 MW operation. Module assembly operations consist of 12 step and repeat transfer machines as follows:

A: Load cut-sorted cells from cassette carts onto step and repeat transfer line load station;
B: Apply interconnect tape;
C: Weld interconnect tape;
D: Apply insulating tape;
E: Apply proprietary grids and grid interconnect busbar;
F: Load grided cells onto step and repeat transfer line load station from cassette carts;
G: Position 10 cells in series in holding fixture;
H: Position end positive and negative busbars and pigtails;
1: Perform interconnect weld operations;
J: Position bypass diodes;
K: Weld bypass diodes; and
L: Unload onto cell-to-module-interconnect cassette carts.

Operation 7: Module Lamination Machine

Three machines are used for the 100 MW operation. Module Lamination Machine operation stations described as follows:

A: Load offline prepared backing plate with polymer;
B: Feed prepared bottom insulating polymer layers;
C: Load interconnected cell-module;
D: Feed prepared bottom insulating polymer layers;
E: Transfer into multiple step lamination chamber;
F: Transfer to cut station; and
G: Transfer onto laminate carts.

Operation 8: Module Finishing Operations Stations

Three machines are used for the 100 MW operation. Module Finishing Operations Stations operates at 1 module per minute as follows:

A: Test laminates;
B: Trim, punch, and grommet laminates;
C: Attach positive and negative connectors; and
D: Label, package, load skids for inventory or shipping.

Summary

Under this Photovoltaic Manufacturing Technology 2A program, we have significantly advanced ECD's continuous roll-to-roll a-Si alloy solar cell photovoltaic technology. The major accomplishments made under this program are:

- Incorporating a high performance Ag/ZnO back-reflector system into our continuous roll-to-roll commercial production line and demonstrated high subcell yield;
- Incorporating deposition of high quality bandgap profiled a-SiGe narrow bandgap solar cells into a commercial continuous roll-to-roll manufacturing process;
- Demonstrating the production of a-Si/a-Si/a-SiGe triple-junction solar cells in 2500 ft. long production runs;
- Demonstrating production of solar cells with 11.1% initial conversion efficiency (0.25 cm^2, 2/93);
- Demonstrating 8% stabilized efficiency on production triple-junction a-Si alloy modules with a total area of at least 0.37 m^2 (4/93);
- Full production runs (700m) with 99.7% subcell yield and high uniformity;
- Reductions of 77% in material costs for germane and 58% for disilane;
- Developing a new grid/busbar design that uses thin wire grids, thereby improving efficiency by approximately 3-4% while also reducing the cost of the grid/busbar by 50%;
- Developing a new 200 kW/yr multipurpose continuous roll-to-roll a-Si alloy solar cell deposition machine for depositing back-reflector, triple-junction solar cell, and transparent conducting oxide layers in multiple passes;
- Designing and constructing a serpentine web, continuous roll-to-roll chamber which is used to demonstrate a compact, low-cost deposition machine design with improved throughput and gas utilization factor for the high throughput deposition;
- Demonstrating a 9.5% triple-junction cell using serpentine technology (0.25 cm^2, 10/94); and
- Developing a concept design for a 100 MW continuous roll-to-roll PV module manufacturing plant to produce large-area, lightweight, frameless PV modules with 10% stable efficiency at less than $1.00/Watt; this manufacturing cost includes material, labor, depreciation, and manufacturing overhead costs.

References

1. Izu, M.; Ovshinsky, S.R. (1983). "Production of Tandem Amorphous Silicon Alloy Cells in a Continuous Roll-to-Roll Process." SPIE Proc. (407, 42).

2. Izu, M.; Ovshinsky, S.R. (1984). "Roll-to-Roll Plasma Deposition Machine for the Production of Tandem Amorphous Silicon Alloy Solar Cells." Thin Solid Films (119:55).

3. Morimoto, H.; Izu, M. (1984). "Amorphous Silicon Solar Cells Production in a Roll-To-Roll Plasma CVD Process:" JARCET (16); (1984) *Amorphous Semiconductor Technology & Devices,* North Holland Publishing Company, Edited by Y. Hamakawa, 212.

4. Ovshinsky, S.R. (1988). "Roll-To-Roll Mass Production Process for Amorphous Silicon Solar Cell Fabrication." Proc. International PVSEC-1, (577).

5. Yang, J.; Ross, R.; Glatfelter, T.; Mohr, R.; Hammond, G.; Bemotaitis, C.; Chen, E.; Burdick, J.; Hopson M.; Guha S.; (1988). "High Efficiency Multiple-Junction Solar Cells using Amorphous Silicon and Amorphous Silicon-Germanium Alloys". Proc. 20th IEEE PV Spec. Conf., 241

6. Yang, J.; Ross, R.; Mohr, R; Fournier J. P. (1987). "Physics of High Efficiency Multiple-Junction Solar Cells". Proc. MRS Symp. Vol. (95:517).

7. Nath, P.; Izu, M. (1985). "Performance of Large Area Amorphous Silicon Based Single and Multiple-Junction Solar Cells". Proc. of the 18th IEEE Photovoltaic Specialists Conf., Las Vegas, Nevada, (939).

8. Nath, P.; Hoffman, K.; Call, J.; Vogeli, C.; Izu, M.; Ovshinsky S.R. (1987). "1 MW Amorphous Silicon Thin-Film PV Manufacturing Plant." Proc. of the 3rd International Photovoltaic Science and Engineering Conf., Tokyo, Japan, 395.

9. Nath, P.; Hoffman, K.; Vogeli, C.; Ovshinsky, S.R. (1988). "Conversion Process for Passivation Current Shunting Paths in Amorphous Silicon Alloy Solar Cells." Appl. Phys. Lett. 53(11), 986.

10. Nath, P.; Hoffman, K.; Call, J.; DiDio, G.; Vogeli, C.; Ovshinsky, S.R. (1988). "Yield and Performance of Amorphous Silicon Based Solar Cells Using Roll-To-Roll Deposition." Proc. 20th IEEE PV Spec. Conf., 293.

11. Nath, P.; Hoffman, K.; Vogeli, C.; Whelan, K.; Ovshinsky S.R. (1988). "A New Inexpensive Thin Film, Power Module." Proc. 20th IEEE PV Spec. Conf.,1315

12. Nath, P.; Hoffman, K.; Ovshinsky S.R. (1989). "Fabrication and Performance of Amorphous Silicon Based Tandem Photovoltaic Devices and Modules." 4th International PV Science and Engineering Conf., Sydney, Australia.

13. Guha, S. (April 1989). "Advances in High efficiency, Multiple-Bandgap, Multiple-Junction Amorphous Silicon Based Alloy Thin-Film Solar Cells." Presented at MRS Spring Meeting, San Diego.

14. Yang, J.; Ross, R.; Glatfleter, T.; Mohr, R.; Guha S. (1989). "Amorphous Silicon-Germanium, Alloy Solar Cells With Profiled Bandgaps." MRS Symposium Proc. (Vol. 149,435)

15. Izu, M.; Deng, X.; Krisko, A.;Whelan, K.; Young, R.; Ovshinsky, H.C.; Narasimhan, K.L.; Ovshinsky, S.R. (1993). "Manufacturing of Triple-Junction 4 ft.^{2} a-Si Alloy PV Modules." Proc. of 23rd IEEE PVSC, 919.

16. Izu, M.; Ovshinsky, S.R.; Deng, X.; Krisko, A.; Ovshinsky, H.C.; Narasimhan, K.L.; Young, R. (1993). "Continuous Roll-To-Roll Amorphous Silicon Photovoltaic Manufacturing Technology." AIP Conf. Proc. 306, 12th NREL PV Program Rev., 198.

17. Guha, S.; Yang, J.; Banerjee, A.; Glatfelter, T.; Hoffman, K.; Ovshinsky, S.R.; Izu, M.; Ovshinsky, H.C.; Deng, X. (1994). "Amorphous Silicon Alloy Photovoltaic Technology - From R&D to Production." Proc. of MRS Spring Meeting.

18. Deng, X.; Izu, M.; Narasimhan K.L.; Ovshinsky, S.R. (1994). "Stability Test of 4 ft.^{2} Triple-Junction a-Si Alloy PV Production Modules." Proc. of MRS Spring Meeting.

19. Izu, M.; Ovshinsky, H.C.; Deng, X.; Krisko, A.; Narasimhan, K.L.; Crucet, R.; Laarman, T.; Myatt, A.; Ovshinsky, S.R. (December 1994). "Continuous Roll-To-Roll Serpentine Deposition for High Throughput a-Si PV Manufacturing." Proc. of the First World Conference on Photovoltaic Energy Conversion, Hawaii, 820.

20. Deng, X.; Narasimhan, K.L., (December 1994). "New Evaluation Technique for Back-Reflector Using Photothermal Deflection Spectroscopy." Proc. of the First World Conference on Photovoltaic Energy Conversion, Hawaii, 555.

21. X. Deng; Narasimhan, K.L.; Evans, J.; Izu, M.; Ovshinsky, S.R. (December 1994). "Dependence of a-Si Solar Cell V_{oc} On Deposition Temperature. Proc. of the First World Conference on Photovoltaic Energy Conversion, Hawaii, 678.

22. Izu, M.; Deng, X.; Ovshinsky, H.C.; Ovshinsky, S.R. (April 2-7, 1995). "Roll-To-Roll RF PECVD Machine for a-Si Solar Cell Manufacturing." Proc. of Annual Conference of Society of Vacuum Coaters, Chicago, IL.

23. Izu, M.; Ovshinsky, S.R.; Deng, X.; Ovshinsky, H.C.; Jones, S.J.; Doehler, J. (May 16-19, 1995). "Continuous Roll-To-Roll a-Si PV Module Manufacturing." Proc. of 13th NREL PV Program Review, Lakewood, CO.

24. Xu, X.; Yang, J.; Guha, S. (1993). "Stability Studies of Component Cells for Multi-junction Amorphous Silicon Solar Cells." Proc. 23rd IEEE PV Specialists Conference, 971.

REPORT DOCUMENTATION PAGE

Form Approved
OMB NO. 0704-0188

1. AGENCY USE ONLY (Leave blank)	2. REPORT DATE	3. REPORT TYPE AND DATES COVERED
	February 1996	Final Subcontract Report, 1 April 1992 - 30 September 1995

4. TITLE AND SUBTITLE

Continuous Roll-to-Roll a-Si Photovoltaic Manufacturing Technology

5. FUNDING NUMBERS

C: ZM-2-11040-7

TA: PV650101

6. AUTHOR(S)

M. Izu

7. PERFORMING ORGANIZATION NAME(S) AND ADDRESS(ES)

Energy Conversion Devices, Inc.
1675 West Maple Road
Troy, Michigan 48084

8. PERFORMING ORGANIZATION REPORT NUMBER

9. SPONSORING/MONITORING AGENCY NAME(S) AND ADDRESS(ES)

National Renewable Energy Laboratory
1617 Cole Blvd.
Golden, CO 80401-3393

10. SPONSORING/MONITORING AGENCY REPORT NUMBER

TP-411-20588

DE96000531

11. SUPPLEMENTARY NOTES

NREL Technical Monitor: R. Mitchell

12a. DISTRIBUTION/AVAILABILITY STATEMENT

12b. DISTRIBUTION CODE

UC-1280

13. ABSTRACT *(Maximum 200 words)*

This report describes work performed by Energy Conversion Devices, Inc. (ECD) to advance roll-to-roll, triple-junction photovoltaic (PV) manufacturing technologies, reduce module production costs, increase stabilized module performance, and expand commercial production capacity using such roll-to-roll technology. The specific goal of this subcontract is to develop advanced large-scale manufacturing technology incorporating ECD's earlier research advances with the capability of producing modules with stable 10.2% efficiency at a cost of about $1.00 per peak watt. The activities reported in this report include: (1) optimization of the high-performance back-reflector system; (2) optimization of the Si-Ge narrow-band-gap solar cell; (3) optimization of the stable efficiency of photovoltaic modules; (4) demonstration of serpentine web continuous roll-to-roll deposition technology; (5) material cost reductions, and (6) improving the module assembly process. Accomplishments made toward these objectives are described.

14. SUBJECT TERMS

manufacturing ; amorphous silicon ; photovoltaics ; solar cells ; roll-to-roll technology ; triple-junction photovoltaics

15. NUMBER OF PAGES
91

16. PRICE CODE

17. SECURITY CLASSIFICATION OF REPORT	18. SECURITY CLASSIFICATION OF THIS PAGE	19. SECURITY CLASSIFICATION OF ABSTRACT	20. LIMITATION OF ABSTRACT
Unclassified	Unclassified	Unclassified	UL